VISCOELASTIC PROPERTIES, GELATION BEHAVIOR AND PERCOLATION THEORY MODEL OF THE TEMPERATURE INDUCED FORMING (TIF) CERAMIC SLURRIES

By

YUNPENG YANG

A DISSERTATION PRESENTED TO THE GRADUATE SCHOOL
OF THE UNIVERSITY OF FLORIDA IN PARTIAL FULFILLMENT
OF THE REQUIREMENTS FOR THE DEGREE OF
DOCTOR OF PHILOSOPHY

UNIVERSITY OF FLORIDA

2001

Dedicated to the memory of my father who loved me.

ACKNOWLEDGMENTS

The author would like to thank his advisor and committee chairman, Dr. W. M. Sigmund, for his generous support, guidance and assistance in performing the research and in writing this dissertation. He would also thank his other committee members, Dr. E. D. Whitney, Dr. R. Baney, Dr. C. Y. Wu, Dr. D. Clark and Dr. L. Gower, for their kindly help in designing and conducting the research. The author also would like to show his great appreciation to Ms. M. Swanson, Dr. M. Kaufman, Dr. R. Abbaschian, Dr. E. Wachsman and Dr. M. Sacks for their kind help so that the author could stay at UF to finish his study. Dr. K. Power, Mr. G. Scheiffele and Mr. G. Brubaker in the Engineering Research Center of the University of Florida are also acknowledged for helping and conducting various kinds of measurements. Dr. A. Rosinus, Dr. E. Laarz and Mr. C. Lofton are acknowledged for their valuable discussions and suggestions on this research topic. He wants to give thanks to all brothers and sisters in Gainesville Chinese Christian Church for their love and encouragement. Finally, the author would like to show his great appreciation to all his family members in China for their love and support throughout his life.

This research is supported in part by the Engineering Research Center for Particle Science and Technology at the University of Florida and the National Science Foundation under Grant No. EEC-94-02989 and BES/9980795.

TABLE OF CONTENTS

Page

LIST OF TABLES

LIST OF FIGURES

Figure Page

Abstract of Dissertation Presented to the Graduate School
of the University of Florida in Partial Fulfillment of the
Requirements for the Degree of Doctor of Philosophy

VISCOELASTIC PROPERTIES, GELATION BEHAVIOR AND PERCOLATION THEORY MODEL OF THE TEMPERATURE INDUCED FORMING (TIF) CERAMIC SLURRIES

By

Yunpeng Yang

August 2001

Chairman: Dr. Wolfgang M. Sigmund
Major Department: Materials Science and Engineering

Controlled ceramic processing is required to produce ceramic parts with few strength-limiting defects and the economic forming of near net shape components. Temperature induced forming (TIF) is a novel ceramic forming process that uses colloidal processing to form ceramic green bodies by physical gelation. The dissertation research shows that TIF alumina suspensions (>40vol%) can be successfully fabricated by using 0.4wt% of ammonium citrate powder and <0.1wt% poly (acrylic acid) (PAA). It is found that increasing the volume fraction of alumina or the molecular weight of polymer will increase the shear viscosity and shear modulus. Larger molecular weight PAA tends to decrease the volume fraction gelation threshold of the alumina suspensions. The author is the first in this field to utilize the continuous percolation theory to interpret the evolution of the storage modulus with temperature for the TIF alumina suspensions. A model that relates the storage modulus with temperature and the volume fraction of solids is proposed. Calculated results using this percolation model show that the storage

modulus of the suspensions can be affected by the volume fraction of solids, temperature, volume fraction gelation threshold and the percolation nature. The parameters in this model have been derived from the experimental data. The calculated results fit the measured data well. For the PAA-free TIF alumina suspensions, it is found that the ionization reaction of the magnesium citrate, which is induced by the pH or temperature of the suspensions, controls the flocculation of the suspensions. The percolation theory model was successfully applied to this type of suspension. Compared with the PAA addition TIF suspensions, these suspensions reflect a higher degree of percolation nature, as indicated by a larger value of percolation exponent. These results show that the percolation model proposed in this dissertation can be used to predict the gelation degree of the TIF suspensions. Complex-shape engineering ceramic parts have been successfully fabricated by direct casting using the TIF alumina suspensions, which has a relative density of ~ 65%. The sintered sample at 1550 °C for 2h is translucent and has a uniform grain size.

CHAPTER 1
INTRODUCTION

1.1 Overview of Ceramic Forming Strategy

Ceramic processing has been one of the heavily studied topics since the emergence of human beings. Ceramic materials are also very appealing for high-performance applications due to their temperature and corrosion resistance, low density, high stiffness, hardness and strength. However, prediction and control of the strength of ceramic materials is insufficiently reliable for many potential applications. In many materials, stress concentrates at microstructural defects. Ceramic materials are brittle, and stress is not relieved by local deformation near the crack tip, as is the case in metals and plastics. The work of fracture is low, so cracks easily propagate. Strength-limiting defects often arise during fabrication of parts and persist through other processing steps, so performance of the part may be limited by the earliest stages of processing. For specimens prepared by powder compaction, defects can arise that are related to the granulated feed material. Compaction is a widely used fabrication process for ceramics. Feed material for compaction processes is commonly in the form of granules, which are free-flowing powder agglomerates with controlled properties and may contain organic additives. Key advantages of compaction are that ceramic parts can be made quickly, the process is easily automated, and the parts need no drying step after forming. A major disadvantage is that the process is prone to internal defects, which can limit the strength

of the final part. A compaction stress needs to be uniformly transmitted through a volume of granules in such a way that all evidence of the granules is eliminated.

Comparatively, the reliability of ceramics can be greatly increased by dispersing the powder in a liquid and filtering the suspension to eliminate strength-degrading heterogeneities prior to forming engineering shapes. To implement this colloidal processing method, forming techniques must be developed that not only are compatible with removing flaws from the suspension by filtration, but also allow economic forming of near net shape components [1-2].

Up to now, the commercialization of advanced ceramic components is still hindered by expensive production processes; especially, the final machining and inspection are currently the major cost factors for complex-shape ceramic products. Powder cost is still a relatively small part of the cost, regardless of the size of the component. Reducing machining costs, eliminating or reducing inspection requirements, and yield improvements are most important for cost reduction. The part also requires excellent finishes and demanding dimensional control. Therefore, the ideal flexible manufacturing process for ceramics would require only such information as the dimensions, surface finish, and microstructure of the component while imposing no process constraints on the component design. Unfortunately, no such "smart" processes currently exist in practice [3-6].

In the future, forming technology will no doubt capitalize on the modern computer-aided-design (CAD) environment to fabricate real objects of complex shape. Software has already been developed to provide a link between solid models and numerical control (NC) machine centers. More recently, processes that build complex

shapes in layers are becoming available. One of the most important tools of an agile manufacturing organization is rapid prototyping (RP) [7-13]. RP refers to the production of a part directly from a computer file generated with a computer-aided design (CAD) program. While RP is sometimes considered to include computer numerical control (CNC) machining, in most cases it refers to building up a part from a stack of thin layers, each of which is patterned from the computer generated 3-D model of the part. This process is also called "solid freeform fabrication" (SFF). Various SFF techniques have been reported, such as laminated object manufacturing (LOM™) [14-18], three dimensional printing (3DP™) [19-21], Sanders prototype (SP™) [22], robocasting [23-26], stereolithography (SL™) [27,28], direct photoshaping [29,30], fused deposition modeling (FDM™) [31-35], selective laser sintering (SLS™) [36-38], shape deposition manufacturing (SDM™) [39-50] and jet printing [51,52]. Stereolithography, for example, constructs successive layers by writing on the surface of a bath containing UV-curable resin. The trajectory the laser takes on the surface is determined by a computer, which mathematically slices a model of the object. Sequential layers are built on top on one another to construct the component. Alternatively, powder processes such as selective laser sintering and three-dimensional printing function in a similar way but seem to be more applicable to ceramics.

1.2 Objective

The objectives of this research are as follows:

(1) Characterize the temperature induced forming (TIF) alumina suspensions with poly (acrylic acid) (PAA) addition and investigate the effect of the composition and temperature on the viscoelastic properties;

(2) Study the feasibility of eliminating PAA so as to decrease the room temperature shear viscosity while keeping higher volume fraction of solids in the suspension for further solid freeform fabrication (SFF) processing;

(3) Build a theoretical model to describe the microstructure evolution of the TIF suspensions, and use the model to predict the gelation condition of the suspension with changes in volume fraction of solids and temperature;

(4) Use TIF alumina suspensions in direct casting to fabricate complex shape ceramic parts for future industrial application.

In this dissertation, Chapter 2 reviews the literature of the stability and flocculation of ceramic suspensions. A brief description and comparison will be given of the up-to-date ceramic shape forming techniques through colloidal processing. Chapter 3 presents how the suspension compositions affect the rheological properties, especially the viscosity, of the suspensions. Gelation diagrams are also given to determine the minimum amount of poly (acrylic acid) to make the suspensions gel. Chapter 4 emphasizes the variation of the shear modulus of the suspensions with composition and thermal history. Chapter 5 gives the proposed percolation theory model for the TIF suspensions to interpret the evolution of the shear viscosity and shear modulus with compositions and temperature for the TIF alumina suspension with PAA addition. The computed results based on this model are compared with the experiment data. Chapter 6 gives the research results on the PAA-free TIF suspensions in order to increase the volume fraction of the suspension while keeping a relatively low viscosity for a direct casting process. DLVO (Deryagin-Landau-Verwey-Overbeek) theory is considered to design the compositions of the suspensions and the explanation using the percolation theory model proposed in Chapter V is discussed. Chapter 7 demonstrates the direct casting results using the TIF suspensions. Chapter 8 is the summary of this dissertation and the future work is

suggested. The Appendix part covers the raw materials characterization, suspension preparation process and the characterization facilities.

CHAPTER 2
LITERATURE REVIEW ON CERAMIC FORMING TECHNIQUES THROUGH COLLOIDAL PROCESSING

2.1 General Concepts of Ceramic Colloidal Processing

Colloidal processing methods to fabricate ceramic parts normally consist of the following steps: (1) the development of a long-range repulsive potential to disperse the sub-micrometer size powder in a suitable liquid. (2) The removal of heterogeneities by filtering the dispersed slurry. (3) Changing the interparticle potentials to produce a weakly attractive particle network. (4) The consolidation of the particles within the slurry to form engineering shape. Removing heterogeneities via filtration requires a low-viscosity slurry containing a high volume fraction of solids, which can only be achieved with long-range repulsive potentials. Once detrimental heterogeneities are removed, the long-range repulsive potential should be replaced with a short-range repulsive potential in order to develop a weakly attractive particle network. With the weakly attractive network, mass segregation due to sedimentation is avoided in the slurry state, particles can be packed to high relative density during consolidation, and the consolidated body can be plastic. The plastic behavior is desired to avoid damage during strain recovery after consolidation and it allows new shape-forming technologies to be used for advanced ceramics, which are commonly used in traditional clay technologies. Thus to fully implement colloidal powder processing, a processor must first disperse a specific powder

to remove heterogeneity via filtration, and then make it weakly attractive for further processing.

2.2 Stabilization and Flocculation of the Ceramic Suspension

A stable suspension is always the first step to consider when studying the colloidal processing of a certain ceramic system. The suspension can be stabilized via three types of mechanisms: the electric double layer stabilization, steric stabilization and the electrosteric stabilization [1, 53-56]. One common method for dispersing ceramic particles is well described by DLVO theory. The surface of a particle containing neutral hydroxide sites can be charged by reactions of the neutral sites with either H^+ or OH^- to produce either positive or negative sites, respectively. DLVO theory proposes that an atmospheric layer of counterions (ions with an opposite charge relative to the dominant surface sites) surrounds and neutralizes each particle. An osmotic pressure (i.e., repulsive potential) arises when the layer of counterions around one particle penetrates another particle's counterion-layer to increase the concentration of counterions between them. Furthermore, DLVO proposes that the thickness of the counterion layer, and thus the separation distance where particles strongly repel one another, is inversely proportional to the concentration of counterions in solution. Where the counterion concentration is small, the repulsive potential extends to a larger separation and overwhelms the pervasive, attractive van der Waals potential. Under these conditions the particles strongly repel one another, and thus they are dispersed within the slurry. DLVO tells that the inter-particle force will become attractive either at high concentration of counterions,

where the layer of counterions is very thin, or near the isoelectric point where the number density of charged surface sites is small.

Destabilization of the stable suspension can be achieved by the following routes. (1) increasing the ionic strength in the suspensions to produce a weakly attractive network. (2) Adjusting the pH of the suspensions toward the IEP so that the net powder surface charge is neutral and Van der Waals attractive force dominates. (3) Removal of part of the solvent so that the volume fraction of powders is increased and the net potential falls into the primary minimum [56].

2.3 Viscoelastic Properties of Ceramic Suspensions

2.3.1 Variation of Shear Viscosity with Volume Fraction of Solids

The colloidal processing for the forming of ceramic green bodies generally requires that the ceramic suspensions fulfill two criteria, maximum possible volume fraction of particles and minimum possible viscosity at low shear rate. These two criteria seem contradictory because the suspension viscosity increases with volume fraction of particles, as can be described by the Dougherty-Krieger equation [57]. This equation has been used widely and successfully for different materials systems to model the correlation between the relative viscosity and volume fraction of solids in the suspensions. Since Dougherty-Krieger model is based on hard sphere interactions, the viscosity values at higher shear rate are normally taken for calculations. This is due to the dominating effect of hydrodynamic force on the suspension viscosity at high shear rate. Excessive amount of organic dispersant and binder might also increase the shear

viscosity, which is a result of the resistance of the organic polymer chains to conformational changes induced by the shear force.

2.3.2 Elastic Response of Ceramic Suspension

The word "viscoelastic" means the simultaneous existence of viscous and elastic properties in a material. At intermediate time-scales a mixed (viscoelastic) response is observed. For many years, much labor has been expended in the determination of the linear viscoelastic response of materials. There are many reasons for this. First there is the possibility of elucidating the molecular structure of materials from their linear-viscoelastic response. Secondly, the material parameters and functions measured in the relevant experiments sometimes prove to be useful in the quality-control of industrial products. Thirdly, a background in linear viscoelasticity is helpful before proceeding to the much more difficult subject of non-linear viscoelasticity [58].

Two types of rheological properties, the shear modulus and the yield stress, can be taken to characterize the strength of an attractive particle network at a given volume fraction of particles by using a sophisticated rheometer. In one method, the shear stress and shear viscosity can be calculated from the measured torque value when the suspension is rotated in one direction at a fixed strain rate. With this method, an apparent elastic response is observed first (linear stress-strain response), followed by a nonlinear "yielding phenomenon" prior to flow (increasing strain at constant stress). The slope of the initial linear region (shear modulus, G') is independent of the applied strain, but the stress where the deviation from linear behavior is observed ("yield stress") is a function of the applied shear rate.

In the second method, a sinusoidal oscillation, at a fixed amplitude and frequency, is applied to the tool, to measure the shear modulus within linear viscoelastic range. A given attractive network will exhibit a fixed value of the shear modulus (G') for conditions where the strain amplitude is small and the frequency is high. A decrease in G' will occur at a "yield strain." At rest, the attractive particle network is elastic and in static equilibrium with body forces produced by gravity. In a frequency sweep experiment, the oscillation frequency is increased at a fixed amplitude (below yield strain), until the shear modulus (G') becomes invariant over a large range of frequencies and both the loss modulus (G'') and the phase angle are small. Strain sweep experiments can also be used to determine the "yield strain" of the network. The strain amplitude is increased, at a fixed frequency, until a stress is reached where the network begins to break apart to initiate flow [59]. For the present research, the measured variation of the shear modulus and shear stress with temperature is used to describe the evolution of the suspension microstructure.

2.3.3 Basic Concepts of the Oscillatory Shear

It is instructive to discuss the response of viscoelastic materials to a small-amplitude oscillatory shear, since this is a popular deformation mode for investigating linear viscoelastic behavior [58].

Let strain be

$$\gamma(t') = \gamma_0 \exp(i\omega t') \qquad (2\text{-}1)$$

where ω is the frequency and γ_0 is a strain amplitude which is small enough for the linearity constraint to be satisfied. The corresponding strain rate is given by

$$\gamma'(t') = i\omega\gamma_0 \exp(i\omega t') \qquad (2\text{-}2)$$

and, if this is substituted into the general integral equation for the total stress

$$\sigma(t) = \int^{t} \phi(t - t') \gamma'(t') \, d\, t' \qquad (2\text{-}3)$$

then we get

$$\sigma(t) = i\omega\gamma_0 \exp(i\omega t) \int \phi(\xi) \exp(- i\omega\xi) \, d\, \xi \qquad (2\text{-}4)$$

In oscillatory shear define a "complex shear modulus' G^*, through the equation

$$\sigma(t) = G^*(\omega) \ \gamma(t) \qquad (2\text{-}5)$$

and, from eqns. (2-1), (2-4) and (2-5), get

$$G^*(\omega) = i\omega \int \phi(\xi) \exp(- i\omega\xi) \, d\, \xi. \qquad (2\text{-}6)$$

It is customary to write

$$G^* = G' + iG'' \qquad (2\text{-}7)$$

And G' and G'' are referred to as the "storage modulus" and "loss modulus," respectively. G' is also called the dynamic rigidity.

For the Maxwell model (assuming a serial connection of the elastic and viscous element), the strains or strain rates are additive. Hence the total rate of shear is the sum of the rates of shear of all elements. Then the following formula can be got

$$G^* = i\omega\eta / (1 + i\omega\tau), \text{ or alternatively } G^* = i\omega\tau G / (1 + i\omega\tau) \qquad (2\text{-}8)$$

And

$$G' = \eta\tau\omega^2 / (1 + \omega^2 \tau^2) \qquad (2\text{-}9)$$

$$G'' = \eta\omega / (1 + \omega^2 \tau^2) \qquad (2\text{-}10)$$

where $\tau = \eta/G$, is the retardation time, η is the viscosity of the pure viscous element, and G is the elasticity of the pure Hookean element in the Maxwell model.

As an alternative to the complex shear modulus, define "complex viscosity" η^*, as the ratio of the shear stress σ to the rate of shear γ'. Thus

$$\sigma(t) = \eta^* \gamma'(t) \quad (2\text{-}11)$$

The similar representation of the general integral of the complex viscosity is

$$\eta^*(\omega) = \int \phi(\xi) \exp(-i\omega\xi)\, d\xi \quad (2\text{-}12)$$

Define

$$\eta^* = \eta' - \eta'' \quad (2\text{-}13)$$

η' is usually given the name "dynamic viscosity." The parameter η'' has no special name but it is related to the dynamic rigidity through $G' = \eta''\omega$. It is also easy to deduce that $G'' = \eta'\omega$.

When the suspension displays a viscous response, $G' \sim 0$. If the response is elastic, then $\eta'' \sim 0$.

Another alternative method of characterizing linear viscoelastic response is to plot G' and the "loss angle" δ. In this method, it is assumed that for an applied oscillatory strain given by Equation (2-1), the stress will have a similar form, but its phase will be in advance of the strain by an angle δ. Then

$$\sigma(t) = \sigma_0 \exp[i(\omega t + \delta)] \quad (2\text{-}14)$$

And it is easy to show that the damping factor is

$$\tan\delta = G'' / G' \quad (2\text{-}15)$$

When the suspension transforms from a elastic to a viscous state or vice versa, tan δ will vary. For pure elastic solid, the stress is in phase with the applied strain. While for pure viscous liquid, the stress is 90° ahead of the strain.

2.3.4 Research Results on the Elastic Properties of the Highly Loaded Suspensions

It is known that aggregation will form flocs in concentrated suspensions. A space-filling network will be created when the characteristic size of a floc is large enough that individual flocs overlap, then the suspension is considered to have undergone gelation [60-62]. The viscoelastic properties, in particular how the elastic modulus scales with volume fraction, have been modeled based on the assumption that the particle network consists of close packed flocs. Two models have been proposed to explain the experimental phenomena, fractal model and percolation model.

The fractal models assume that suspensions can gel at all volume fractions; therefore, there is no gelation threshold. Several authors interpreted the elasticity of aggregated dispersions in terms of the fractal concept. The fractal models depend on the assumption that the aggregated structure transmits stress through its elastic backbone (a chain of particles). Fractal models of gelation predict that a space-filling network will be created when the characteristic size of floc, ξ is large enough so that individual flocs overlap. In the suspensions that a weak attraction causes slower aggregation and is reaction limited, the viscoelastic properties, in particular how the elastic modulus scales with volume fraction, have been modeled based on the assumption that the particle network consists of close packed fractal flocs. The models predict a power law behavior of elastic modulus with respect to volume fraction,

$$G = G_0 \cdot \phi^P \qquad (2\text{-}16)$$

where G_0 is the pre-exponential factor, ϕ is the volume fraction of clusters, and p is an exponent that relates to the structure through the fractal dimension of the flocs. P is about 4.5 for reaction limited cluster aggregation (RLCA) [63-66].

Percolation models deal with the effects of varying the richness of interconnections present in a random system. The basic idea of percolation is the existence of a sharp transition at which the long-range connectivity of the system disappears or occurs. This transition occurs abruptly when some generalized density in this system reaches a critical value (percolation threshold). The models based on percolation concepts describe the importance of the gelation threshold ϕ_g to the rheological properties of aggregating suspensions. Percolation models can be divided into two categories: site/lattice percolation network and continuous percolation network. For the lattice percolation model, it is assumed that each particle has a fixed site to fill. Each lattice site represents one polyfunctional unit, and two reacted neighboring units are linked by a bond. This is analogous to the electrical conductivity of an electrical network. For the continuous percolation network, particles do not have fixed positions to fill but rather deposit randomly as isolated islands. One example of this type of network is the physical vapor deposition of the electrical conducting thin film. In the initial stage of deposition, the deposited particle forms random isolated islands and they do not give an electrical conductivity. When the number of the deposited particle increases to a critical number, these originally isolated particles start to connect somehow and give electrical conductivity.

Rueb and Zukoski used an octadecyl silica system to obtain a scaling for the moduli which follows:

$$G = G_0 \cdot (\phi / \phi_g - 1)^{s} \qquad (2\text{-}17)$$

where the exponent, s is related to the microstructure of the network [66,67].

But experimental results of Yanez et al. on AKP-30 alumina / poly(12-hydroxy stearic acid) suggested that the expression $G' = G'_0 \cdot (\phi - \phi_g)^s$ captured the generic mechanical behavior of particle gels. Here, $\phi - \phi_g$ is the distance from the gel transition and thus relates to the number of stress carrying bonds. G'_0 characterizes the elasticity of the interparticle bonds, which might be temperature dependent [68].

Although both models predict that the modulus of the suspension increases with increasing volume fraction of the flocs, there are no reports on how to model the temperature dependence of the suspension modulus. Because temperature is an important parameter that will affect the rheological properties of the suspension, it is desirable for industrial application to understand and control the variation of these properties with temperature.

2.4 Consolidation Techniques through Colloidal Processing

2.4.1 Consolidation through Removing of Solvent

All of the drained casting techniques, e.g. slip casting, pressure casting and centrifugal casting, involve a solid-liquid separation process to form a dense green body. Considerable effort has been put forth to optimize the properties of the slurries used for slip casting [56,69,70]. But there are generic problems with the traditional drained casting methods, including the following: stress gradient may lead to non-uniform densities of the green body, and the liquid flow will affect the suspension microstructure and tend to orient non-spherical constituents such as whiskers. All these factors will decrease the properties and the reliability of the sintered materials.

2.4.2 Constant Volume Consolidation through Injection Molding

Injection molding is based on mixing of the ceramic powder with a binder system (usually a mixture of polymers) to create a viscous feedstock, and forming the part by injecting the powder/binder mixture into an impermeable mold where the binder is solidified by a temperature control. Injection molding has proven to be an excellent forming technique for smaller parts although there are potential problems with the die filling process. Also the removal of the binder must be carried out at a very slow rate and might take up to several days in order to avoid slumping and crack formation. The binder removal time will increase dramatically with the size of the green body. Another challenge for injection molding is to produce parts with thick cross sections [71-74].

2.4.3 Near-Net-Shape Forming Techniques through Gelation

The near-net-shape forming techniques are also called direct casting methods. According to the fundamental physical and chemical principles of the dispersing mechanism and gelation reaction, the direct casting methods can be classified as either physical gel method or chemical gel method. For a more detailed review paper, see Sigmund et al. [56]. Physical gel techniques include direct coagulation casting (DCC), temperature induced coagulation casting (TICC), temperature induced forming (TIF), temperature induced gelation (TIG) and clay-like forming/vibraforming, etc. Chemical gel techniques include hydrolysis assisted solidification (HAS), aqueous injection molding (AIM), gelcasting etc.

DCC uses chemical reactions of some enzymes that can either shift the pH or increase the salt concentration so as to induce coagulation. DCC allows casting at room temperature and uses inexpensive molds. This technique has the advantages of a room

temperature reaction and is independent of the component size and wall thickness. Typically less than 0.5wt% of organic compounds (dispersants and enzymes) based on ceramic powder are required. Therefore, a separate burnout step is not required. Since the physical gelling was done by thermal activated chemical reaction before enzymatic reactions were introduced, it is important to design these reactions far from the boiling point of the dispersing media so that bubble formation can be avoided [75-78].

For the electrosterically stabilized TICC slurry with the minimum amount of polymer dispersant, the flocculation might be due to the entropy driven increase in polymer adsorption with increasing temperature, and which suggests that a fully covered surface at room temperature will have more sites available for adsorption at higher temperature. Since there is no additional free polymer in solution, the only way to fill the empty sites is by bridging. Therefore, flocculation occurs at elevated temperatures for slurries that have an exact balance of adsorbed polymer. In the case of excessive polymer addition, no flocculation is observed. Limitation for this technique is to use maximum solid loading because the process requires a precise control of the polymer dispersant concentration [79].

Since the adsorbed polymers at the interface can generate long-range steric forces, the extension of the adsorbed polymer can be beyond the van der Waals attraction and form a dispersed particle system. Temperature induced gelation (TIG) originates from the incipient flocculation effect of sterically stabilized suspensions. The magnitude and range of the interaction between polymer layers can be related to the solution properties of the polymer and the conformation of the polymer at the solid-liquid interface. When the solvency reaches a critical level, the sterically stabilized dispersion flocculates, so

called incipient flocculation. Decrease in solvency of the polymer by temperature change or addition of non-solvent has been utilized in several previous studies to induce flocculation in sterically stabilized concentrated suspensions. In principle, all sterically stabilized suspensions should be able to flocculate by making the stabilizing moieties insoluble. For many systems, however, this effect can only be obtained far from room temperature, which makes these systems difficult to apply for ceramic processing. One example is the TIG formed Al_2O_3 and composite Al_2O_3 / SiC_w from suspensions dispersed with Hypermer KD3 (copolymer). Choosing a continuous medium with intermediate polarity, such as pentanol, will result in a transition temperature close to room temperature. At temperatures above 30°C, the suspension has a low viscosity and negligible elasticity due to extension of the polymer dispersant. Below 20°C, the viscosity increases significantly due to a change in the solvation parameter of the adsorbed polymer, and the viscoelastic behavior becomes predominantly elastic.

The elasticity and the associated particle network strength are sufficiently high for a highly concentrated gelled suspension to support its own weight. TIG produces a fully reversible gel and can recycle excess material easily. For the same reason gelled saturated bodies must be kept at the solidification temperature to avoid slumping [80,81].

In comparison to the physical gels, chemical gels usually require a higher amount of organic processing aids and thus a separate burnout step. Since larger amount of polymer is available, the green bodies have higher strength than the physical gels. Another major difference from the physical gels lies in the irreversibility of chemical gelling since covalent bonds between molecules are formed. Hydrolysis Assisted Solidification (HAS) uses this mechanism that the green strength of physical gels can be

increased when the salt created for gelation precipitates to form particle necks. For example, AlN in water has a thermally activated decomposition reaction, and AlN is stable in aqueous system at room temperature due to a thin inert protective coating of alumina. But when heating, this layer dissolves and the exposed AlN surface will react with water. Dissolving aluminum nitride in water yields gibbsite and ammonia and creates the pH shift [82].

The first Aqueous Injection Molding (AIM) process was reported in the late 1970's where methylcellulose derivatives were used. These polymers are highly soluble at room temperature due to polymer hydration. When increasing temperature, the polymer becomes more and more dehydrated until the chain-chain interaction is stronger than the chain-water interaction. And at above 50°C, the slurry suddenly gels. The process is reversible on cooling. The gel strength is related to the molecular weight and thus requiring a compromise for the maximum solid loading and the wet green body strength [83]. Another approach is to use other polymers to gel the slurry on cooling, such as agarose (a purified polysaccharide) gels through a change of its conformation. But the slurry has to be handled close to the boiling point and gels below 37°C. The agar dissolves in the water at slightly elevated temperatures and results in a viscous but fluid material that is readily injectable into molds using standard thermoplastic injection molding equipment. The agar re-gels in the mold upon cooling, utilizing water as part of its gel structure. Molding cycle time of 5 min are achievable for components such as turbine blades and nozzles. The AIM process can result in Si_3N_4 components with equivalent mechanical properties to slip cast Si_3N_4 [84]. Although AIM is a faster gelation process than gelcasting, but is more limited to thickness and size of parts that can

be formed because it is a viscous filling process. And the critical technical issues for AIM remain: (1) Generation of defect-free part in high yield since the sintered body has a porous structure; (2) Dimension control of complex-shaped surfaces such as airfoils.

Gelcasting technology is another type of direct casting method through chemical gelation. The gelcasting concept originates in the early 1960's when metallic particles in the slurry were first consolidated using the polymerization of monomers, and its application towards ceramics was first described in the 1990's. The general process follows a dispersion of the particles by electrostatic or steric stabilization using a dispersant for maximizing solid loading. The monomer is dissolved in the dispersing media and provides a low viscosity vehicle for transporting the fluid into the mold. After a small amount of cross-linker is added to the Si_3N_4 aqueous slurry, the monomer is polymerized in situ and permanently gels around the ceramic powder to retain the desired shape. Because the monomers and cross-linking agents undergo a free-radical chain polymerization reaction, the setting is very rapid. For example, gelation times are as short as 15 min for turbine wheels. The gelled powder compact is then dried to remove the water, leaving a powder compact with an open pore network and 2-4 wt% dried gel. The gel can be removed by a pyrolysis cycle.

The gelcasting process has some advantages over pressure slip casting, including: being 50-80% faster, generating more uniform powder packing, having a much higher part strength after forming and after drying, and requiring simpler molds (no need for de-watering surfaces). But there are some remaining technical issues for gelcasting: (1) requires an appropriate combination of mold materials and mold release agents to ensure that the part can be removed form the mold. Mold release agent selection is often the

most difficult aspect of developing an effective gelcasting system; (2) Densification is another issue. Gelcasting parts typically shrink 23% during densification. Distortion in the densified part is an inherent outcome of the densification process. Controlling the distortion using furnace cycles, fixturing and a combination of the two is a constant challenge; (3) Achieving full density in a thick cross section such as the hub of a turbine wheel is a challenge; (4) Burnout process usually takes a long time [85,86].

2.4.4 Temperature Induced Forming (TIF) Process

TIF method was first proposed by F. Aldinger and W. M. Sigmund [87]. Similar to TICC, the TIF process also applies to the electrosterically stabilized slurry and the slurry is flocculated by temperature control. But TIF employs a low molecular weight dispersant for stabilization at room temperature, and uses the ceramic powder dissolution with increasing temperature to exchange the molecular dispersant for a higher molecular weight polymer. Since the polymer concentration is maintained below the level necessary for stabilization, the gelation occurs via bridging flocculation (Figure 2-1). The polymer molecular weight is a critical factor for this process. Normally high molecular weight polymer results in a stronger gel. After drying, the precipitation of dissolved materials at particle contacts increases the green strength [87,88].

The effect of the PAA amount on the viscosity and relative viscosity (at shear rate 20 s^{-1}) of the 50vol% AKP53 alumina TIF suspensions was reported by Bell et al [88]. The molecular weight of the PAA was 50,000 and the amount of PAA ranged from 0.02wt% to 0.20wt% of dry alumina particles. The viscosity of all suspensions increased when the temperature is above 45 °C. But there are also some contradictions in the data reported, for example, the viscosity data for the 0.12wt% PAA addition suspension is

lower than that of the 0.065wt% PAA addition suspension. These contradictions might be due to the mill jars that are made out of polymer materials, which will erode into the suspensions and affect the viscoelastic properties. The paper also reported that the TIF process could be used for direct casting ceramic parts with good surface finish, and that the sintered ceramic parts had a uniform microstructure.

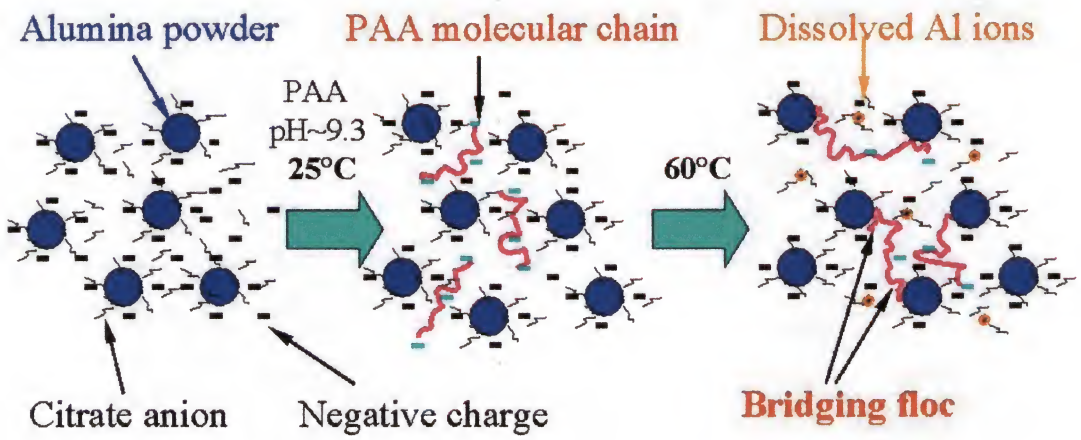

Fig. 2-1. Proposed gelation mechanism for TIF suspensions. The initial slurry is stable because of electrostabilization, and the negative-charged PAA chains do not adsorb on alumina surface because of complete surface coverage by negative-charged citrate anions. The desorption of citrate anion from alumina surface with the increasing solubility of alumina in water at elevated temperatures leaves adsorption sites for poly (acrylic acid) chains, and the bridging flocculation results [87,88].

Compared with other direct casting techniques and the conventional slip casting techniques discussed above, the TIF process has some evident advantages. First, TIF uses water as solvent and a higher volume fraction of solid is accessible. Therefore, a dense green body of complex shape parts can be obtained. Another virtue of TIF is that it

only uses temperature to control the rheological properties of the suspensions. Third, TIF is a constant volume method using gelation mechanism for consolidation; and principally less stress in the green body compared to drained techniques. Also, TIF uses less than 0.5 wt% of organic materials during the processing, therefore the burnout step can be omitted, and the density of the resulting green body can be above 65% theory density. From the industrial point, TIF technology is readily automatable. Another important character of TIF process is that it is through physical gelation, which indicates that the gelation degree can be tailored by alternating the process parameters, such as temperature and time. This makes it possible to build ceramic parts layer by layer using TIF suspension without causing any layer delamination.

Therefore, in this research, the author will focus on the viscoelastic characterization and evaluation of the TIF suspensions, and try to tailor the compositions to get higher volume fraction suspensions while having a relatively lower shear-rate viscosity for direct casting fabrication of complex shape, engineering ceramic parts. The qualitative and quantitative understanding of the microstructure evolution with compositions and temperature will enable us to design the appropriate processing parameters and control the degree of gelation of the TIF suspensions.

CHAPTER 3
EFFECT OF COMPOSITION ON THE VISCOSITY OF THE TIF AQUEOUS ALUMINA SUSPENSIONS WITH POLY(ACRYLIC ACID) (PAA)

3.1 Adsorption of Citrate Anions on Alumina Particle Surfaces

3.1.1 Shift of the Isoelectric Point by Adsorption of Citrate Anions

Ammonia citrate (TAC) powder is soluble in water in the basic pH region. The adsorption of citrate on the alumina particles has been studied [24,89,90]. These results show that the adsorption of negatively charged citrate ion on alumina can prepare high volume fraction stable suspensions for slip casting. The competitive adsorption of citrate with polymers such as polyethylene oxide (PEO) has been reported by Hidber et al. [91]. The exis tence of PEO will not impede the adsorption of citrate on alumina, while the adsorption of citrate will decrease the adsorption of PEO because citrate is negatively charged and is preferably adsorbed on the polar alumina surface. This indicates that adsorption energy between citrate-alumina is higher than that of PEO-alumina. The effect of PAA on the adsorption of citrate in alumina suspensions has not been reported, but it can be estimated that citrate is apt to adsorb on alumina more easily than that of PAA because of its smaller size. When citrate is first added into suspensions, the alumina particle surfaces will be covered and saturated by citrates. The late addition of PAA will not affect the adsorption amount of citrate on alumina particles.

The pH dependence of the zeta potential for the AKP53 alumina suspensions with and without TAC is shown in Figure 3-1. For the pure AKP53 alumina powders, the point of zero charge (PZC) is ~ pH9.2. When the pH > 9.2, the zeta potential, ξ, is

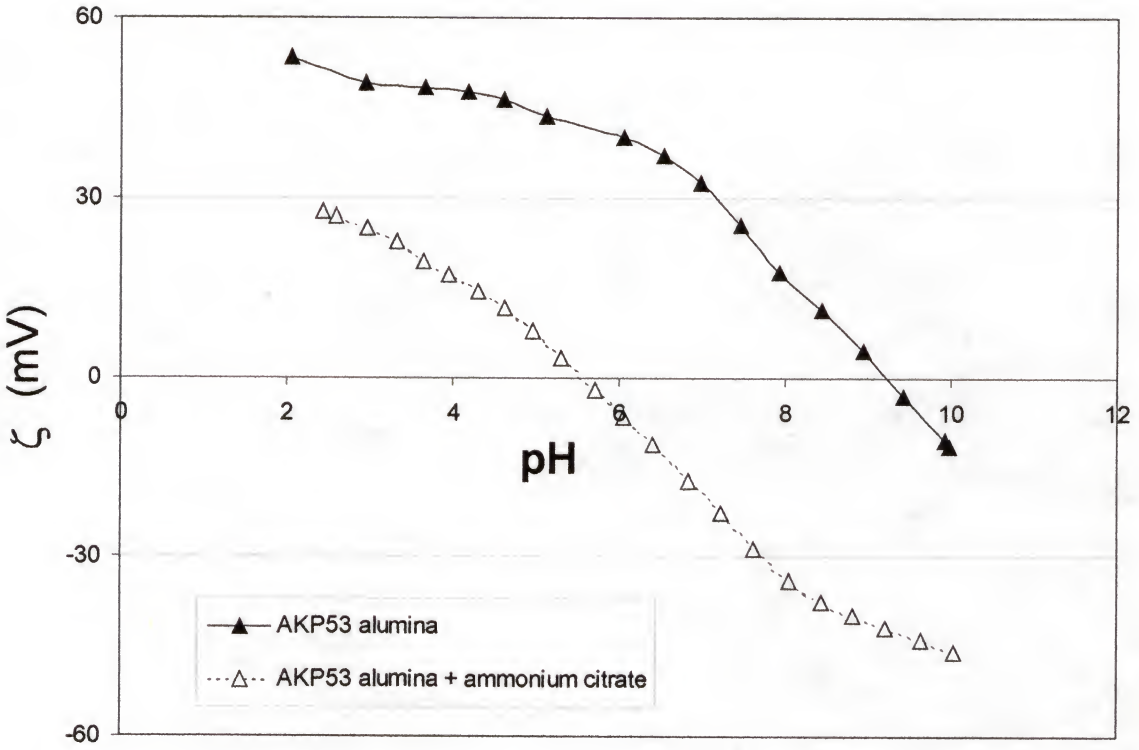

Fig.3-1. The pH dependence of the zeta potential for the 3vol% AKP53 alumina suspensions. The amount of TAC is 0.4wt% of alumina powder.

negative; at pH < 9.2, $\xi > 0$. The surface charge comes from the hydrolysis of the ceramic powder in water. At alkaline region of pH>9.2, adsorption of the negative hydroxyl groups on the particle surface yields a net negative surface charge. While at pH<9.2, the proton in water will react with the hydroxyl groups on the particle surface to yield a net positive surface charge and thus a positive surface potential. Since a higher magnitude of the zeta potential is required to prepare a stable suspension by the electrostatic mechanism, the pH of the suspensions needs to be adjusted to the highly acidic region. The acid condition is not favorable to industrial application because of erosion of the steel containers.

The data shows that the addition of TAC shifts the PZC of alumina to the acidic region, or IEP of about pH5.5, which is in agreement with the reported results on the shift the PZC of alumina suspensions to the acidic region by poly (acrylic acid) or citric acid as dispersant [24,89,90,92]. The shift of PZC of the alumina particles is due to the adsorption of these charged dispersant s on the ceramic powder surface so that more protons are needed to neutralize the surface charge. Therefore, at pH>9, the zeta potential of the alumina particles in the suspension with TAC is about –50 mV and this value is large enough to stabilize the suspensions. The pH of the TIF suspensions is then adjusted to above pH9 for dispersion.

3.1.2 Minimum Amount of Citrate Anion for Complete Surface Coverage

The adsorption of citrate on alumina surfaces creates a higher EDL repulsive potential to overcome the van der Waals attractive potential and enables the preparation of stable concentrated suspensions. When the surface of the alumina surface is fully covered, the excessive citrate will stay in the suspension. Even though these citrate molecules carry the same sign charge as the particle surface, they will increase the resistance to the movement of the water molecules under shear, which results in increase of the viscosity. Therefore, determination of the minimum amount of citrate needed to stabilize the alumina particles is necessary in order to get a concentrated suspension with minimum shear viscosity.

Figure 3-2 illustrates the TAC concentration dependence of viscosity for the 40vol% AKP53 alumina suspension, which is the value at shear rate of 100 s^{-1}. It can be seen that the plot has a minimum at about 0.4wt% TAC. Above this value, the viscosity increases gradually. When the TAC concentration is less than 0.4wt%, the viscosity

increases sharply. Therefore, it can be concluded that the optimum amount is about 0.4wt% TAC, which will yield full surface coverage of citrate on alumina particle surface while maintaining a low viscosity. The measured adsorbed amount of citrate anions on AKP53 alumina at 25 °C is 5.7 ±0.1 μg / m^2 Al_2O_3 (BET surface area) using the UV-Persulfate TOC Analyzer (DOHRMANN, Phoenix 8000). This value is in good agreement with the value (~ 5.0 μg / m^2 Al_2O_3) reported by Hidber et al [89].

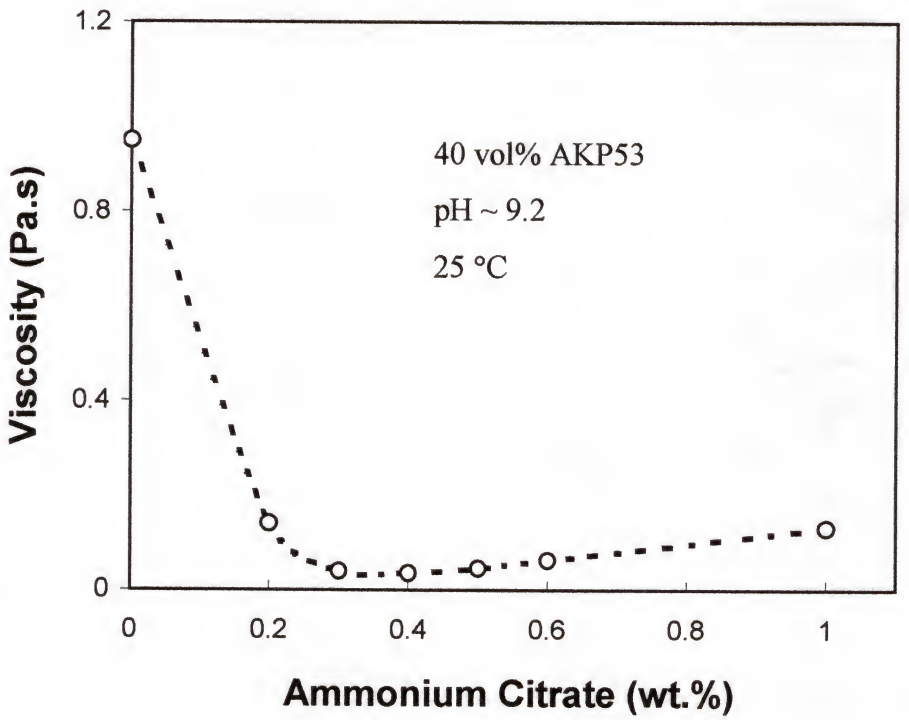

Fig.3-2. TAC amount dependence of the suspension viscosity at shear rate of 100 s^{-1}.

3.2 Determination of the Minimum Amount of PAA

3.2.1 Gelation Experiments

PAA is not used as dispersant in TIF suspension, but as a gelation agent to form bridging flocculation when the suspension temperature is raised. Although the effect of

the PAA amount on the viscosity and relative viscosity (at shear rate 20 s^{-1}) of the 50vol% AKP53 TIF suspensions has been reported by Bell et al. [88], the data reported can not be adopted for the experiments directly because of the difference in jar materials used. In this section, qualitative gelation experiments are used to determine the minimum amount of PAA that is necessary to gel the suspension.

Gelation experiments are performed by injecting the TIF suspensions into borosilicate glass tubes (Fisher Scientific) to a height of 30 mm. The suspension surface at the open end is covered with a thin layer of vegetable oil to prevent water evaporation. Additionally, tubes are sealed with stoppers as tight as possible. Then the tube is put into an oven at 70°C for 4 hours. Finally, the suspension cylinder is taken out carefully and the gelation condition is checked qualitatively by measuring the height of the freestanding suspension cylinder. These experiments are quite different from sedimentation experiments in that when the TIF suspension is gelled, all the solvent is trapped in the gelled body. Here, we define that the suspension is well gelled if the freestanding wet suspension cylinder height is more than 15 mm after 10 min of demolding (define the gelation degree as 50%). Complete gelation yielded cylinders of 30-mm height without any collapse (defined the gelation degree as 100%). Some gelation results are shown in Figure 3-3 and Figure 3-4 to illustrate the definition of gelation degree. The amount of PAA is base on the weight of dry alumina powder.

3.2.2 Gelation Diagrams for PAA 50,000 and PAA 10,000 Addition Suspensions

The gelation diagrams for alumina suspensions with PAA of Mw ~ 50,000 and 10,000 are shown in Figure 3-5 and Figure 3-6, respectively. These diagrams relate the

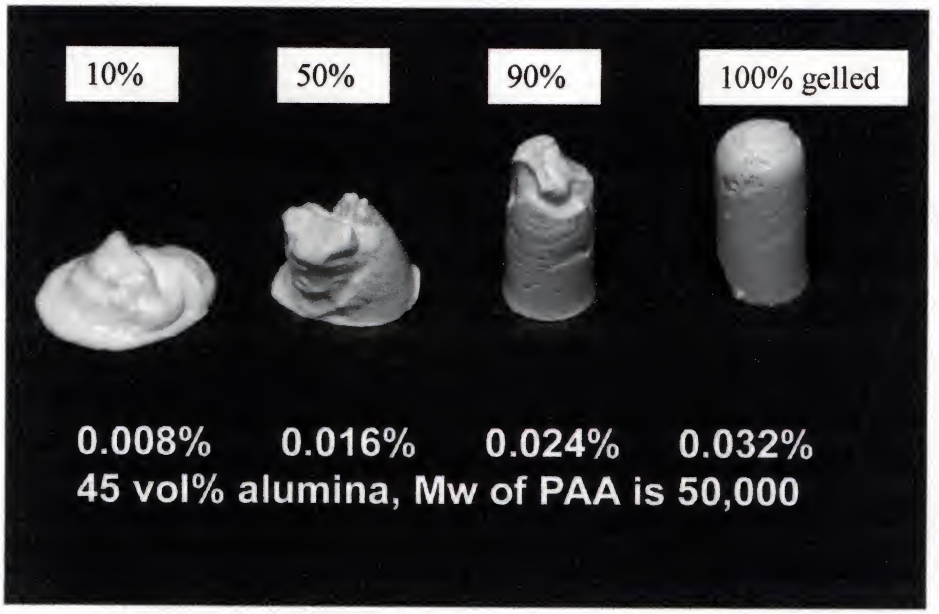

Fig.3-3. Gelation results of the 45vol% AKP53 suspensions while varying the amount of PAA 50,000. All suspensions are put in oven of 70 °C for 4h before they are removed from their container. The gelation degree is also shown.

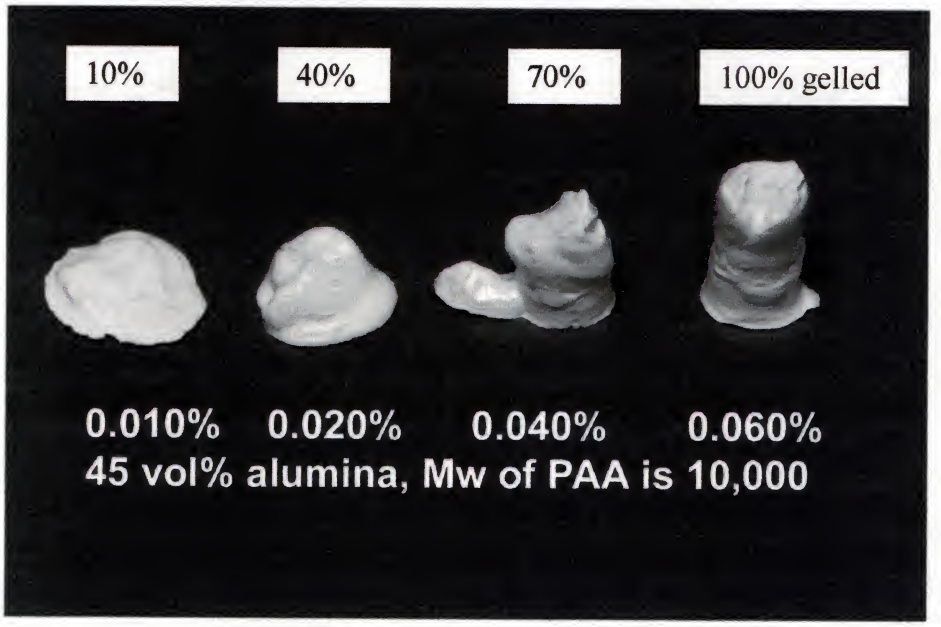

Fig.3-4. Gelation results of the 45vol% AKP53 suspensions while varying the amount of PAA 10,000. All suspensions are put in oven of 70 °C for 4h before they are removed from their container. The gelation degree is also shown.

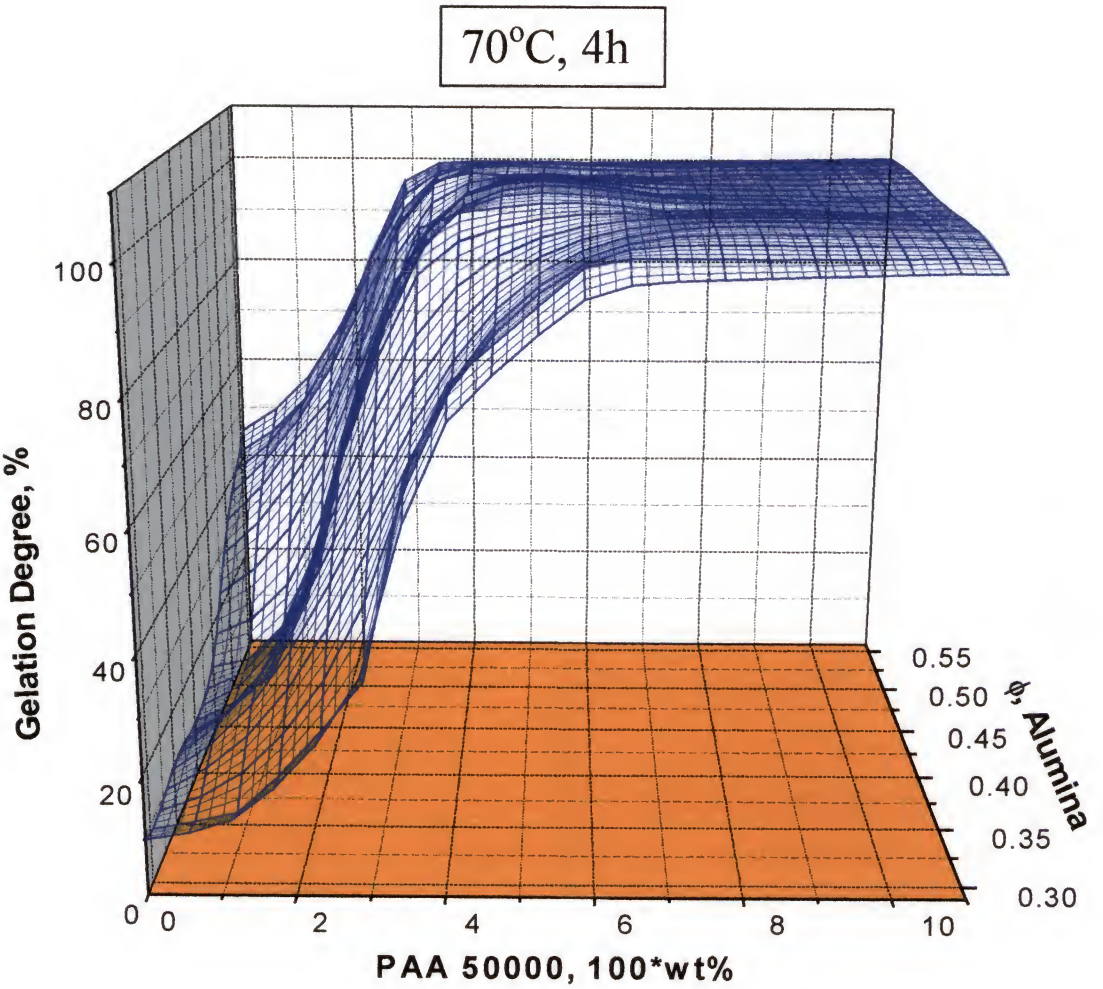

Fig.3-5. 3D gelation diagram that relates the gelation degree to the volume fraction of AKP53 alumina and the amount of PAA 50,000. The plot shows that when the volume fraction is > 0.3, the suspension can be gelled if the amount of PAA is > 0.035wt% of alumina powder when the suspensions are put in oven of 70 °C for 4h.

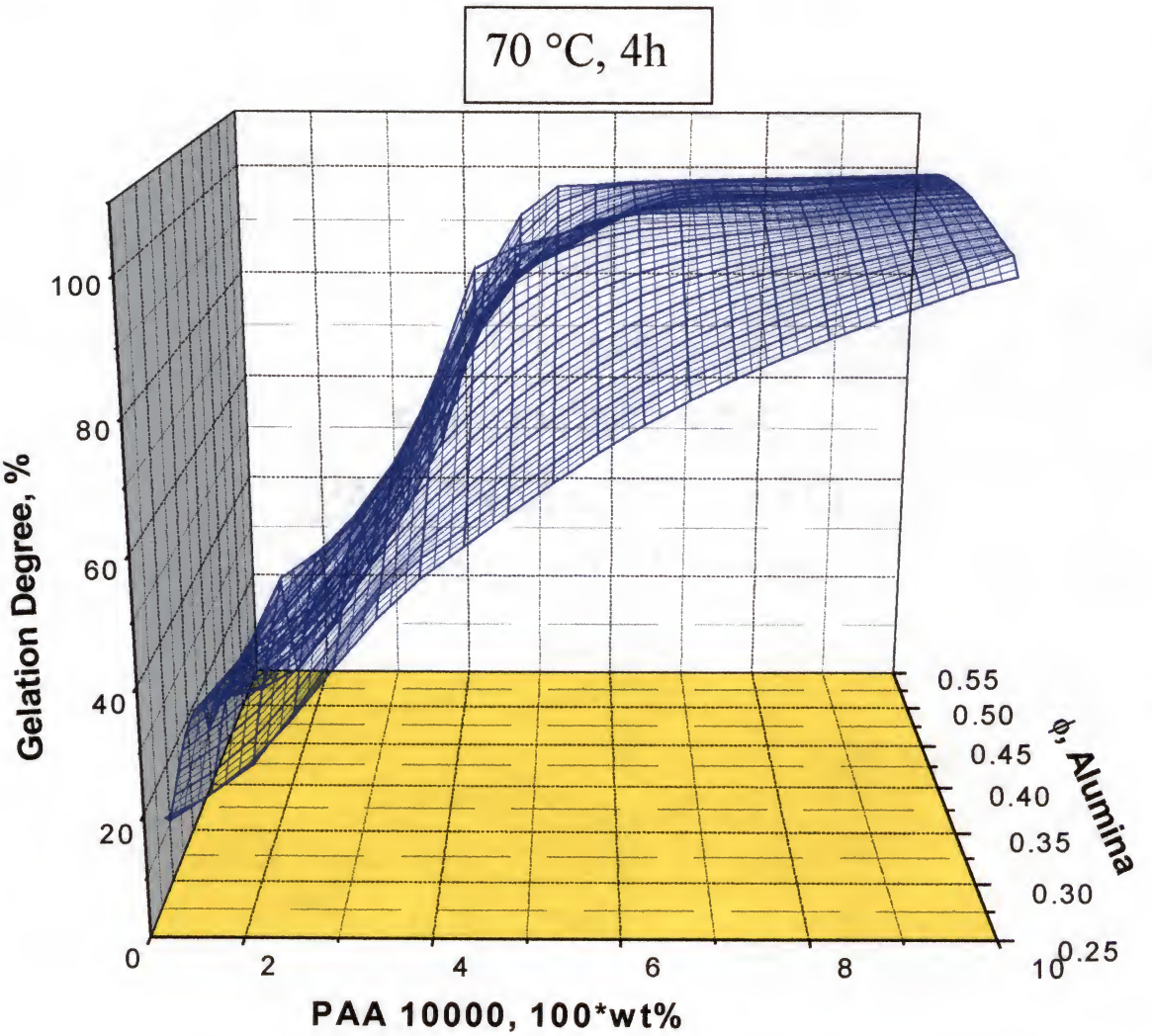

Fig.3-6. 3D gelation diagram that relates the gelation degree to the volume fraction of AKP53 alumina and the amount of PAA 10,000. The plot shows that when the volume fraction is > 0.3, the suspension can be gelled if the amount of PAA is > 0.035wt% of alumina powder when the suspensions are put in oven of 70 °C for 4h.

gelation condition of the suspensions with volume fraction of particles and PAA amount under a fixed experimental condition. The minimum amount of PAA (~ 0.035wt%) required to gel the suspension at 70°C for 4 hours seems independent of the volume fraction of particles for the present experimental volume fraction of particles (from 30 to 50vol%). This observation does not indicate that the polymer concentrations that are required to gel the suspensions are independent of the volume fraction of particles under all experimental conditions. But it can be concluded that ~ 0.035wt% PAA is enough to gel the suspension that is used for direct casting. Therefore, a PAA amount of 0.04wt% (based on the weight of dry alumina particles in respective suspension) is chosen for the following experiments.

3.3 Effect of Composition on Room-Temperature Viscosity

3.3.1 Effect of the Volume Fraction of Alumina Particles

The room temperature shear flow property is important for the direct casting process in that it governs the filling capability of the suspension in the mold. Low viscosity at low shear rate is preferred to reduce the defects (i.e. pores) in the green body. Figure 3-7 shows the variation of the steady shear viscosity with shear rate at 25 °C for different volume fraction suspensions with 0.4wt% TAC and 0.04wt% PAA of molecular weight 50,000. All suspensions show shear-thinning behavior in the experimental shear range, where the viscous force affects the suspension structure more than that of thermal motion. The shear thinning is also thought to be the result of the perturbation of the suspension structure by shear [60]. It can also be seen that higher suspension loading

results in higher viscosity, which might be due to the stronger interaction between the electric double layer (EDL) when the EDL overlaps more.

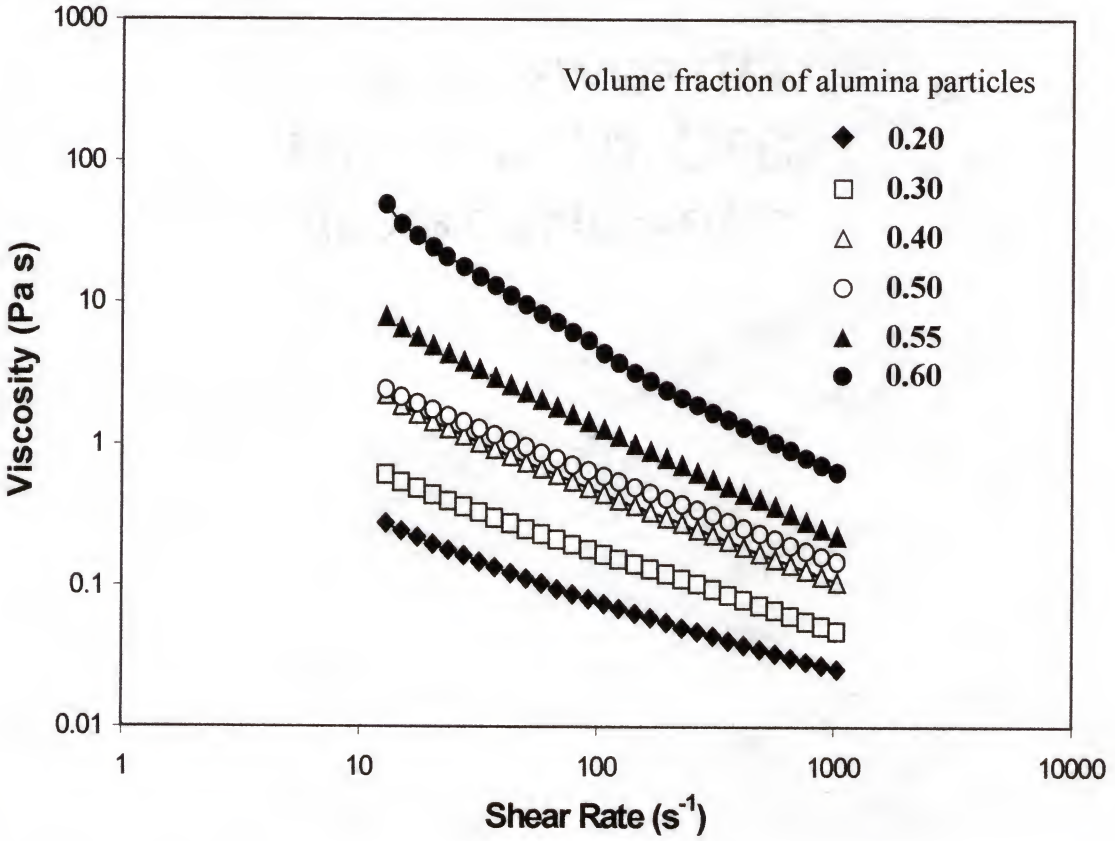

Fig.3-7. The shear rate dependence of viscosity at 25 °C for different volume fraction alumina suspensions. The amount of TAC and PAA (Mw=50,000) are 0.4 and 0.04wt%, respectively.

3.3.2 Volume Fraction Dependence of the Relative Viscosity

The variation of relative viscosity of the suspensions with volume fraction of solids is given in Figure 3-8. The viscosity data are taken at the shear rate of 1030 s^{-1}. The relative viscosity is defined as the ratio of the measured suspension viscosity to that

of water at 25 °C. At very high shear rate, the electrostatic stabilized system could be thought to behave similarly to hard sphere system, and hydrodynamic interaction is the main contribution to the flow of the suspensions. The Dougherty-Krieger equation is

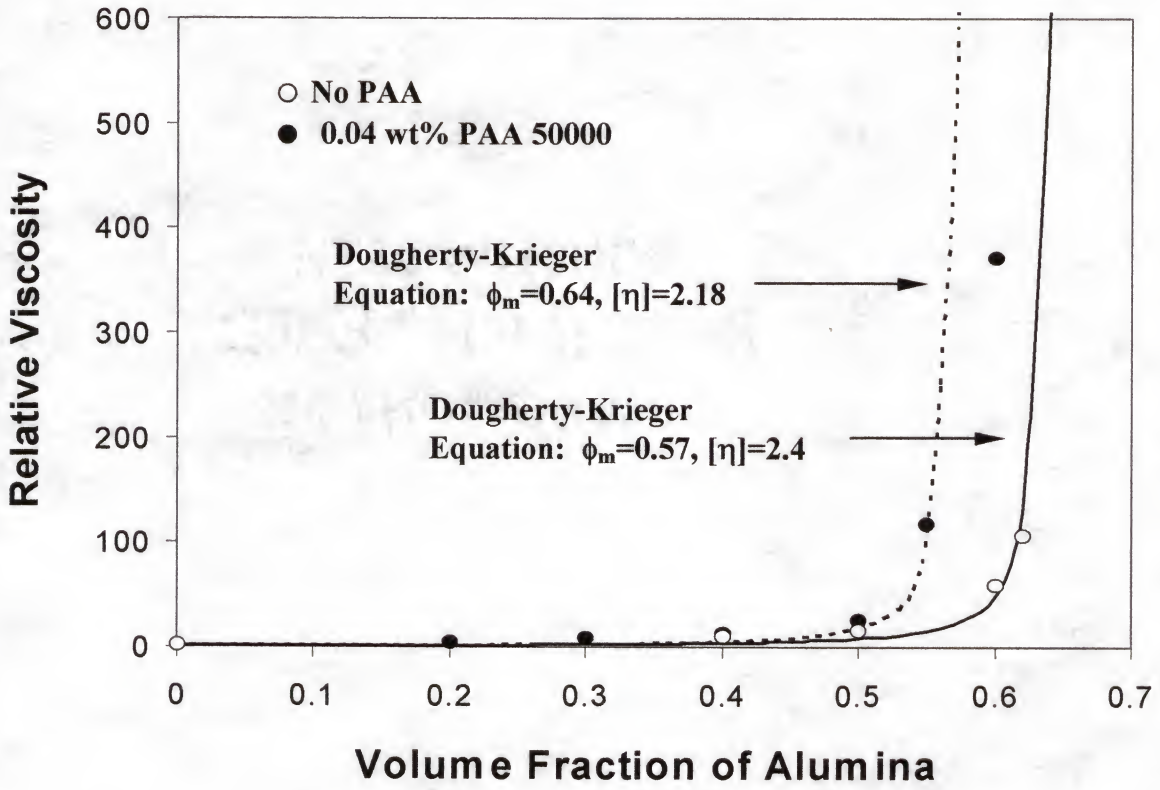

Fig.3-8. The slurry loading dependence of the relative viscosity for the AKP53 alumina suspensions at shear rate of 1030 s^{-1}. All slurries have 0.4wt% TAC and 0.04wt% PAA 50,000. The relative viscosity data of the PAA-free suspensions can fit the Dougherty-Krieger equation more closely than that of the PAA addition suspensions.

commonly used to relate the relative viscosity with suspension loading for hard sphere systems:

$$\eta_r = [1 - (\phi / \phi_m)]^{-[\eta]\phi_m} \qquad (3\text{-}1)$$

where ϕ is the suspension loading, ϕ_m is the maximum packing fraction, which is of the order of 0.64 for random packing, $[\eta]$ is the asymptotic slope of the curve as ϕ goes to zero, and normally it is taken as 2.5. But in most cases, both ϕ_m and $[\eta]$ are chosen as variables at the same time to fit the experimental data and analyze the suspension structures [1,53-56,60,93,94].

Using the above Dougherty-Krieger equation to fit the viscosity data of the suspensions in the absence of PAA gives $\phi_m = 0.64$ and $[\eta] = 2.18$. The calculated results (solid line in Figure 3-8) fit the experimental data (open circles) well for volume fraction up to 0.62. For the PAA addition suspensions (filled circles in Figure 3-8), the Dougherty-Krieger equation with $\phi_m = 0.57$ and $[\eta] = 2.4$ (dashed line in Figure 3-8) could only fit the experimental data well at volume fraction less than 0.55. This deviation might be due to the "wall-slip" effect using the concentric cylinder measuring system when the suspension viscosity is very high. The measurement data indicates that PAA addition increased the viscosity at the respective volume fraction of particles, and this increment became larger at higher volume fraction of particles. When the volume fraction is more than 0.55, the interparticle distance would be very small and the depletion flocculation might occur. The depletion flocculation might also cause the formation of agglomerates in the suspension, which makes contribution to the larger increment of the shear viscosity. When the volume fraction is further increased, the interparticle distance might fall into the primary minimum of the interaction potential, then the possibility of forming weak-attractive particle agglomerates increases, which could also contribute to the increase of the shear viscosity.

3.3.3 Effect of the Molecular Weight of PAA

Figure 3-9 and Figure 3-10 give the shear flow curves for PAA 10,000 and PAA 5,000 addition suspensions, respectively. It is found that shear thinning only happens for high volume fraction suspensions at low shear rate, and shear thickening will take place at higher shear rate. The shear thickening might be due to the deformation of the ordered structure of the suspension formed at a lower shear rate, and this will cause rearrangement of its microstructure such that the resis tance to flow increases with shear rate. In almost all known cases of shear thickening, there is a region of shear thinning at lower shear rate [67].

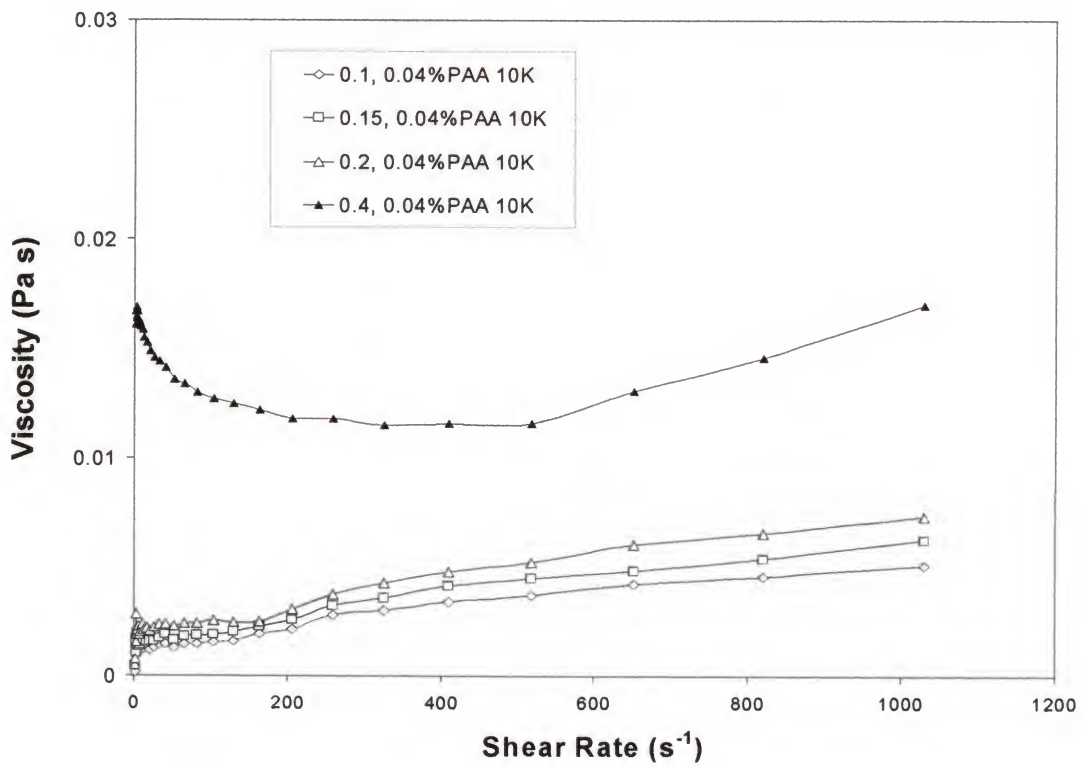

Fig.3-9. The shear rate dependence of viscosity at 25 °C for different volume fraction alumina suspensions. The amount of TAC and PAA (Mw=10,000) are 0.4wt% and 0.04wt%, respectively.

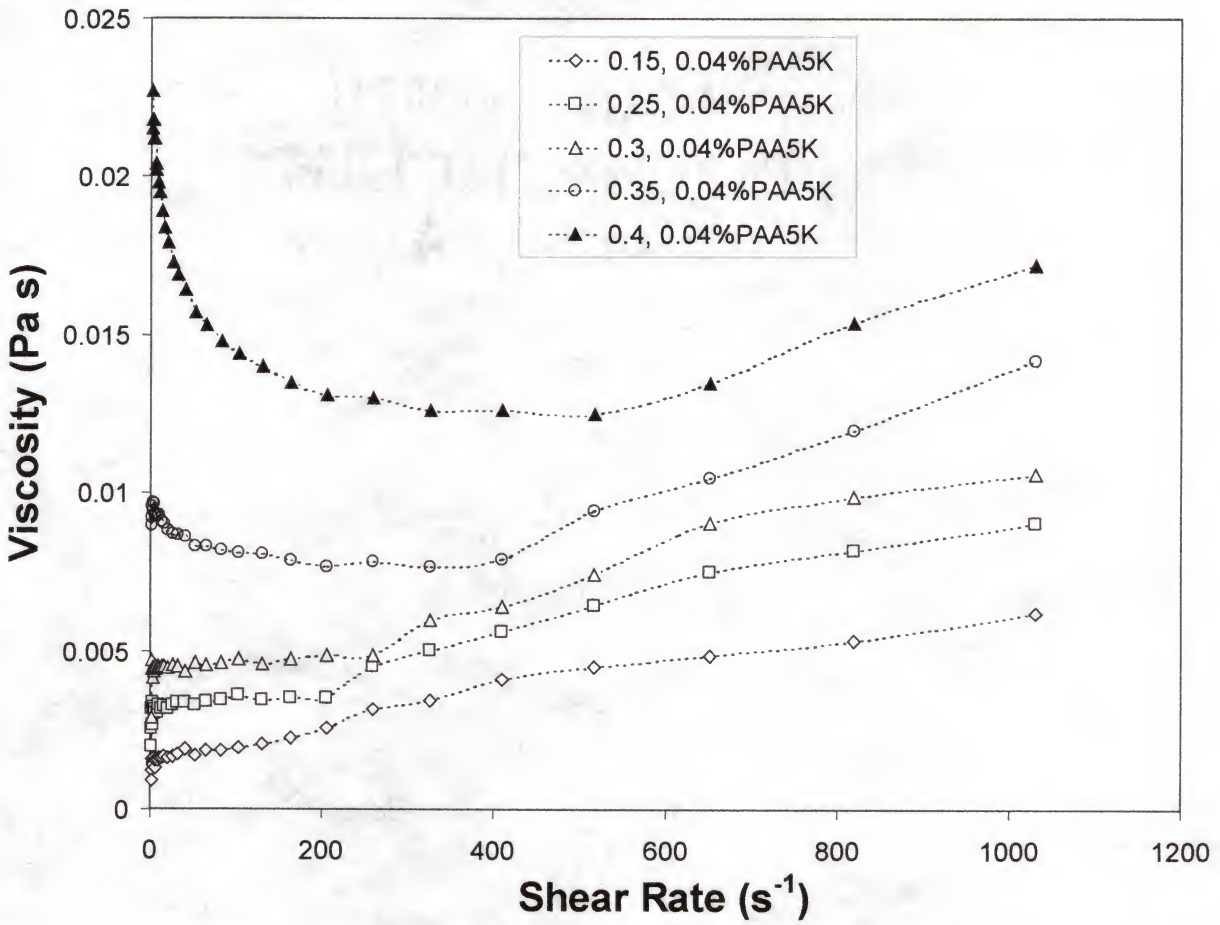

Fig.3-10. The shear rate dependence of viscosity at 25 °C for different volume fraction alumina suspensions. The amount of TAC and PAA (Mw=5,000) are 0.4wt% and 0.04wt%, respectively.

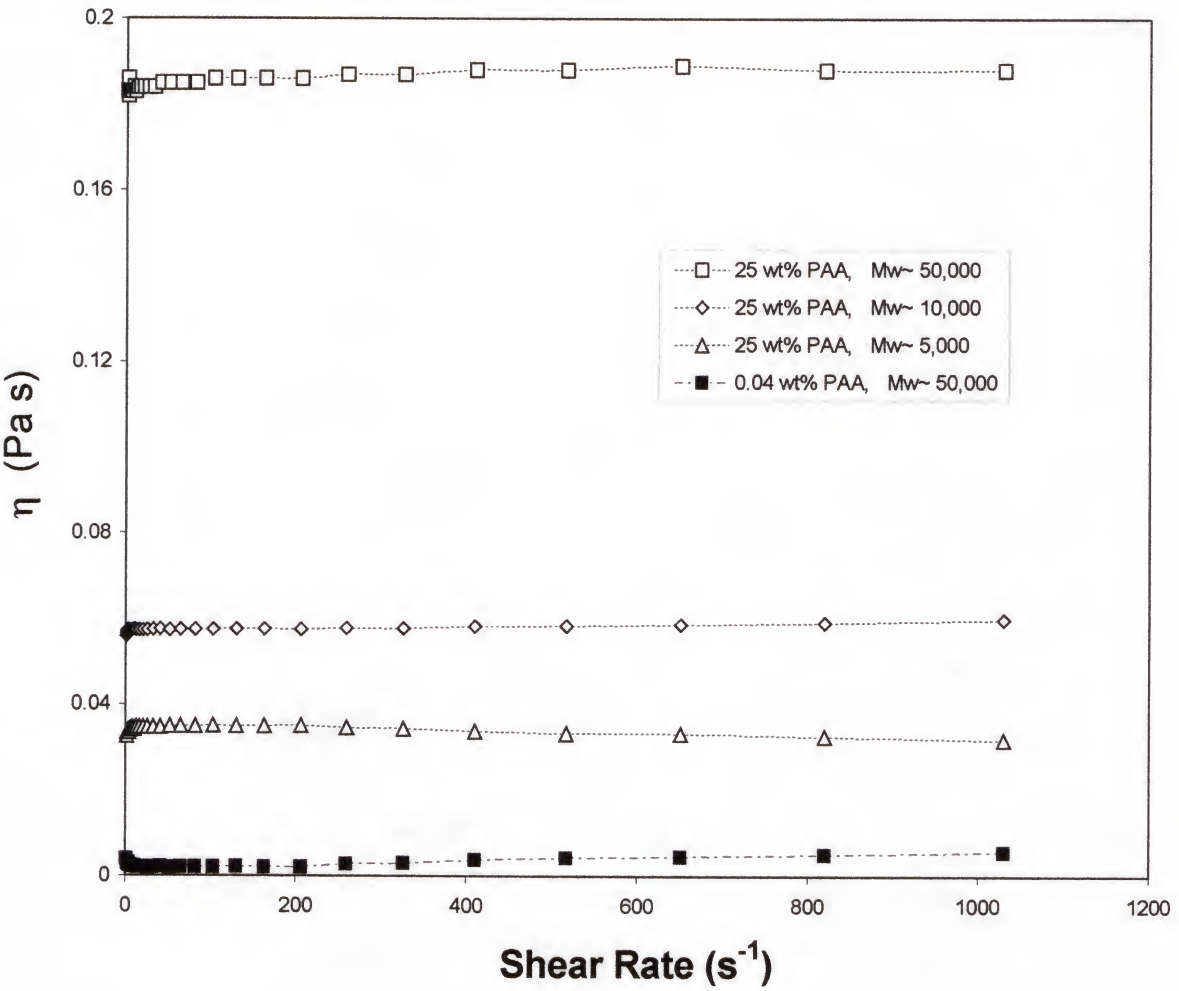

Fig.3-11. The shear rate dependence of viscosity at 25 °C for the pure PAA aqueous solutions. 25wt% PAA solutions show Newtonian shear behavior. It can be seen that higher molecular weight of PAA yields a higher viscosity at the experimental shear rate range. 0.04wt% PAA 50,000 solution shows shear thickening at higher shear rate.

For the same volume fraction suspension with same weight percent of PAA, higher molecular weight of PAA yields a higher shear viscosity. This variation is especially large for high volume fraction suspensions, where the amount of PAA is also high compared with the low volume fraction suspensions. It is assumed that the resistance of the PAA molecular chains to the movement of water molecules increases with the increasing of both molecular weight and amount of PAA in the suspensions. The intrinsic shear flow characters of 25wt% of PAA aqueous solutions with different molecular weight is shown in Figure 3-11. It is evident that higher molecular weight of PAA yields a higher viscosity at the experimental shear rate range.

3.4 Temperature Dependence of the Suspension Viscosity

Figure 3-12 gives the temperature dependence of the relative viscosity (ratio of the measured viscosity to that of water at the same temperature) for suspensions with 0.04wt% PAA 50,000 addition. The relative viscosity of all suspensions starts to increase monotonously with temperature when the temperature is above 35 °C. The variation of relative viscosity becomes larger with increasing suspension loading. The addition of PAA in a concentrated suspension not only increases the viscosity of zero shear rate, but also bridges the particles and flocculated the suspension [61,87,88], which can be reflected from the larger variation of relative viscosity. For suspensions in absence of PAA, the relative viscosity has changed little in the experimental temperature range for the suspension loading of 40 or 50vol%, as shown in Figure 3-13. These results suggest that PAA play an important role in the temperature induced forming suspensions.

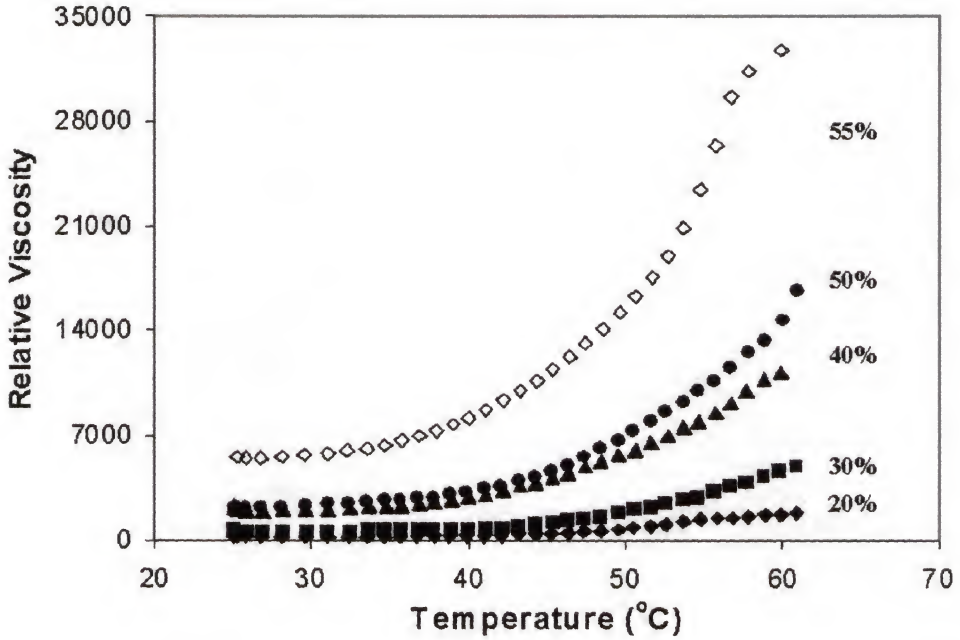

Fig.3-12. Temperature dependence of the relative viscosity of TIF alumina slurries with variation in solids loading while keeping TAC and PAA 50,000 constant at 0.4 and 0.04wt%, respectively.

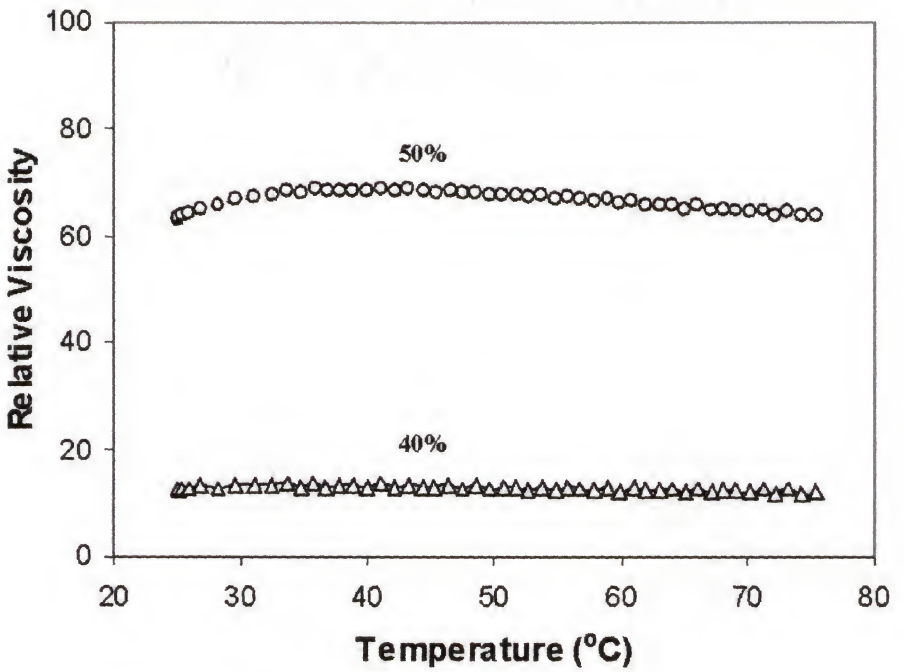

Fig.3-13. Temperature dependence of the relative viscosity of 40 and 50vol% alumina slurries without PAA addition. The TAC amount is 0.4wt% for both slurries.

The temperature dependence of the suspension viscosity is due to the evolution of the suspension microstructure with increasing temperature. Both bridging flocculation and depletion flocculation could make contributions to the flocculation of the suspension when the temperature is raised, especially for the high volume fraction suspensions. It is proposed that the dissociation of citrate anions from the alumina particle surface with increasing temperature would leaving adsorption sites available, and this followed by the exchange of the lower molecular weight dispersant for a higher molecular weight polymer [88]. Since the adsorption/desorption process for TAC on alumina is dynamic,

and an increase in temperature would likely cause an increase in the kinetics of desorption, leading to a more liable TAC bound fraction. Since TAC may effectively block PAA from adsorption (both species interact with alumina through COOH groups), and because TAC adsorbs first during slurry preparation, TAC must desorb before PAA could adsorb. Being a long chain molecule, it is likely that PAA adsorbs at multiple points on the alumina surface, giving it a stability advantage over TAC. TAC desorption is facilitated by increasing the temperature. In this scenario, bridging is the most likely mechanism for temperature induced coagulation. The resultant aggregates will grow with increasing temperature and finally form a space-filling network.

The data in Figure 3-13 also shows that the increase in the kinetic energy of the particles, which could cause them to overcome the electrostatic repulsive barrier more easily and to aggregate, would not appear to be a factor in the present case. This indicates that sufficient electrostatic repulsion, and or steric hindrance, is present to prevent primary aggregation.

For the 0.04wt% PAA 10,000 and PAA 5,000 addition suspensions, the variations of the relative viscosity with temperature are shown in Figure 3-14 and Figure 3-15, respectively. It seems that there is a minimum volume fraction of particles, 0.3, for the PAA 5,000 addition suspensions, and only above this value can the suspensions start to show an increase in the relative viscosity with temperature. In the percolation model, this value is called the gelation threshold. For example, 0.04wt% PAA 10,000 and PAA 50,000 addition suspensions have a volume gelation thresholds ~ 0.15 and 0.25, respectively. Increasing PAA molecular weight also decreases the temperature where the suspensions begin to show an increase in relative viscosity, which might be due to the

larger chain length and surface adsorption energy on alumina [95]. Therefore, larger molecular weight PAA would be more efficient to cause gelation than lower molecular weight PAA. One problem that should be addressed is that higher molecular weight of PAA will increase the room temperature viscosity, especially for the highly loaded suspensions. This necessitates a compromise between the volume fraction of particles and the selection of the molecular weight of PAA.

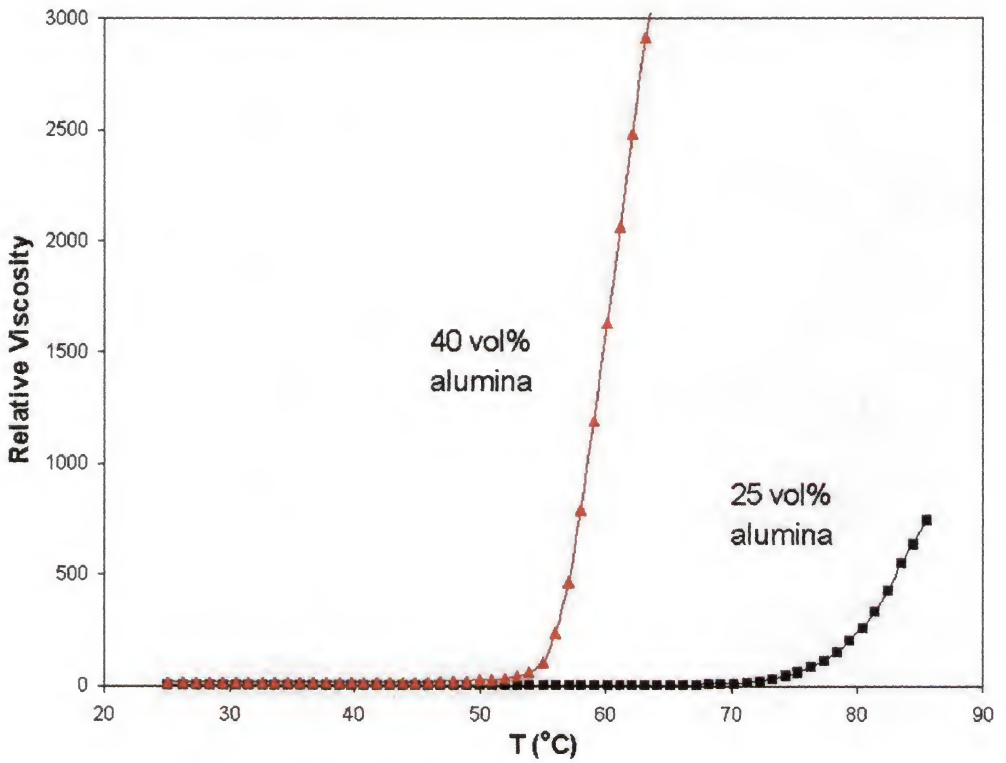

Fig.3-14. Temperature dependence of the relative viscosity of TIF alumina slurries with variation in solids loading while keeping TAC and PAA 10,000 constant at 0.4 and 0.04wt%, respectively.

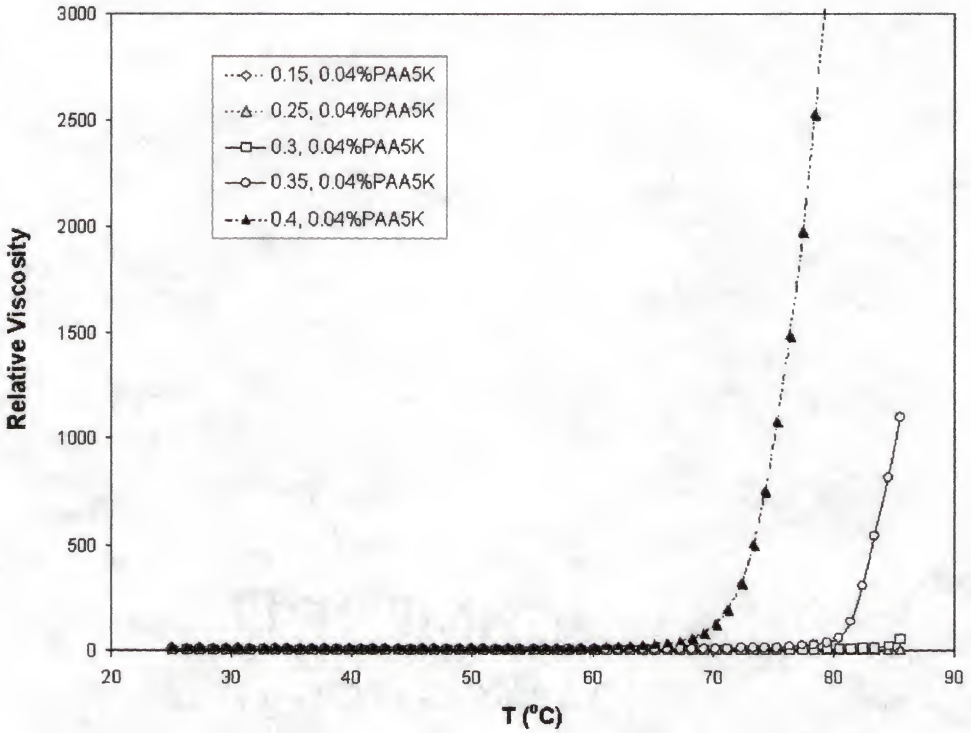

Fig.3-15. Temperature dependence of the relative viscosity of TIF alumina slurries with variation in solids loading while keeping TAC and PAA 5,000 constant at 0.4 and 0.04wt%, respectively.

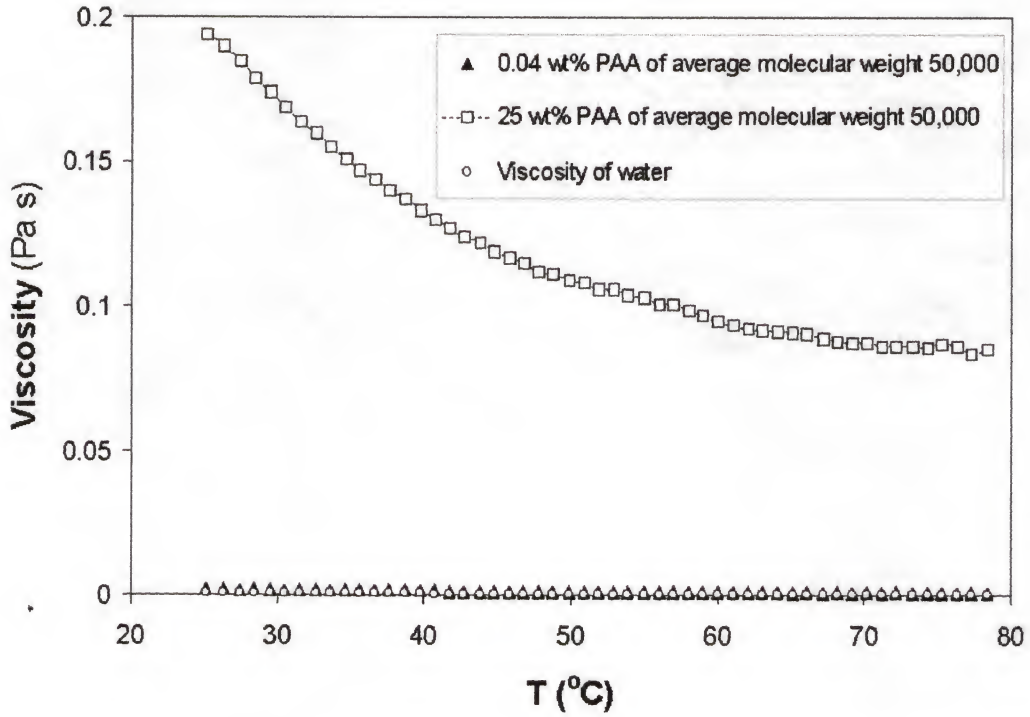

Fig.3-16. Variation of the shear viscosity at shear rate 20 s^{-1} with temperature for the 0.04wt% PAA, 25wt% PAA (molecular weight ~ 50,000) aqueous solutions and water. The temperature ramp is 1 °C/min.

In order to exclude the effect of the viscosity of PAA itself on the total slurry viscosity, variation of the viscosity of the pure PAA aqueous solutions with temperature are measured and shown in Figure 3-16. It is clear that the viscosity of the PAA solutions decreases with increasing temperature. Therefore, the increase of the TIF alumina slurry viscosity can not be attributed to the variation of the PAA intrinsic viscosity with temperature.

3.5 Summary of This Chapter

TIF alumina suspensions are successfully fabricated by adding 0.4wt% of ammonium citrate powder and <0.1wt% poly (acrylic acid) into the suspensions.

The optimum amount of ammonium citrate powder is determined experimentally to be ~ 0.4wt% of the dry alumina particles.

The gelation diagrams that related the volume fraction of particles and PAA amount to the gelation degree are experimentally determined and plotted. The results show that ~ 0.04wt% of either PAA50,000 or PAA 10,000 is enough to flocculate and gel the TIF alumina suspensions when the volume fraction of particles is no less than 0.3.

Incremental increases in the volume fraction of alumina increases the shear viscosity, which is described by the Dougherty-Krieger equation. For the PAA 50,000 addition suspensions, the D-K equation used to fit the measured data is $\eta_r = [1 - (\phi / \phi_m)]^{-[\eta]\phi_m} = [1 - (\phi / 0.57)]^{-2.4\times 0.57}$, while for the PAA-free suspensions, the D-K equation is $\eta_r = [1 - (\phi / \phi_m)]^{-[\eta]\phi_m} = [1 - (\phi / 0.64)]^{-2.18\times 0.64}$.

Molecular weight of PAA has a significant effect on the 25 °C shear viscosity of the alumina suspensions. Larger molecular weight PAA increases the shear viscosity, especially for the highly loaded suspensions. Higher volume fraction of particles increases the viscosity more strongly.

Higher molecular weight of PAA decreases the critical temperature where the suspension relative viscosity starts to increase rapidly.

CHAPTER 4
ELASTIC PROPERTIES OF THE TIF AQUEOUS ALUMINA SUSPENSIONS WITH PAA ADDITION

4.1 Temperature Dependence of the Shear Modulus of the Suspensions

4.1.1 Determination of the Strain Amplitude for Oscillation

Figure 4-1 illustrates the results of a typical strain sweep experiment, showing that the behavior of the suspension changes from an elastic response (storage modulus, G' remains constant) to a flow response (G' decreases) with increasing strain amplitude. It can be seen that 1% strain is in the linear viscoelastic region at a frequency of 1Hz. Therefore, 1% strain is chosen as the strain amplitude in the following measurements.

4.1.2 Effect of the Volume Fraction of Particles

Figure 4-2 shows the variation of the shear modulus with temperature for the TIF alumina suspensions with 0.04wt% PAA (Mw~50,000) addition. The shear modulus (both the storage modulus G' and the loss modulus G'') of all suspensions does not have visible change at lower temperature, and then it starts to increase when the temperature is raised to a certain value for specific volume fraction suspensions. It can also be observed that there is a "crossover" between the storage and loss modulus for all suspensions except the 0.5 volume fraction one, which shows that G'>G'' in the whole temperature range (Figure 4-2). Transition from "fluid-like" to "solid-like" behavior takes place when the temperature is above this "crossover" temperature. The results in Figure 4-2 also

show that the magnitude of G' and G'' varies with volume fraction of particles, and a higher volume fraction yields a higher G' and G'' at each respective temperature.

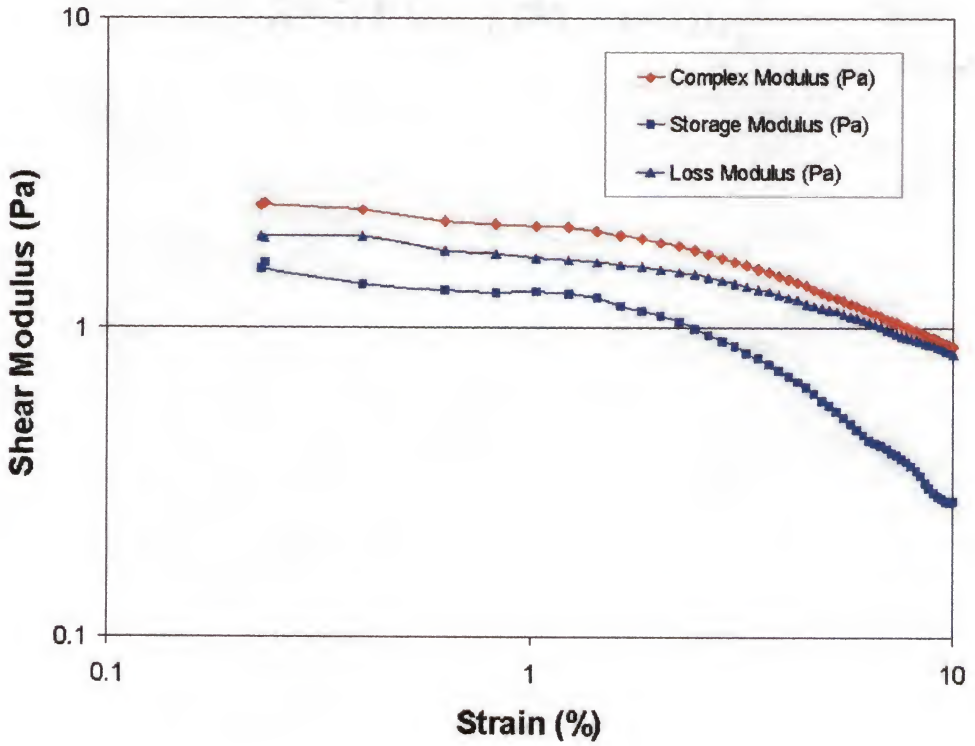

Fig.4-1. Variation of shear modulus with shear strain for the 40vol% AKP53 alumina suspension with 0.4wt% TAC and 0.04wt% PAA 50,000. The frequency is 1Hz.

Similar to the effect of the volume fraction of particles on the suspension viscosity, the shear modulus is also related to the formation of aggregates and its growth with increasing temperature. When the size of the aggregates is not large enough to form a space-filling network, aggregates can only increase the shear viscosity of the suspension. It is only when the aggregates connect to form a space-filling network that the suspension can start to manifest evident changes in the storage modulus, which is in

the "crossover" point in Figure 4-3. Below the "crossover" temperature, the suspension behaves "fluid-like" and G''>G'. When the temperature is raised higher than this temperature, G'>G'', the suspension shows "solid-like" character.

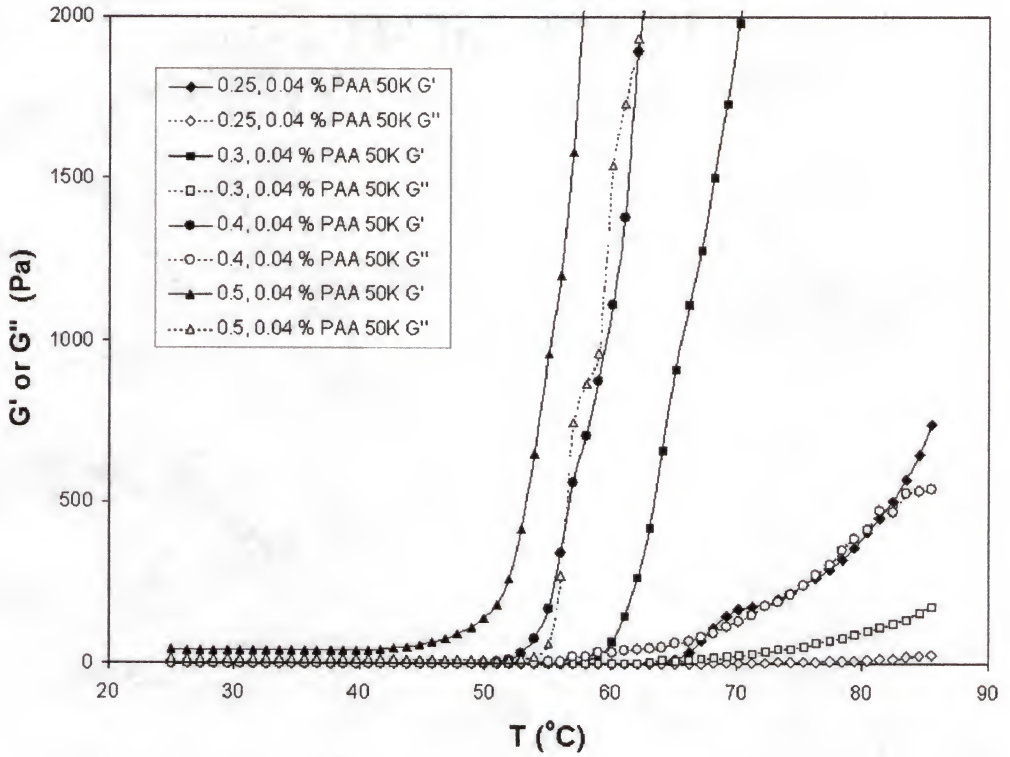

Fig.4-2. Variation of the shear modulus with temperature and volume fraction of alumina for the TIF suspensions with 0.04wt% PAA (Mw~50,000) addition. The measurements are conducted under 1% strain and 1Hz. The temperature ramp is 1°C/min.

In lower volume fraction suspensions, the bridging floc grows slower than that in higher volume fraction suspensions since the number of particles available is fewer. Therefore, higher volume fraction suspensions can form percolation network easier

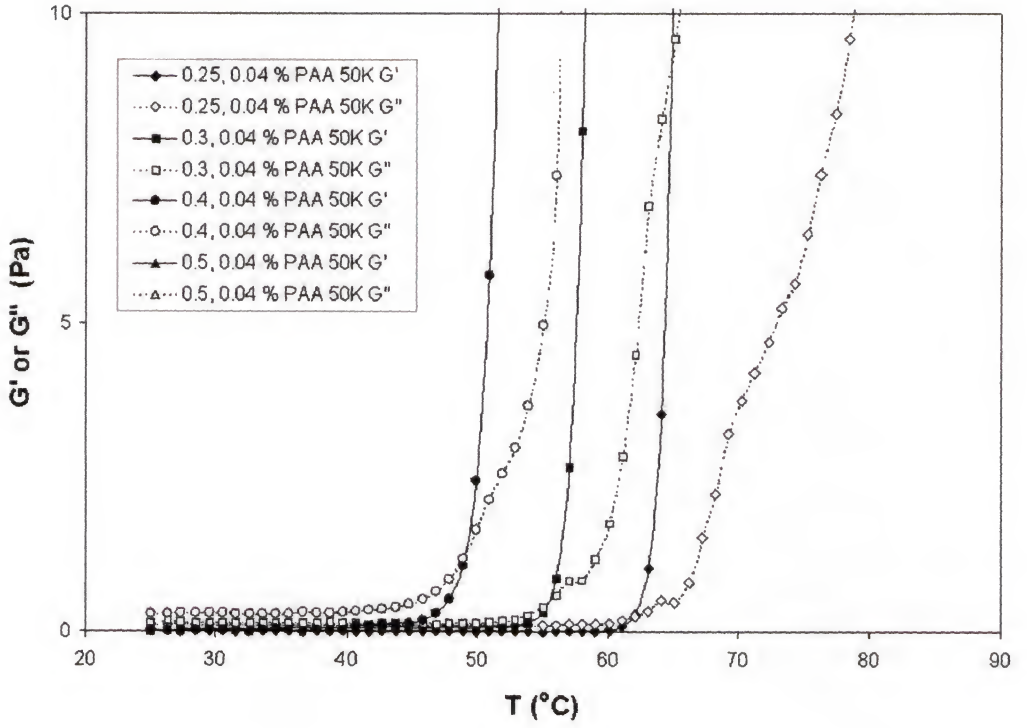

Fig.4-3. The same plots as in Fig.4-2 to show the "cross-over".

than that of the lower volume fraction suspensions, which correspondings to the lower "crossover" temperature shown in Figure 4-3. But when the volume fraction of alumina is higher than 0.5, the EDL overlaps. When the interparticle distance is close to the distance of the primary minimum, van der Waals attraction will take effect and a weak attractive network yields. The weak agglomerate formation is thought to contribute to the G'>G'' at 25 °C for the 0.5 volume fraction suspension.

The transition from "fluid-like" to "solid-like" behavior can also be seen from the variation of the damping factor (tan δ = G''/G') with temperature, as is shown in Figure 4-4. Before the transition temperature (the temperature of crossover), the damping factor

value is large, which indicates that G''>>G'. Above the transition temperature, the damping factor value drops to nearly zero, indicating that G'>>G'' and the gelation of the suspensions.

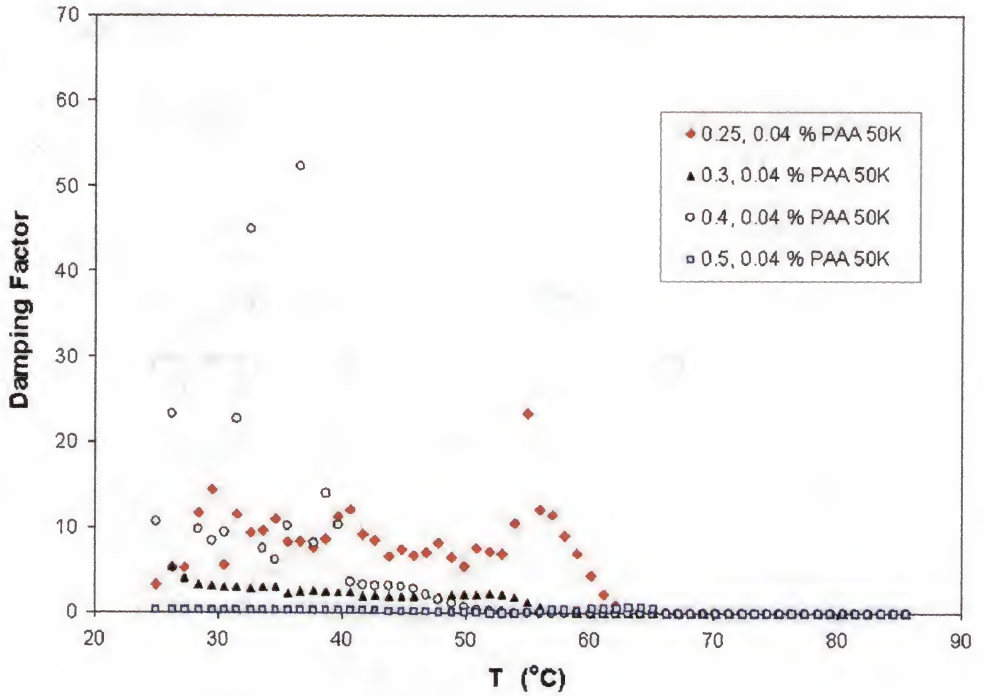

Fig.4-4. Variation of the damping factor (tan δ = G''/G') with temperature and volume fraction of alumina for the same suspensions as shown in Fig.4-2 and Fig.4-3. All suspensions have 0.4wt% TAC and 0.04wt% PAA (Mw~50,000). The measurements are conducted under 1% strain and 1Hz. The temperature ramp is 1°C/min.

4.1.3 Effect of the Amount of PAA

The effect of the amount of PAA (Mw~50,000) on the variation of shear modulus with temperature is shown in Figure 4-5, and "crossover" is also noticed in Figure 4-6. This "crossover" temperature decreases with increasing amount of PAA, indicating that

the space-filling network can be formed at a lower temperature when the PAA amount is increased, because increasing PAA amount will increase the number of aggregates formed by bridging flocs. Therefore, larger amount of PAA will enhance the formation of the space-filling network and yield a lower "crossover" temperature. Figure 4-7 gives the variation of damping factor with temperature for the same suspensions in Figure 4-5 and Figure 4-6, and the transition temperature can be easily determined from it.

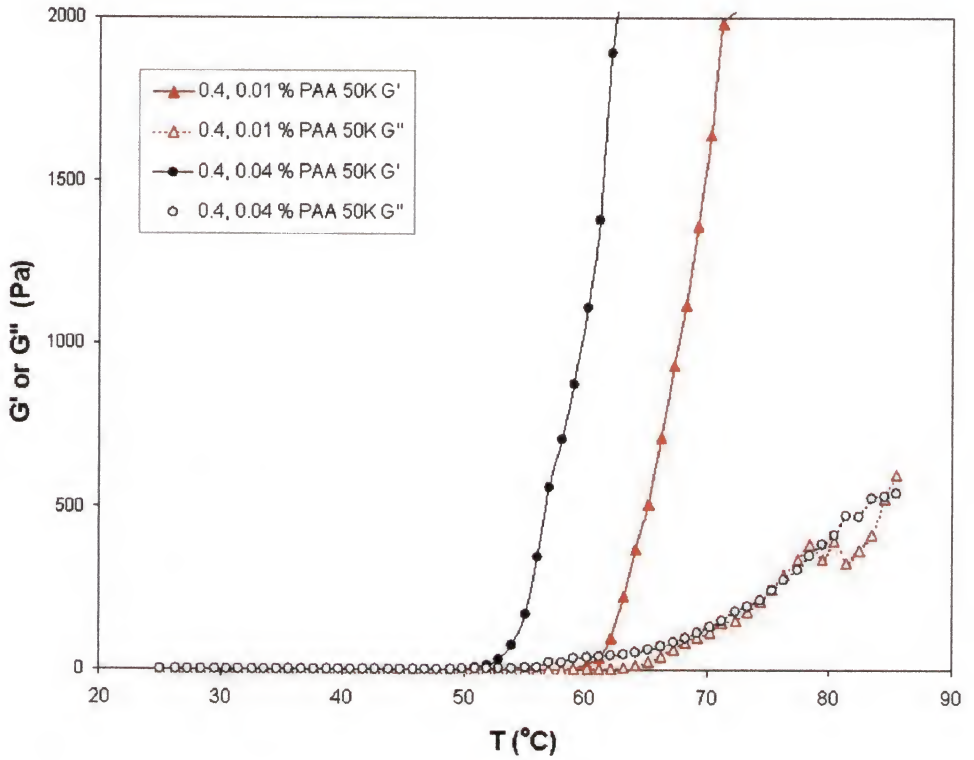

Fig.4-5. The effect of the amount of PAA (Mw~50,000) on the variation of shear modulus with temperature. The volume fraction of alumina is 0.4. The measurements are conducted under 1% strain and 1Hz. The temperature ramp is 1°C/min.

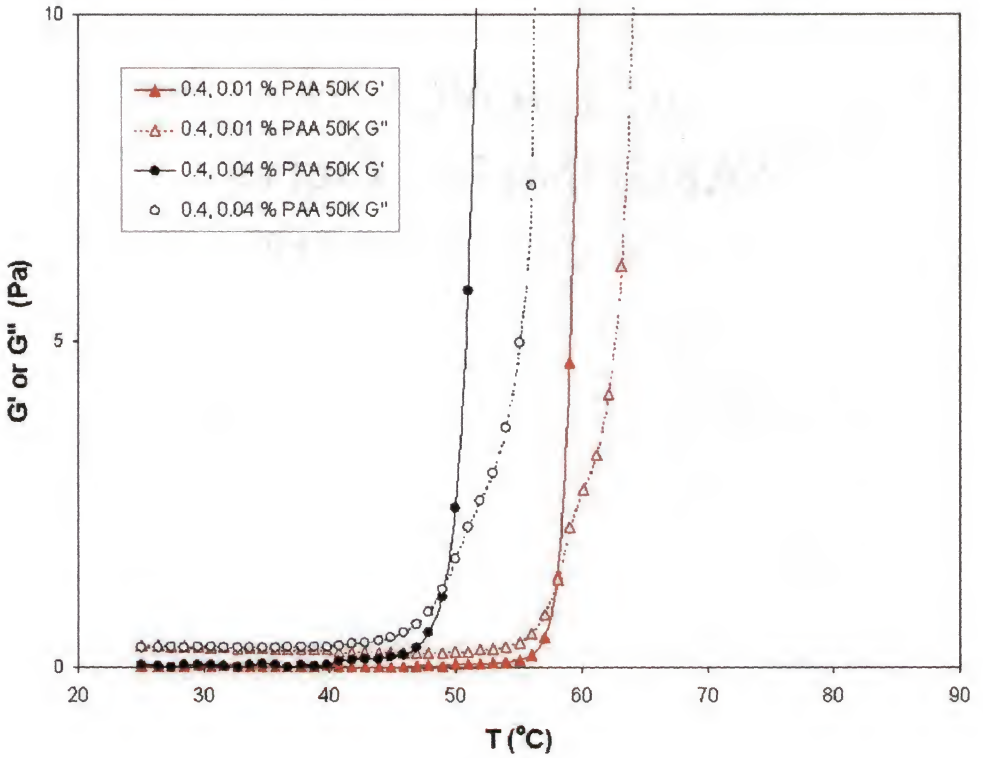

Fig.4-6. The same plots as in Fig.4-4 to show the "cross-over".

4.1.4 Effect of the Molecular Weight of PAA

Figure 4-8 and Figure 4-9 illustrates the influence of the PAA molecular weight on the variation of shear modulus with temperature for the 0.4 volume fraction suspensions. It is observed that increasing molecular weight of PAA will slightly increase the starting shear modulus value and decrease the "crossover" temperature. The corresponding damping factors varying with temperatures are shown in Figure 4-10.

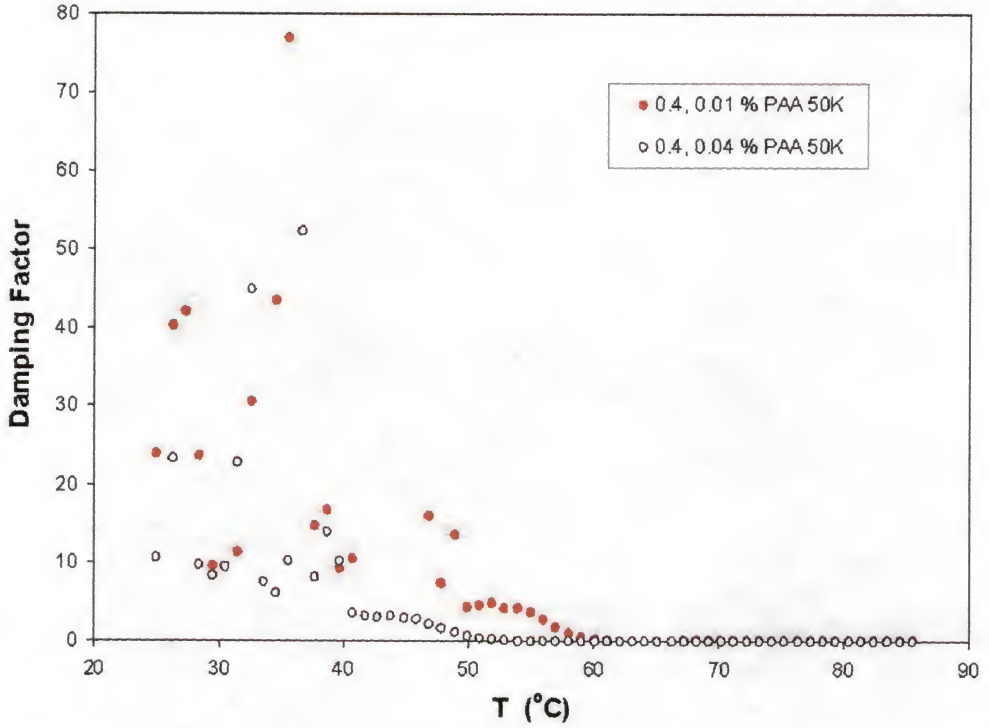

Fig.4-7. Variation of the damping factor (tan δ = G''/G') with temperature and the amount of PAA for the same suspensions as shown in Fig.4-5 and Fig.4-6. The volume fraction of alumina is 0.4. The measurements are conducted under 1% strain and 1Hz. The temperature ramp is 1°C/min.

For the suspension without PAA addition, the loss modulus will dominate over the storage modulus in the experimental temperature range. The corresponding value of the damping factor is very large and does not vary with increasing temperature, as shown in Figure 4-11. This behavior also indicates that the suspension in the absence of PAA is very stable and the thermal energy is less than the EDL repulsive potential barrier. Therefore, PAA is a crucial component in the TIF suspension to form bridging flocs and causes gelation of the suspensions.

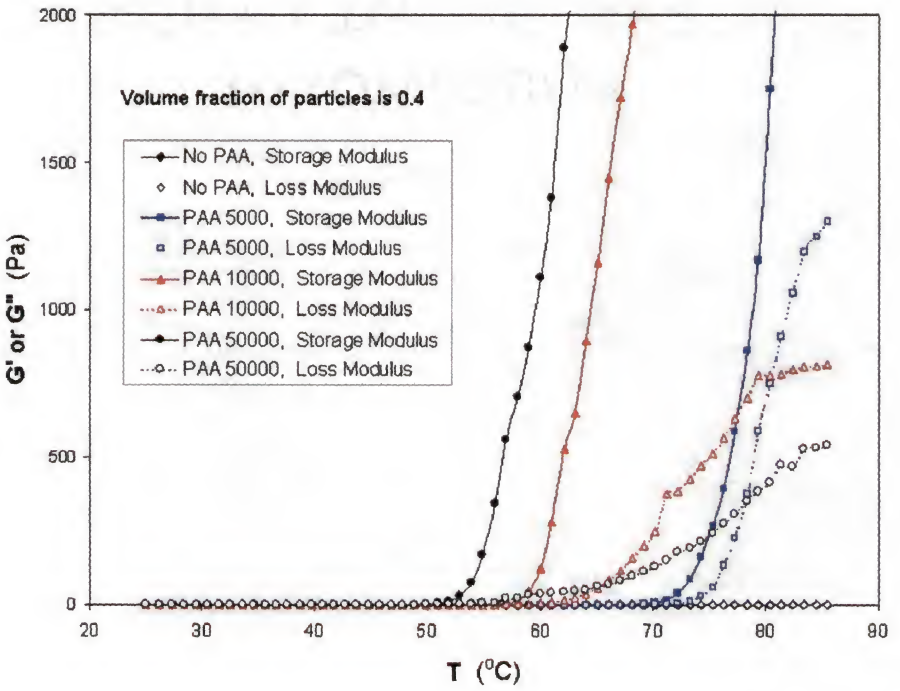

Fig.4-8. Effect of the PAA molecular weight on the variation of shear modulus with temperature for the 0.4 volume fraction suspensions with 0.04wt% PAA. The measurements are conducted under 1% strain and 1Hz. The temperature ramp is 1°C/min.

The contribution from the molecular weight of PAA might be due to two aspects. First, the adsorption energy between PAA chains and alumina particles is higher for the larger molecular weight PAA. [95] Therefore, larger molecular weight PAA can interact with alumina particles more easily to form bridging flocs. Second, being a longer PAA chain, it is likely that it adsorbs at multiple points on the alumina surface easier, thus giving it a stability advantage over shorter PAA chains. Therefore, the "crossover" temperature can be lowered by larger molecular weight PAA.

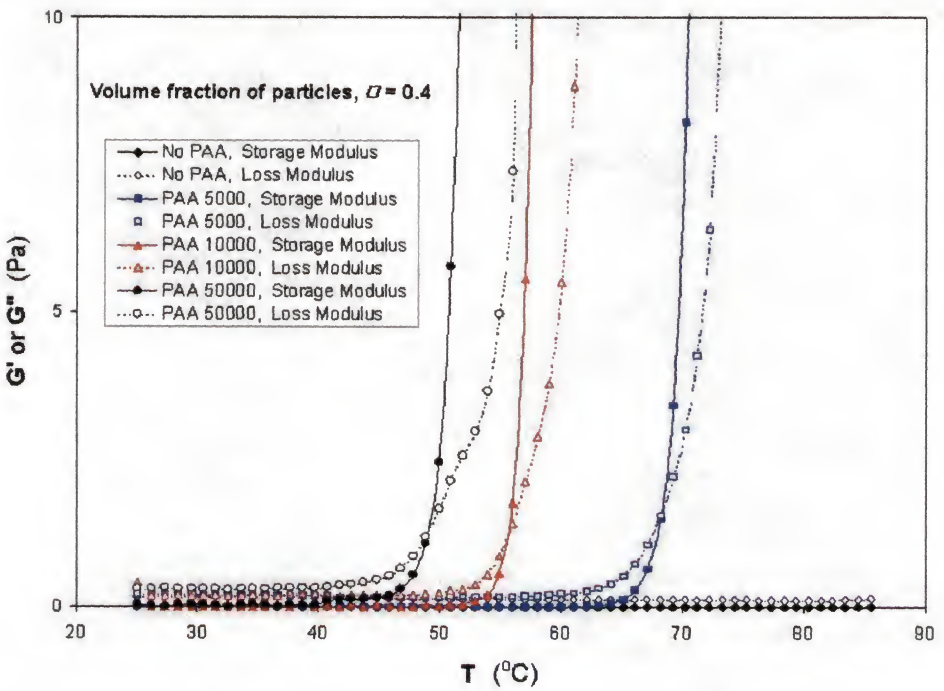

Fig.4-9. The same plots as in Fig.4-8 to show the "cross-over".

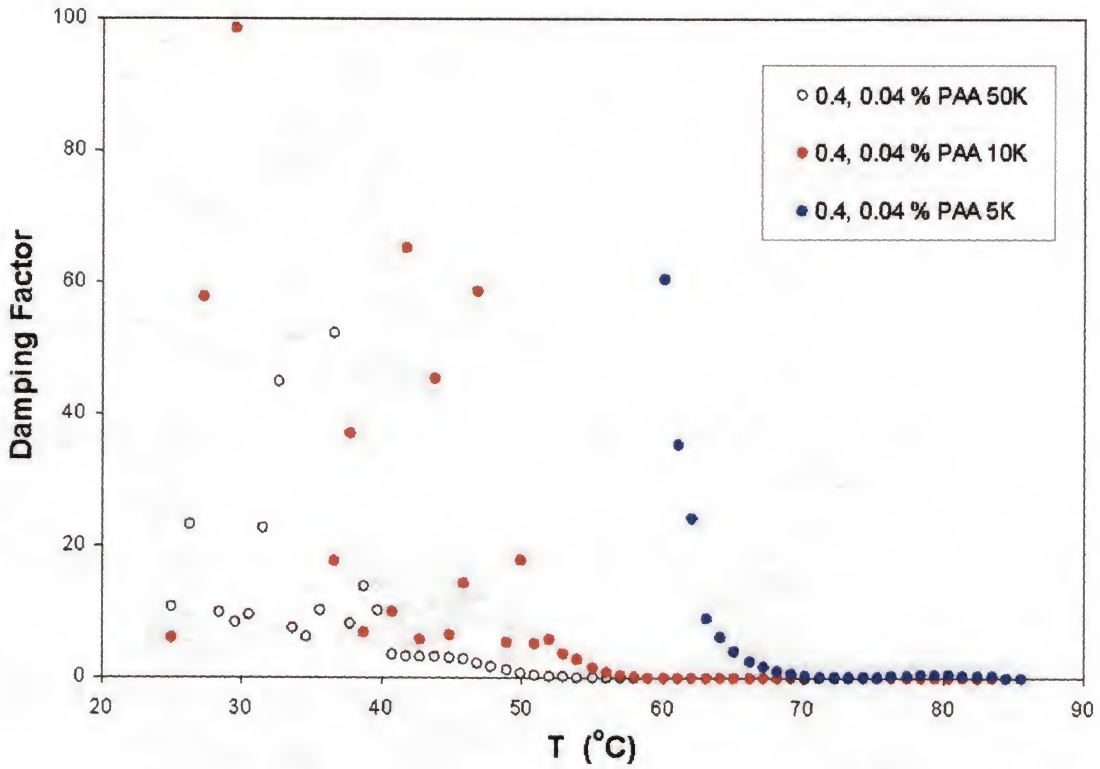

Fig.4-10. Variation of the damping factor for the 0.4 volume fraction of alumina suspensions with temperature and molecular weight of PAA. The suspensions are the same as those shown in Fig.4-8 and Fig.4-9. 1% strain, 1Hz, 1°C/min.

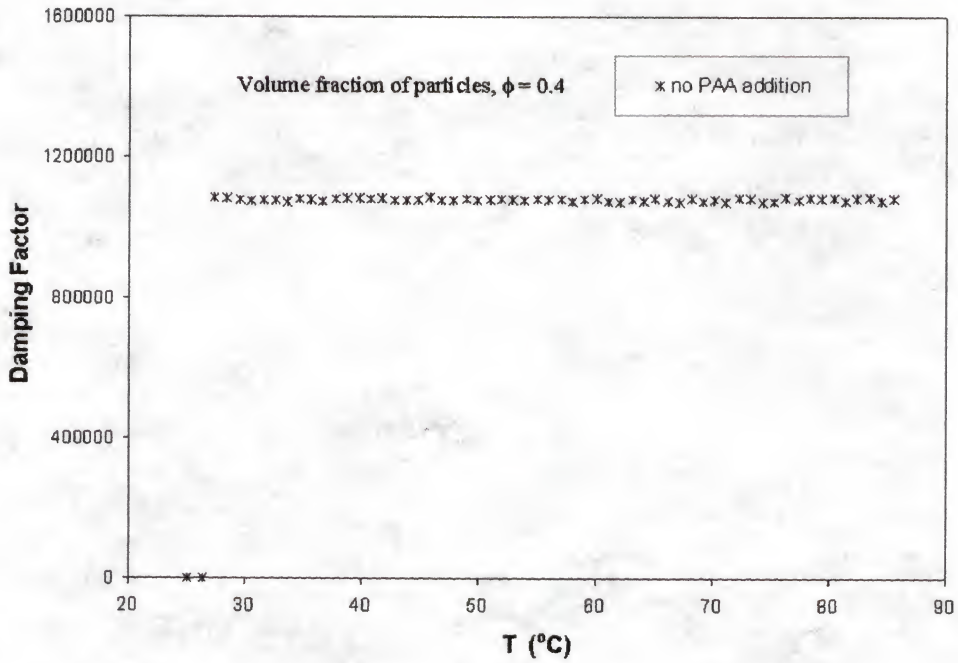

Fig.4-11. The damping factor for the PAA-free suspension of 0.4 volume fraction of alumina. The damping factor is very large and does not vary with increasing temperature indicating loss modulus dominates over storage modulus. 1% strain, 1Hz, 1°C/min.

4.2 Time Dependence of the Shear Modulus

The curves in Figure 4-12 demonstrate the time dependence of the suspension modulus at 45 °C for 0.4 volume fraction suspensions with PAA 10,000 and 50,000 addition, respectively. It is evident that both the storage and the loss modulus of the suspension with PAA 50,000 increase much more than those of the suspension with PAA 10,000 do. Therefore, higher PAA molecular weight can improve the gelation degree under the same experimental conditions, but at an expense of increasing the zero shear

rate viscosity that is not favorable for the direct casting process. Since the 0.4 volume fraction is above the volume fraction gelation threshold, the remaining alumina particles will fill in the interstice space of the percolation network and increase the density of the network and thus contribute to the further increase of the suspension shear modulus with temperature or time.

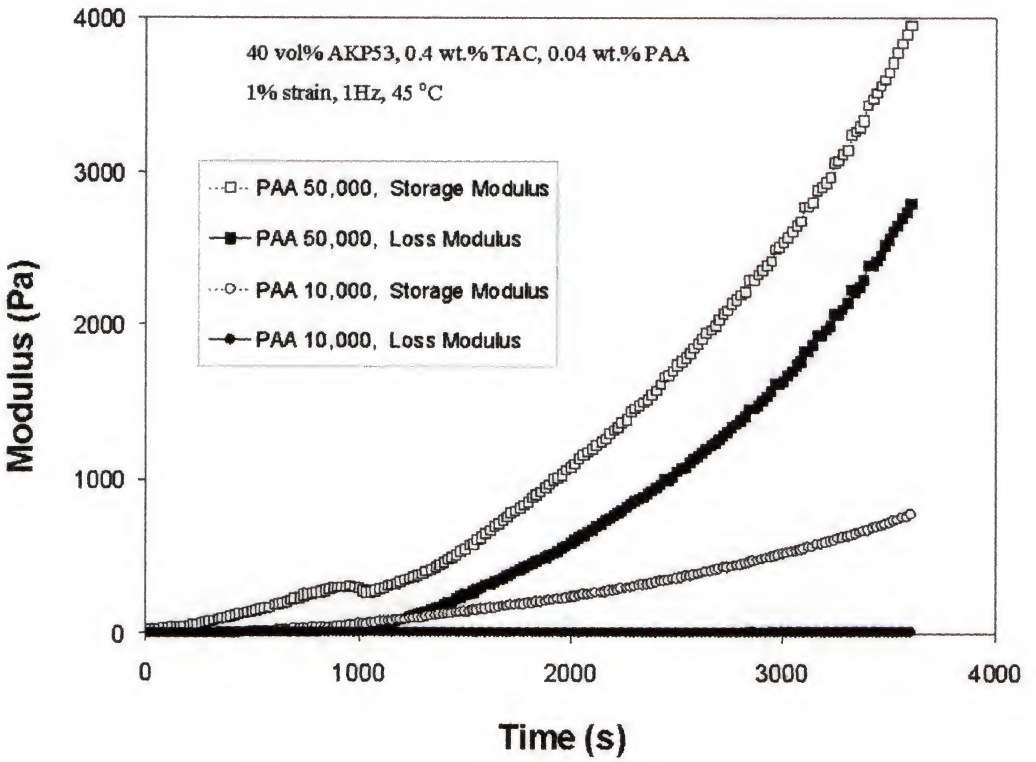

Fig.4-12. Time dependence of the suspension modulus at 45 °C for 0.4 volume fraction suspensions with 0.04wt% PAA 10,000 and 50,000 addition, respectively. It is evident that both the storage and the loss modulus of the suspension with PAA 50,000 increase much more than those of the suspension with PAA 10,000 do. The measurements are conducted under 1% strain at a frequency of 1Hz.

Figure 4-13 gives the time dependence of modulus at different temperatures for the 0.4 volume fraction AKP53 suspensions with 0.04 wt.% PAA 10,000 addition. It is

very clear that the magnitude of the shear modulus of the suspensions increases more at a higher temperature than that at lower temperature, although here there is only 5 °C difference. This might be due to the earlier space network formation and higher particles-polymer reaction rate at higher temperature, then the remaining particles can fill into the interstice of network and increase the density of the network more efficiently. Therefore, such network shows higher shear modulus.

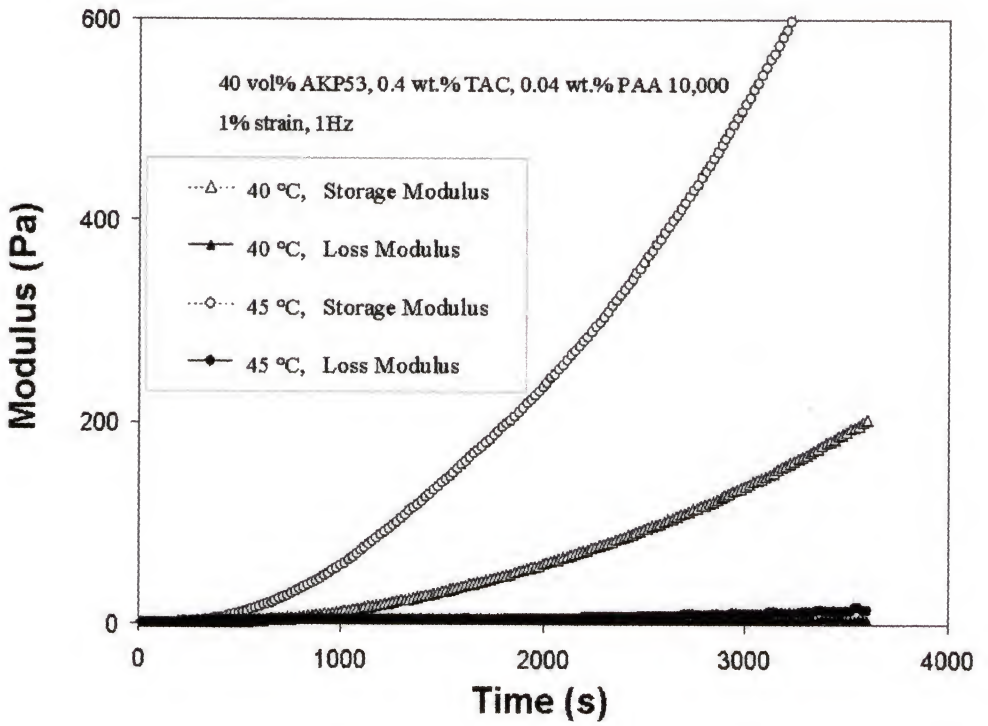

Fig.4-13. Time dependence of the suspension modulus at 40 and 45°C for the 0.4 volume fraction AKP53 suspensions with 0.04wt% PAA 10,000 addition. The magnitude of the shear modulus of the suspensions increases more at a higher temperature than at lower temperature. The measurements are conducted under 1% strain at a frequency of 1Hz.

These results also suggest that temperature is one important parameter to control the gelation degree of the TIF alumina suspensions. Figure 4-14 shows the time

dependence of the damping factor. As can be seen from the curves, the damping factor decreases with the treatment time at both 40 °C and 45 °C, and finally levels off to a small value, which indicates that the storage modulus is increasing much more with time than the loss modulus. The variations of the damping factor with time in Figure 4-13 also verify the suspension structure transitions from "fluid-like" to "solid-like" behavior. When the damping factor levels off to a very small value at the longer period of time, the storage modulus totally dominates over loss modulus.

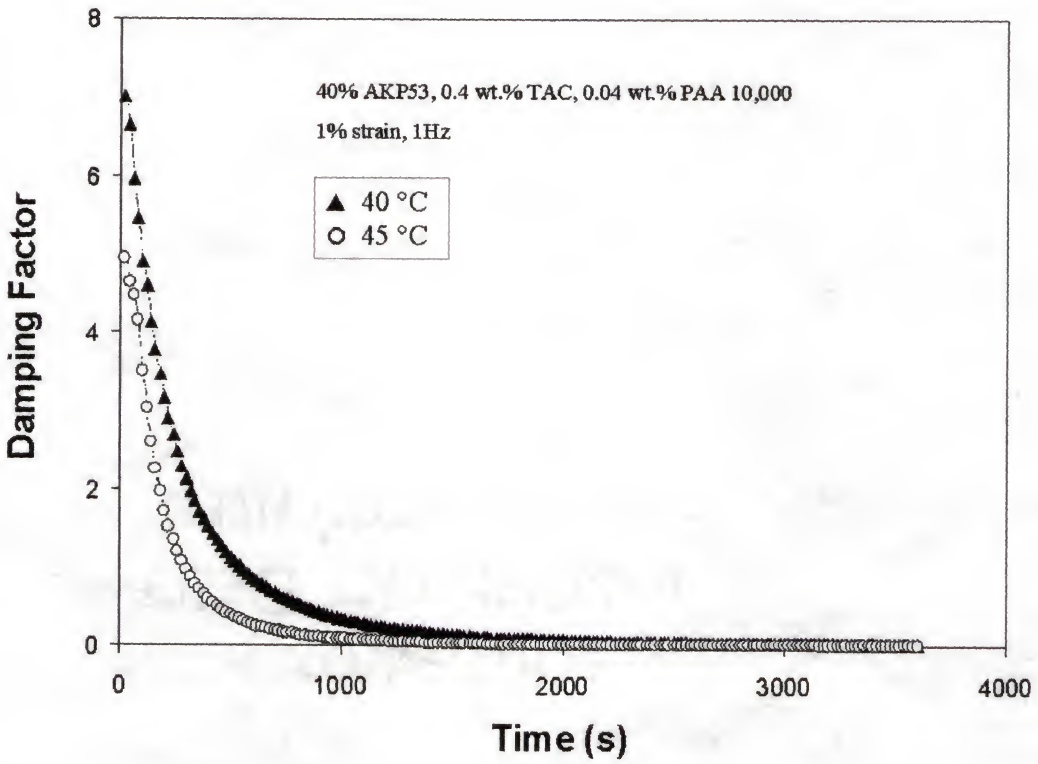

Fig.4-14. Time dependence of the suspension modulus at 40 and 45°C for the 0.4 volume fraction AKP53 suspensions with 0.04wt% PAA 10,000 addition. The measurements are conducted under 1% strain at a frequency of 1Hz.

4.3 Summary of This Chapter

The storage modulus and the loss modulus can be used to characterize the viscoelastic properties of the TIF suspensions. For the suspensions with volume fraction less than 0.5, there is a "crossover" point where above this temperature, the suspensions behave "solid-like" with G'>G'', and "fluid-like" with G''>G' when the temperature is below this transition point. This "crossover" point can be easily observed in the damping factor vs. temperature plots.

Higher volume fraction of particles tends to shift the "crossover" to a lower temperature and increases the magnitude of the storage modulus at each respective temperature. Increasing the PAA amount will shift the "crossover" to a lower temperature and results in the formation of a particle space-filling network at lower temperature. Larger molecular weight of PAA tends to decrease the "crossover" temperature for the same volume fraction suspensions and enhance the formation of the particle space-filling network.

The evolution of the shear modulus with time at a temperature shows that higher temperatures increase the shear modulus more rapidly than at lower temperature. Both the storage and the loss modulus of the suspension with PAA 50,000 increases much more rapidly than the suspensions with PAA 10,000. Therefore, higher M_w PAA can improve the gelation degree under the same experimental conditions, but at an expense of increasing the zero shear rate viscosity that is not favorable for a direct casting process.

CHAPTER 5
PERCOLATION THEORY MODEL FOR THE TIF ALUMINA SUSPENSIONS

5.1 Assumptions to the TIF Percolation Gelation Model

Experimental results in Chapter 3 and Chapter 4 showed that for the PAA addition TIF alumina suspensions, several processing parameters affected the rheological properties of the TIF suspensions, such as volume fraction of solids, dispersant amount and molecular weight of PAA, etc. In Chapter 2 it was also mentioned that aggregation would form flocs and grow in concentrated suspensions. The formation of a space-filling network occurred when the characteristic size of the floc was equal to the total volume of the suspension. Fractal model and percolation model had been proposed to explain the experimental phenomena, which stated that the modulus of the suspension increased with increasing volume fraction of the flocs. In the percolation model, the properties of the investigated sample show "transition" behavior around a threshold composition. It was realized from the experimental results that the temperature dependence of the viscoelastic properties of the TIF suspensions also showed transition behavior, i.e. gelation. Therefore, the author thought that the variation of the shear modulus with temperature for the TIF suspensions could be described using the percolation theory model if the particle percolative network did form. The following assumptions are proposed to evaluate the evolution of the microstructure of the TIF suspensions when the temperature is raised.

(1) Aggregate forms because of bridging flocculation, which arises from the interaction between particles and polymer chains with increasing temperature.

(2) The number of aggregates formed might be affected by the magnitude of the EDL repulsive potential between particles, the initial volume fraction of particles and the amount of the polymer.

(3) The size of aggregates grows with increasing temperature.

(4) Viscoelastic properties, such as storage modulus and shear viscosity, increase with the number density of the stress carrying bonds.

(5) TIF alumina suspension has a volume fraction threshold, above which the slurry can be gelled to form a continuous filling network as the temperature is raised. This volume fraction threshold should vary with the molecular weight of PAA because of the increasing possibility of the interactions between PAA chains and particles.

(6) There is a temperature threshold that is related to the balance of the thermal energy, the particle/PAA adsorption energy, van der Waals attraction potential and the EDL repulsive potential. This temperature should decrease with increasing molecular weight of PAA.

(7) A new concept, the effective volume fraction of particles, ϕ_{eff}, is introduced. Compared with the initial volume fraction of particle (ϕ_0), ϕ_{eff} increases with temperature because of the growth of the aggregate floc and it reaches maximum value of 1 in the completely gelled suspension.

5.2 Continuous Percolation Theory Model

Considering the high order of stochastic geometry in concentrated suspensions, and the disorder–generating statistical variable (stable region / aggregates) being superimposed on a background structure that is itself topologically disorder (no lattice for aggregates positions), the space filling network in TIF suspension is treated as continuous percolation. The whole system of a concentrated suspension has a two-fold disorder, statistical (for the state of aggregates to link to each other) and geometrical (for background structure).

Adopting the similar form as Eq. (2-17) to relate the storage modulus with the volume fraction and temperature of the TIF alumina suspensions, Eq. (5-1) is obtained.

$$G'(T, \phi) = G'_0(T) \cdot [\phi_{eff}(T) / \phi_g - 1]^s \quad (5\text{-}1)$$

where ϕ_{eff} is the effective volume fraction of the flocs instead of the initial volume fraction ϕ_0. The concept of ϕ_{eff} can be thought as the total volume of the particles in a aggregate and the volume of the solvent trapped inside the backbone of the aggregate, where $\phi_{eff} \geq \phi_0$. ϕ_g is the volume fraction gelation threshold. $G'_0(T)$ is a reflection of the strength of the aggregate backbone, which might vary with the molecular weight of polymer and the deviation from the thermal equilibrium condition. The exponent, s is related to the microstructure of the network, which can be taken as $s \approx 2 - 5$ [96-100].

Considering the intrinsic similarities (i.e. by thermal activation) between the formation and growth of the aggregate flocs in the TIF suspension, and the nucleation and growth of crystalline phase from solution, $G'_0(T)$ and ϕ_{eff} are defined as the expressions shown in Eq. (5-2) and Eq. (5-3), respectively.

$$G'_0(T) = G_0 \cdot e^{\beta T} \quad (5\text{-}2)$$

$$\phi_{eff}(T) = \phi_0 \cdot e^{-\Delta U / kT} \cdot F(\Delta T) \quad (5\text{-}3)$$

where ϕ_0 is initial volume fraction of powders, ΔU is the total interaction energy barrier for particles to overcome to form agglomerate flocs, G_0 is a constant that relates to the interparticle bonding strength, and $F(\Delta T)$ is a function of the temperature and reflects

the effect of temperature on the growth of the agglomerate flocs. The parameter β varies with material system and temperature ramp rate. ***k*** is the Boltzmann constant.

Assume F (ΔT) has the following form

$$F(\Delta T) = e^{d_1 \cdot [d_2 + (T-T_0)/T_0]} \tag{5-4}$$

Then the final expression for the storage modulus is

$$G'(T, \phi_0) = G_0 \cdot e^{\beta T} \cdot \{\phi_0 \cdot e^{-\Delta U/kT} \cdot e^{d_1 \cdot [d_2 + (T-T_0)/T_0]} / \phi_g - 1\}^s \tag{5-5}$$

where d_1 and d_2 are constants, T_0 is the characteristic temperature for a molecular weight polymer system, and T_0 is independent with the amount of polymer and volume fraction of particles. The physical meaning of T_0 might be the balance temperature between the repulsive interaction potential and the affinity potential that ties particles together to form agglomerates, i.e. the thermal energy, the particle/PAA adsorption energy, van der Waals attraction potential and the EDL repulsive potential.

5.3 Calculation Results Using the Model

In this section the calculated results using Eq. (5-5) will be given and discussed. Several parameters in the equation were fixed during calculation: $d_1 = 1.3$, $d_2 = 0.1$, $\beta = 0.016\ K^{-1}$.

5.3.1 Effect of G_0 and ΔU on the Storage Modulus

Figure 5-1 shows how the magnitude of G_0 affects the storage modulus of the 0.4 volume fraction suspensions. Figure 5-2 shows the 3D plots that relate the storage modulus with G_0 and temperature. It is obvious that increasing G_0 can increase the value of storage modulus, G'. As mentioned above, G_0 is indicative of the bonding strength between particles; and higher interparticle strength will form a stronger particle percolation network and can transport larger stress along the backbone of the clusters. Therefore, the storage modulus will increase with increasing of G_0.

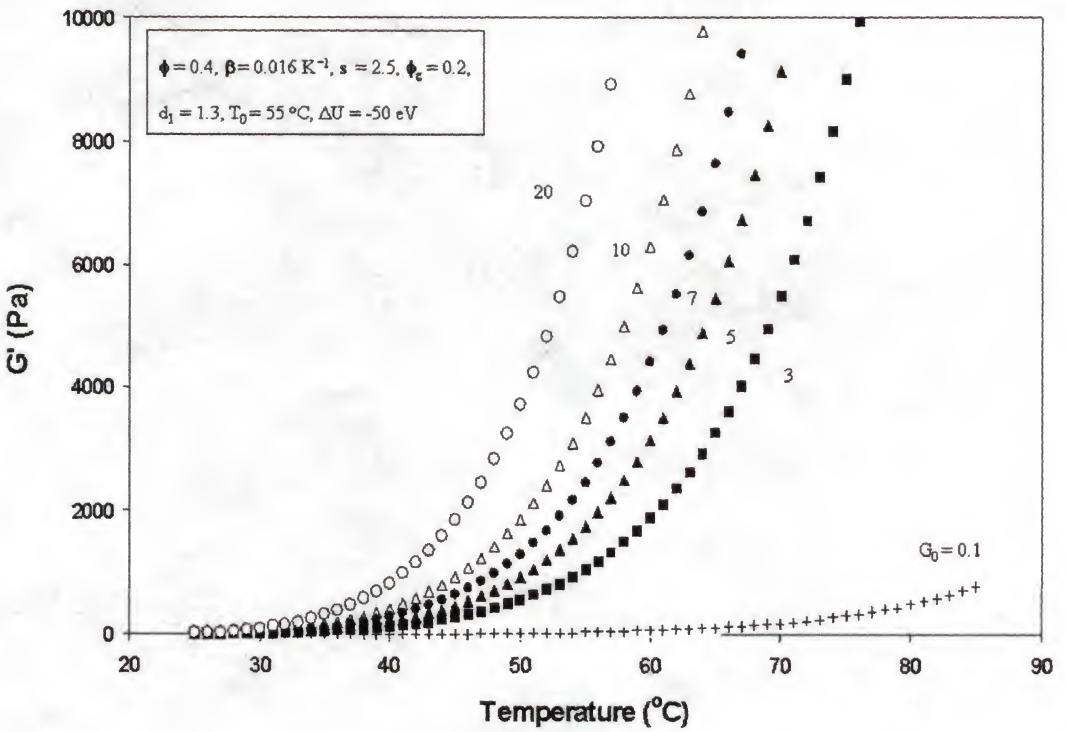

Fig.5-1. The G_0 dependence of the storage modulus using Eq.(5-5). Other parameters are $\phi = 0.4$, $\beta = 0.016\ K^{-1}$, $\mathbf{s} = 2.5$, $\phi_g = 0.2$, $d_1 = 1.3$, $T_0 = 55\ ^{\circ}C$, and $\Delta U = -50$ eV.

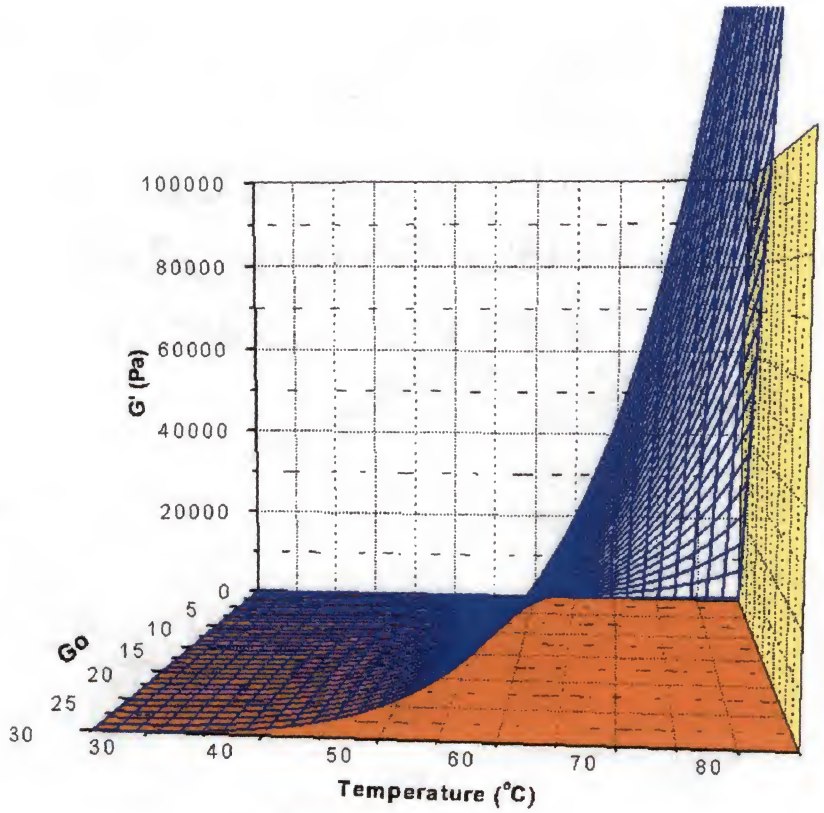

Fig.5-2. 3D plots using Eq.(5-5) to relate the storage modulus with G_0 and temperature. Other parameters are $\phi = 0.4$, $\beta = 0.016\ K^{-1}$, $s = 2.5$, $\phi_g = 0.2$, $d_1 = 1.3$, $T_0 = 55\ ^{\circ}C$, and $\Delta U = -50$ eV.

5.3.2 Effect of Initial Volume Fraction ϕ_0 on the Storage Modulus

Figure 5-3 gives the calculated results of the temperature dependence of the storage modulus while varying the volume fraction of solids, ϕ_0, in the suspensions. During calculations, the volume fraction threshold is set as $\phi_g = 0.2$; and the characteristic temperature is assumed as $T_0 = 55\ ^{\circ}C$. The exponent factor is $s = 2.5$. As can be seen from the plots, larger volume fraction of solids yields a higher storage modulus value at a

given temperature. Since the volume fraction threshold is 0.2, all the suspensions show increasing storage modulus as the temperature is raised when the volume fraction is larger than 0.2. There is no significant variation of G' for the 0.1 volume fraction particle suspension.

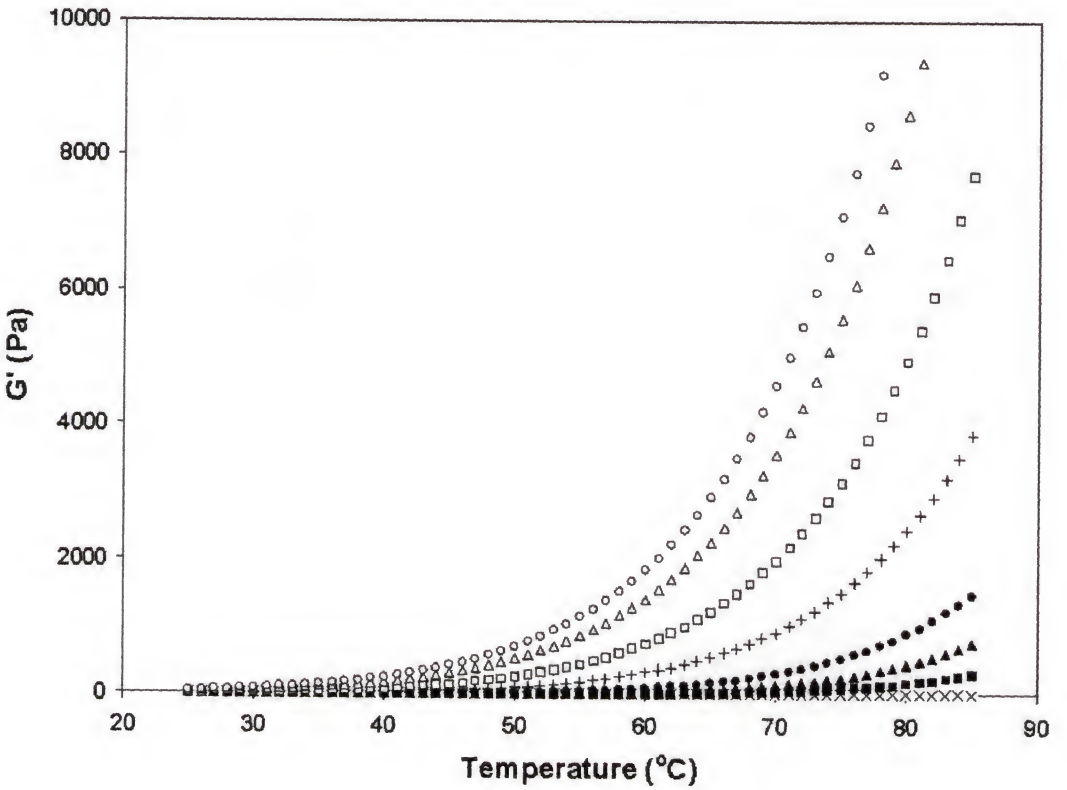

Fig.5-3. The effect of volume fraction on the storage modulus. Other parameters are β = 0.016 K^{-1}, **s** = 2.5, ϕ_g = 0.2, d_1 = 1.3, T_0 = 55 °C, ΔU = -50 eV, G_0 = 0.5. (×) ϕ = 0.1, (■) ϕ = 0.2, (▲) ϕ = 0.25, (●) ϕ = 0.3, (+) ϕ = 0.4, (□) ϕ = 0.5, (△) ϕ = 0.6, (○) ϕ = 0.65.

The volume fraction dependence of the storage modulus at various temperatures is computed and shown in Figure 5-4. During calculations, the parameters are chosen as ϕ_g = 0.2, T_0 = 55 °C, ***s*** = 2.5, G_0 = 5 and ΔU = –50 eV. The plots clearly manifest a

storage modulus increase with the volume fraction of the suspension in a power law relationship as is shown in Eq. (5-5). The plots also show that at higher temperature, the storage modulus starts to increase at a volume fraction that is smaller than ϕ_g. Higher volume fraction of particles will give a dense aggregate network and therefore can sustain larger stress before breaking, and therefore yields a higher storage modulus value.

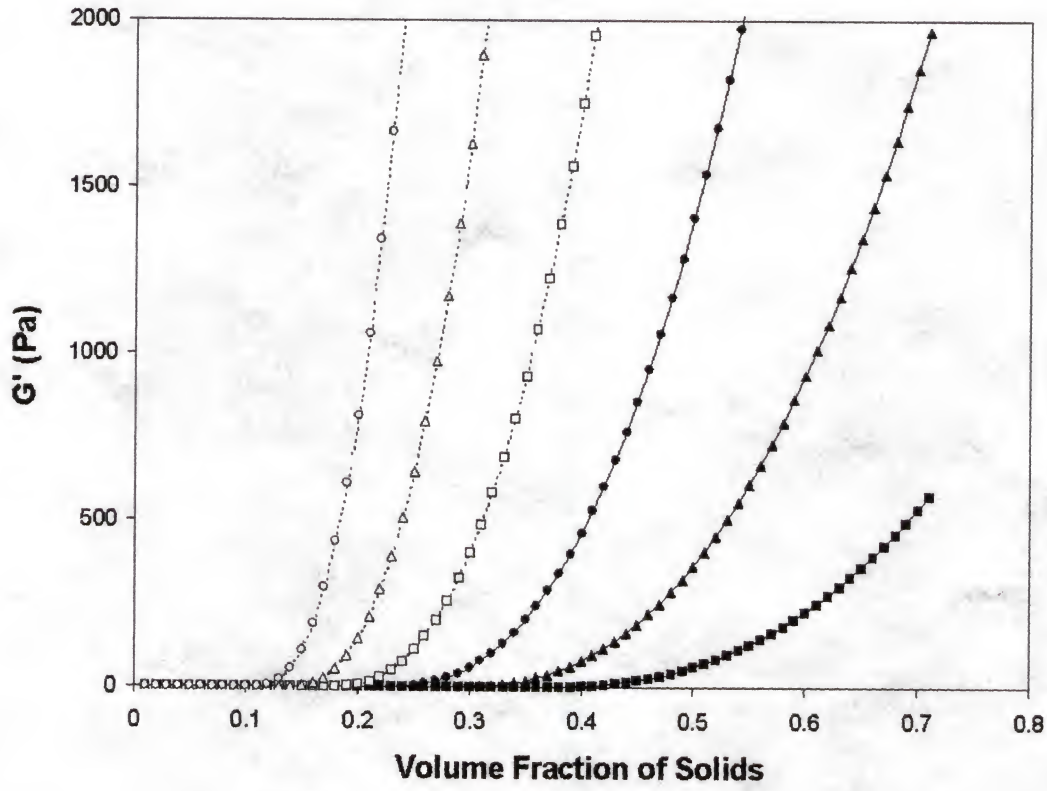

Fig.5-4. Volume fraction of solids dependence of the storage modulus at different temperature. Other parameters are $\beta = 0.016\ K^{-1}$, $s = 2.5$, $\phi_g = 0.2$, $d_1 = 1.3$, $T_0 = 55\ ^{\circ}C$, $\Delta U = -50$ eV, $G_0 = 5$. At (■) $T = 25\ ^{\circ}C$, (▲) $T = 35\ ^{\circ}C$, (●) $T = 45\ ^{\circ}C$, (□) $T = 55\ ^{\circ}C$, (△) $T = 65\ ^{\circ}C$, (○) $T = 75\ ^{\circ}C$.

The power law dependence of shear modulus on volume fraction of particles has been documented often in the literature. Some investigators suggest that there is a simple

function to relate the storage modulus with the volume fraction as $G' \propto \phi^n$, considering that the particle connectivity is very tortuous at all volume fractions so that many interpenetrating, percolative paths exist to support applied pressures at high volume fractions. For example, Sen et al. proposed a model for such a tortuous network and yielded $n = 4.4$ [96]. During modeling, they changed the volume fraction of particles by randomly removing particles from a periodic array (face-centered cubic) of identical, spherical particles. The results of Yanez et al. showed that $n = 4.75 \pm 0.25$ for the attractive alumina particle networks in aqueous slurries [97]. Sonntag and Russel have found n to be 2.5 and 4.4 for fresh and aged polystyrene networks, respectively [98]. Shih et al. have experimentally determined that n = 4.1 for the modulus of agglomerated, platelike, boehmite alumina crystallites [99]. Buscall et al. have found n = 4.3 for the compressive yield stress of polystyrene latex systems aggregated with barium chloride [100]. It is clear that these large values of n are due to the percolative nature of particle networks.

5.3.3 Effect of Characteristic Temperature T_0 on the Storage Modulus

Figure 5-5 shows how the characteristic temperature T_0 affects the temperature dependence of storage modulus. During calculation, the parameters are set as $\phi_g = 0.2$, $s = 2.5$, $G_0 = 0.5$, $\phi_0 = 0.4$ and $\Delta U = -50$ eV. The plots show that reducing T_0 can increase the storage modulus value dramatically. It seems that smaller T_0 gives a sharper "transition" from "fluid-like" to "solid-like" starting from a lower temperature. It is assumed that the value of T_0 is related to the molecular weight of the polymers added to the suspensions. Higher molecular weight of polymers gives a smaller value of T_0.

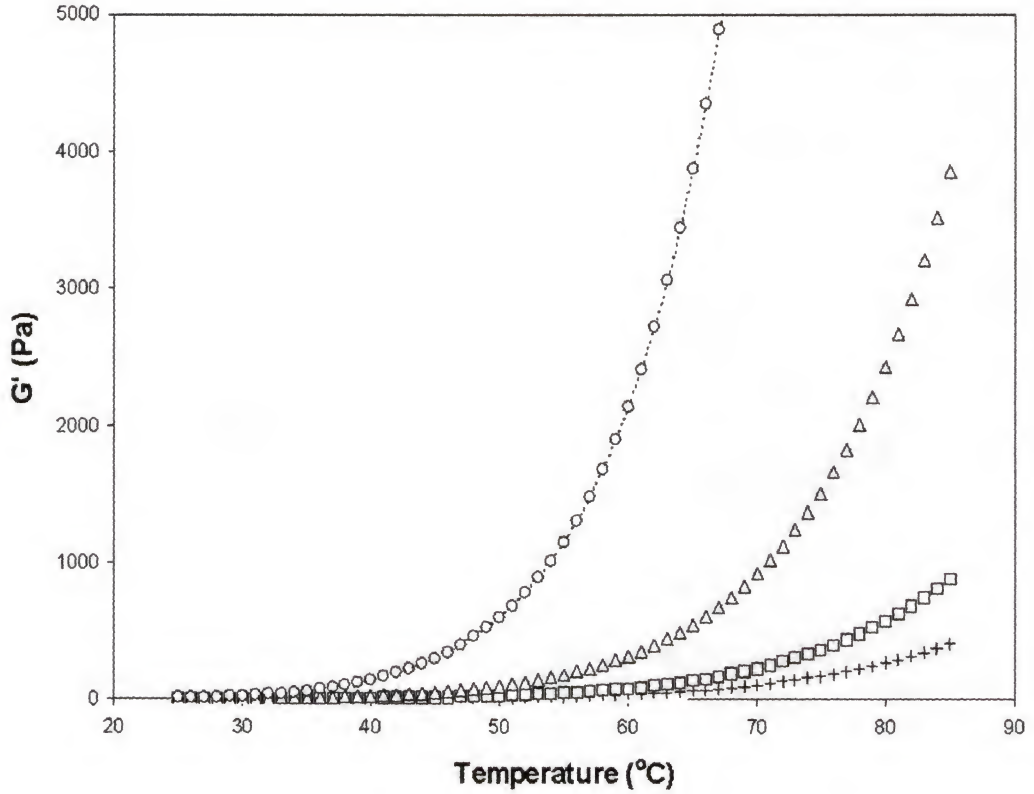

Fig.5-5. The effect of varying T_0 only on the storage modulus for 0.4 volume fraction suspensions. The parameters are $\phi = 0.4$, $\beta = 0.016\ K^{-1}$, $s = 2.5$, $\phi_g = 0.2$, $d_1 = 1.3$, $\Delta U = -50$ eV, and $G_0 = 0.5$. (+) $T_0 = 80$ °C, (□) $T_0 = 70$ °C, (△) $T_0 = 55$ °C, (○) $T_0 = 40$ °C.

5.3.4 Effect of Volume Fraction Threshold ϕ_g on the Storage Modulus

The volume fraction threshold, ϕ_g, is also related to the molecular weight of polymers when its amount is just enough for bridging flocculation. Higher molecular weight of polymers yields a smaller value of ϕ_g. For large amount of polymer addition suspensions, the ϕ_g can be reduced even more. In most cases, ϕ_g and T_0 need change at the same time.

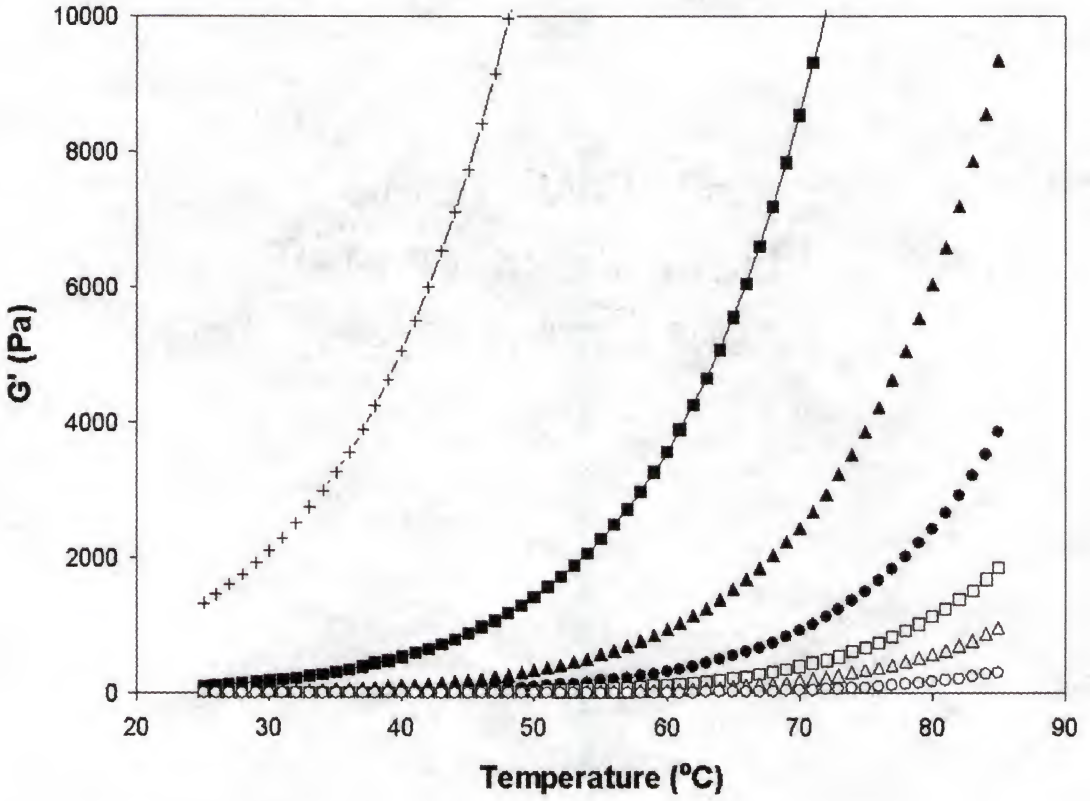

Fig.5-6. The effect of varying gelation threshold on the storage modulus for 0.4 volume fraction suspensions. The parameters are $\phi = 0.4$, $\beta = 0.016\ K^{-1}$, $s = 2.5$, $d_1 = 1.3$, $\Delta U = -50$ eV, $G_0 = 0.5$, $T_0 = 55\ ^{\circ}C$. (+) $\phi_g = 0.05$, (■) $\phi_g = 0.1$, (▲) $\phi_g = 0.15$, (●) $\phi_g = 0.2$, (□) $\phi_g = 0.25$, (△) $\phi_g = 0.3$, (○) $\phi_g = 0.4$.

Figure 5-6 shows how the storage modulus varies with temperature for different values of ϕ_g. The volume fraction of the suspensions is 0.4. It is evident that smaller volume fraction threshold produces a higher value of the storage modulus. The sharper "transition" also happens at lower temperature for smaller ϕ_g. Since ϕ_g is the minimum amount of particles in the suspensions to form a connective network; therefore, lowering this threshold can result in more remaining particles to join the building of the percolation

network so that a denser backbone of the aggregates is produced. If the value of ϕ_g is very large, such as 0.4, the calculation shows that the suspension storage modulus has no significant change over the temperature range.

Altering ϕ_g and T_0 at the same time can tailor the "sharpness" of the "transition" and the magnitude of the low temperature storage modulus, as is shown in Figure 5-7. These results agree with the experimental data better than those results by only varying either one parameter.

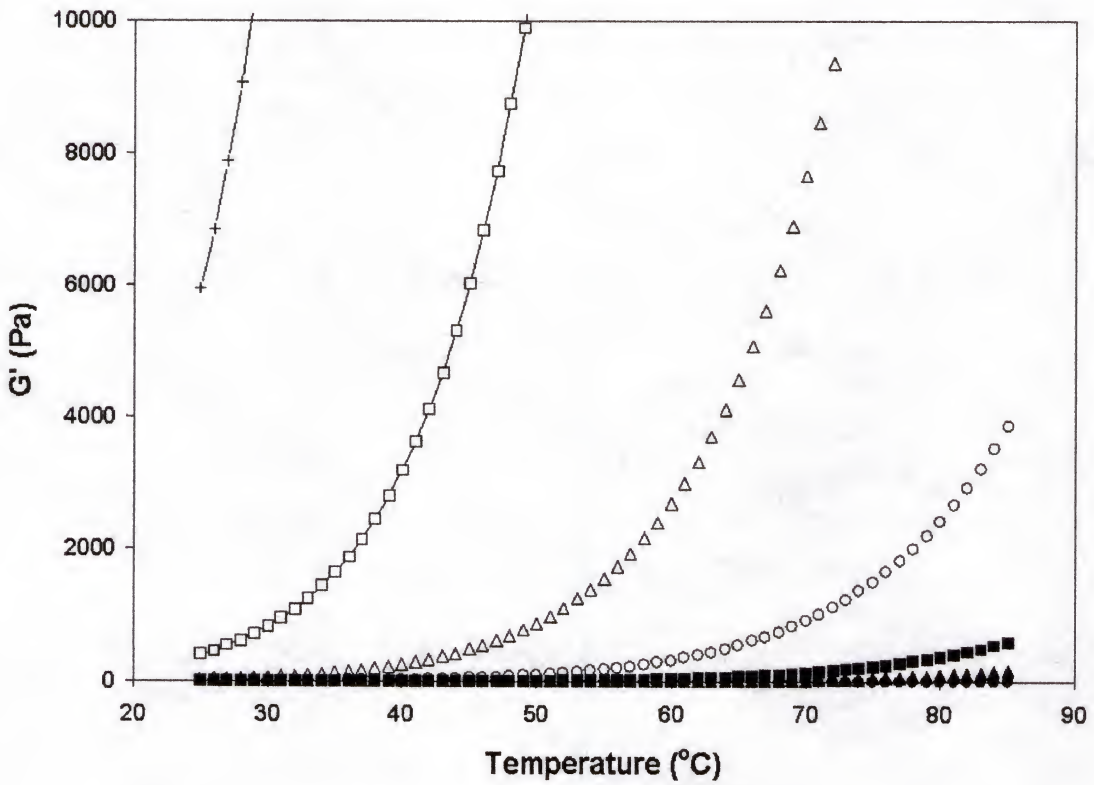

Fig.5-7. The effect of varying gelation threshold and T_0 at the same time on the storage modulus for 0.4 volume fraction suspensions. The parameters are $\phi = 0.4$, $\beta = 0.016\ K^{-1}$, $s = 2.5$, $d_1 = 1.3$, $\Delta U = -50$ eV, $G_0 = 0.5$. (+) $\phi_g = 0.05$, $T_0 = 30\ ^\circ C$; (□) $\phi_g = 0.1$, $T_0 = 35\ ^\circ C$; (△) $\phi_g = 0.15$, $T_0 = 45\ ^\circ C$; (○) $\phi_g = 0.2$, $T_0 = 55\ ^\circ C$; (■) $\phi_g = 0.25$, $T_0 = 65\ ^\circ C$; (▲) $\phi_g = 0.3$, $T_0 = 70\ ^\circ C$; (●) $\phi_g = 0.4$, $T_0 = 80\ ^\circ C$.

5.3.5 Effect of Exponent *s* on the Storage Modulus

Figure 5-8 and Figure 5-9 shows the effect of exponent ***s*** on the temperature dependence of the storage modulus. It is apparent from the plots that larger ***s*** value gives a "sharper" "transition" trend as predicted by the exponential power law. One interesting result is the "crossover" of the plots at T ≈ 50 °C. Below this "crossover" temperature, a larger ***s*** value gives a lower storage modulus. Above this "crossover" temperature, the change is the reverse. Larger values of ***s*** are due to the more extensive percolative nature of particles.

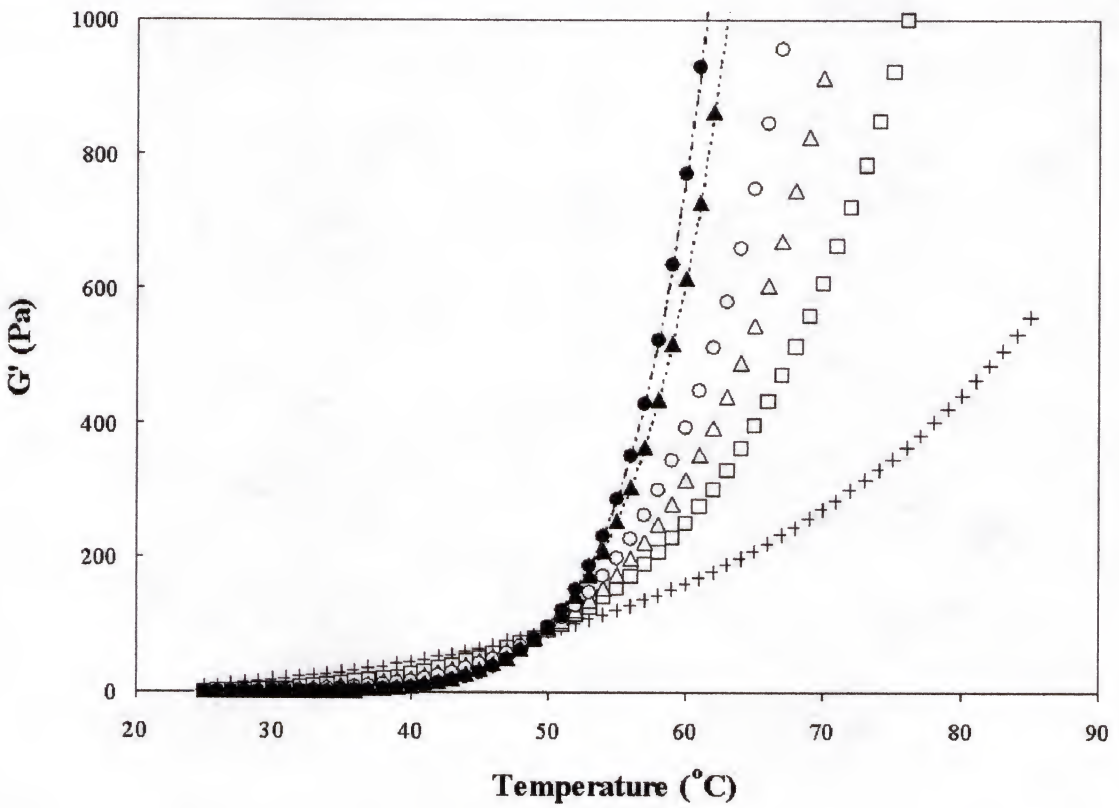

Fig.5-8. The effect of exponent s on the storage modulus for 0.4 volume fraction suspensions. The parameters are $\phi = 0.4$, $\beta = 0.016\ K^{-1}$, $d_1 = 1.3$, $\Delta U = -50$ eV, $G_0 = 0.5$, $\phi_g = 0.2$, $T_0 = 55\ ^{\circ}C$. (+) **s** = 1.0, (□) **s** = 2.0, (△) **s** = 2.5, (○) **s** = 3.0, (▲) **s** = 4.0, (●) **s** = 4.5.

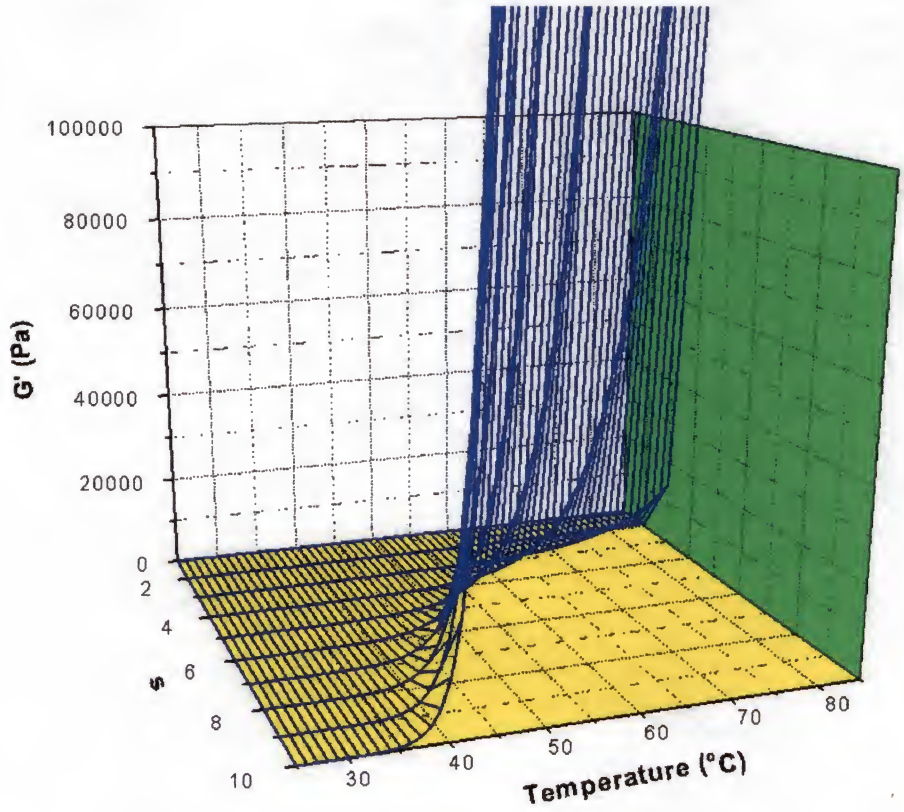

Fig.5-9. 3D plots to illustrate the variation of the storage modulus with the value of exponent s and temperature calculated from Eq. (5-5). The parameters are $\phi = 0.4$, $\beta = 0.016\ K^{-1}$, $d_1 = 1.3$, $\Delta U = -50$ eV, $G_0 = 0.5$, $\phi_g = 0.2$, $T_0 = 55$ °C.

5.4 Determination of the Parameters from Experiments

According to the above calculations, it can be seen that several parameters are critical for us to understand the percolation nature of the TIF alumina suspensions. The exponent, s reflects the nature of the particle percolation structure, and the gelation threshold, ϕ_g, gives the minimum volume fraction of particles under the experimental conditions to form a space-filling percolation network. The pre-exponent coefficient,

$G'_0(T)$, reflects the stiffness and strength of the backbone of the percolation network. The following section discusses how to determine these three parameters.

5.4.1 Determination of the Volume Fraction Threshold, ϕ_g

The volume fraction gelation threshold is the minimum amount of alumina particles required to form a continuous percolation network when the amounts of other components are fixed. Since the basic idea of percolation theory is the existence of a sharp transition at which the long-range connectivity of the system disappears or appears, this transition occurs abruptly when some generalized density in this system reaches a critical value (percolation threshold). Here it is proposed to use the temperature dependence of the shear modulus to find the volume fraction gelation threshold, and the oscillation mode of 1% strain and 1 Hz frequency is taken. The reason for using storage modulus is that it reflects the elastic response of the suspension structure to the shear stress. It is only after the formation of a particle space-filling network that the suspension can show an abrupt change in storage modulus such that the suspension manifests the solid-like behavior to withstand deformation.

Figure 5-10 is the temperature dependence of shear modulus for the alumina suspensions with 0.04wt% PAA of Mw~50,000. From these curves, it can be seen that both the storage and loss modulus do not experience change when the volume fraction of particles is 0.1. At 0.15 volume fraction, the storage modulus shows some increase at about 80 °C, but the magnitude is rather small. When the volume fraction is above 0.15, all suspensions show significant variation of storage and loss modulus with temperature. Therefore, a conclusion can be drawn from our above assumptions that the critical volume fraction of alumina with PAA 50,000 addition is about 0.15, or $\phi_g \sim 0.15$.

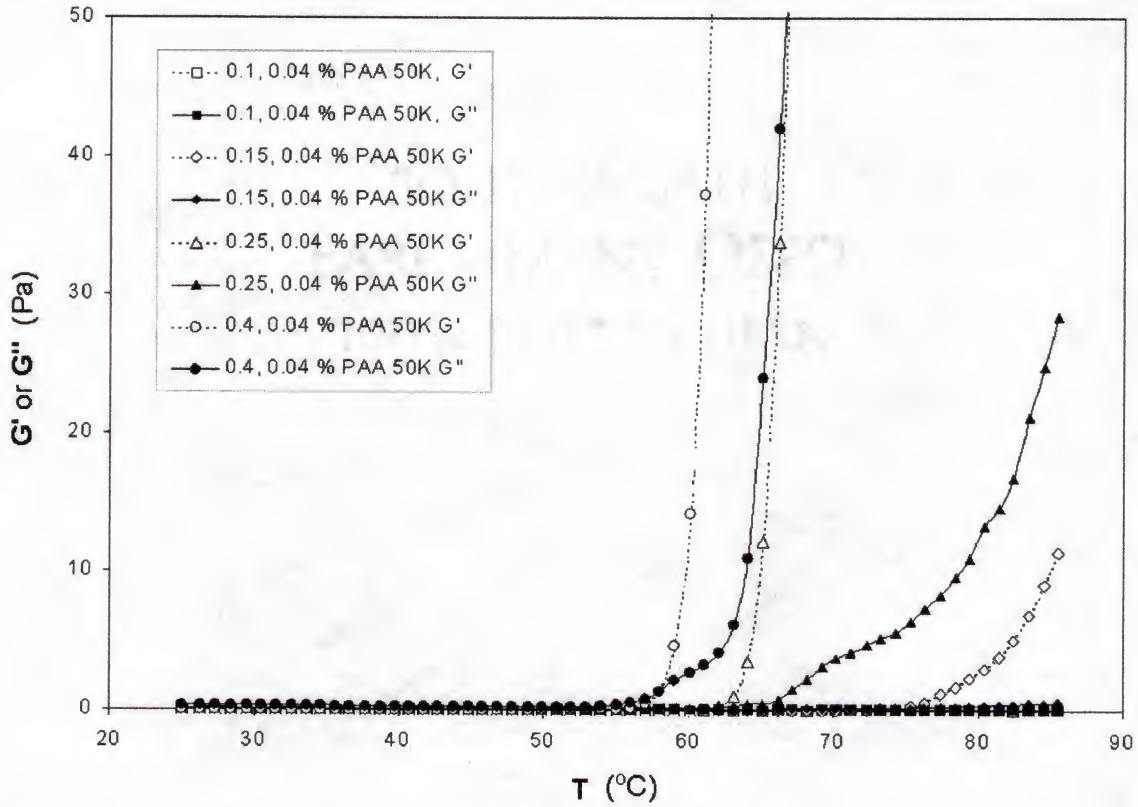

Fig.5-10. The temperature dependence of shear modulus for the alumina suspensions with 0.04wt% PAA of Mw~50,000. The filled symbols are for loss modulus, and the empty symbols are for storage modulus. The volume fraction gelation threshold can be determined to be around 0.15. The measurements are conducted at 1% strain and 1Hz, with a temperature ramp of 1 °C/min.

Figure 5-11 gives the temperature dependence of the damping factor of the same suspensions with respective to Figure 5-10. The sharp decrease of the damping factor with temperature indicates that the suspension microstructure has a relatively dramatic change when the temperature of the suspension is above a specific point. The smaller the value of the damping factor is, the more significantly the storage modulus dominates over the loss modulus for the suspension. Figure 5-11 shows that the damping factor of the

suspension starts to show this type of "transition" behavior when the volume fraction of particles is above the gelation threshold over the experimental temperature range. For the suspensions that the volume fraction of particles is less than the gelation threshold, the damping factor data are scattered randomly.

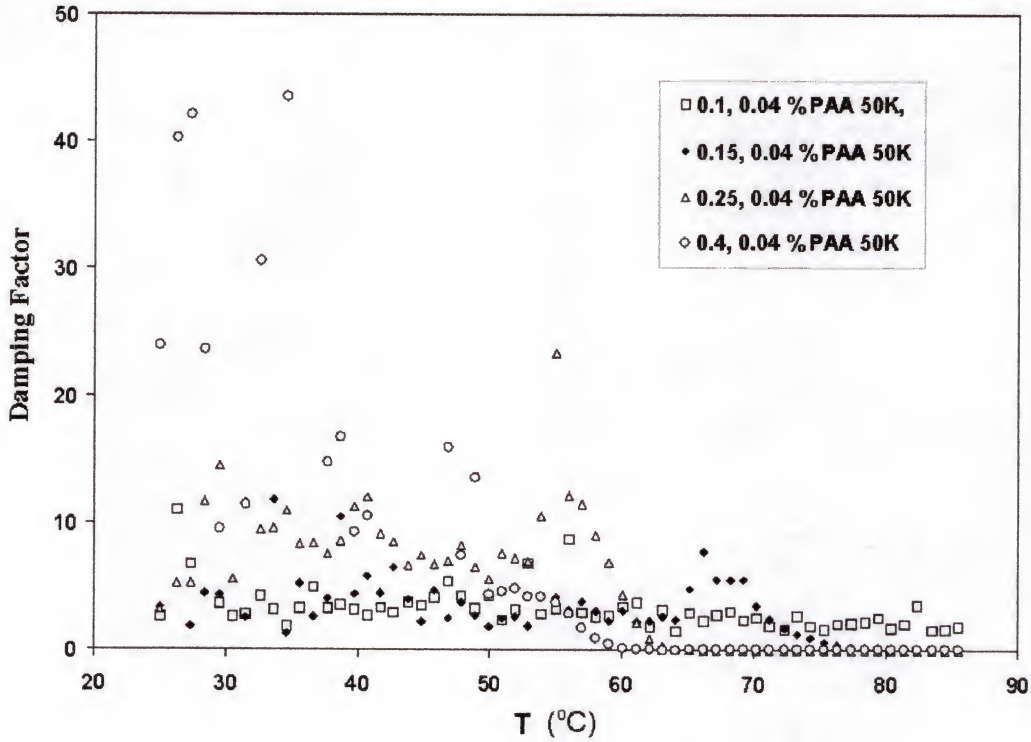

Fig.5-11. Variation of damping factors with temperature for the suspensions in Fig.5-10. Measurements are conducted at 1% strain and 1Hz, the temperature ramp is 1 °C/min.

The amount of PAA should be a concern to determine the volume fraction gelation threshold, because the probability of the interaction between PAA molecular chains will be increased with the increment of PAA. Figure 5-12 gives the temperature

dependence of the shear modulus for the 10vol% alumina suspensions with the PAA (Mw~50,000) amount fixed as 0.04wt%, 0.5wt%, 1.0wt% and 1.5wt%, respectively. Here the slurry loading is chosen as 10vol% because it is just below the gelation threshold determined above, 15vol%. It seems that up to PAA amount of 1.0wt%, the 10vol% suspensions do not have a significant change in storage modulus during the experimental temperature range. When the PAA amount is 1.5wt%, the storage modulus did show increase when T > 70 °C and reach a maximum value of about 50 Pa at 85 °C.

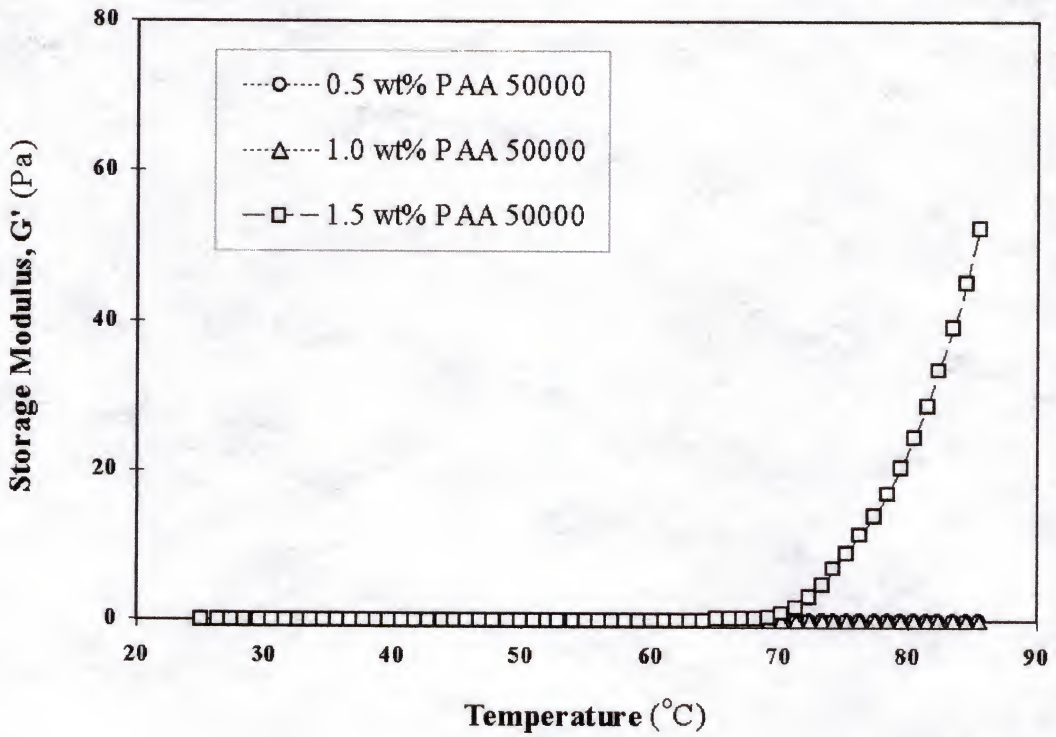

Fig.5-12. Effect of the amount of PAA (Mw~50,000) on the variation of storage modulus with temperature for the 10vol% alumina suspensions. It seems that up to 1.0wt% PAA, the suspensions do not have a significant change in storage modulus. The measurements are conducted at 1% strain and 1Hz, with a temperature ramp of 1 °C/min.

This increase in storage modulus at relatively higher amount of PAA (>1.5wt%) indicates the formation of the particle percolative microstructure, because a larger amount of PAA tends to form more agglomerates. But in the concentration range of PAA in our TIF suspensions (<< 0.5wt%), the conclusion can be drawn that the amount of PAA will not have a significant effect on the volume fraction gelation threshold of the AKP alumina particles.

Another issue will be whether the volume fraction gelation threshold varies with the molecular weight of PAA because the polymer chain length varies. Figure 5-13 and Figure 5-14 demonstrate the temperature dependence of storage modulus and damping factor for the 0.04wt% PAA 10,000 addition suspensions with variation in the volume fraction of the alumina particles. Similar procedures can be used to determine that the volume fraction gelation threshold for these suspensions is about 0.20, or $\phi_g \sim 0.20$. For the 0.04wt% PAA (Mw~5,000) addition suspensions shown in Figure 5-15 and Figure 5-16, the volume fraction gelation threshold can be taken as $\phi_g \sim 0.35$.

Therefore, it seems that for the 0.04wt% PAA alumina suspension, the volume fraction gelation threshold decreases with increasing molecular weight of PAA. This might be due to the higher adsorption energy between the longer polymer chains and particles. Therefore, bridging flocculation will occur more readily when higher molecular weight PAA is used. As a result, less amount of particles are required to form the percolation network in the suspension with increasing temperature.

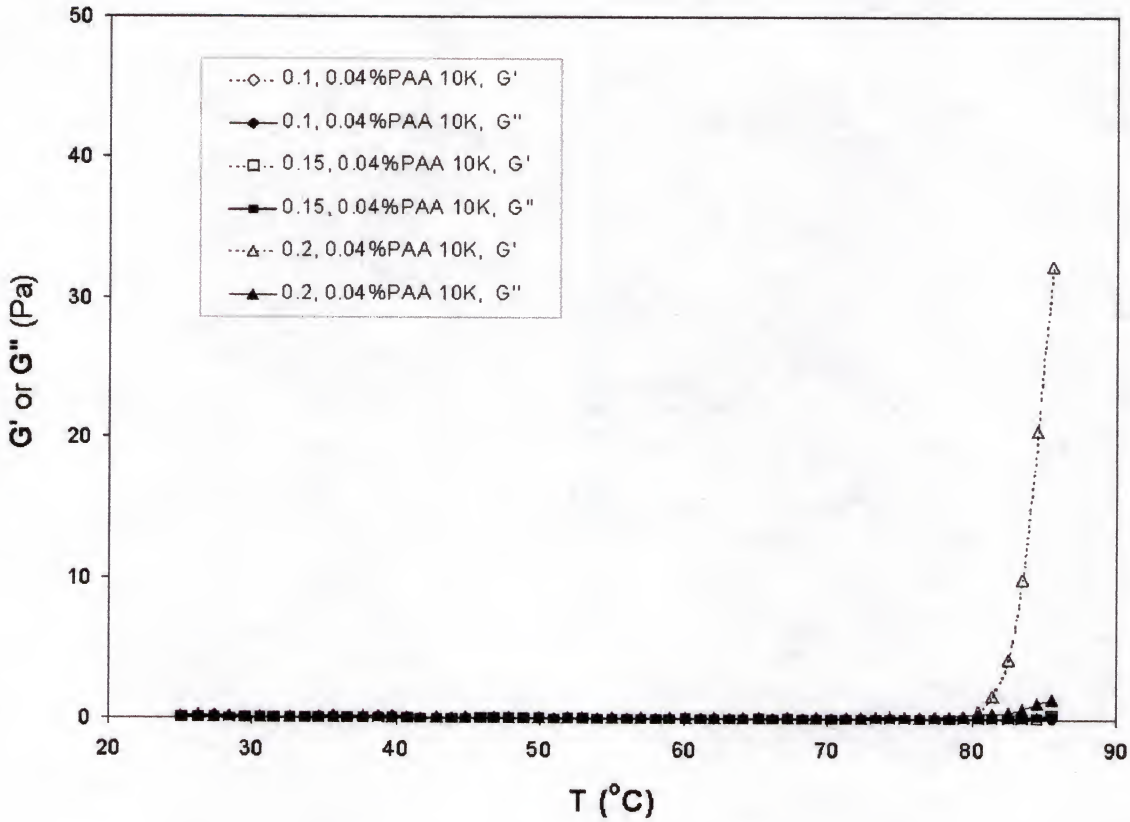

Fig.5-13. Variation of the shear modulus with temperature for the 0.04wt% PAA 10,000 addition suspensions. The volume fraction gelation threshold is about 0.2. Measurements are conducted at 1% strain and 1Hz, with a temperature ramp of 1 °C/min.

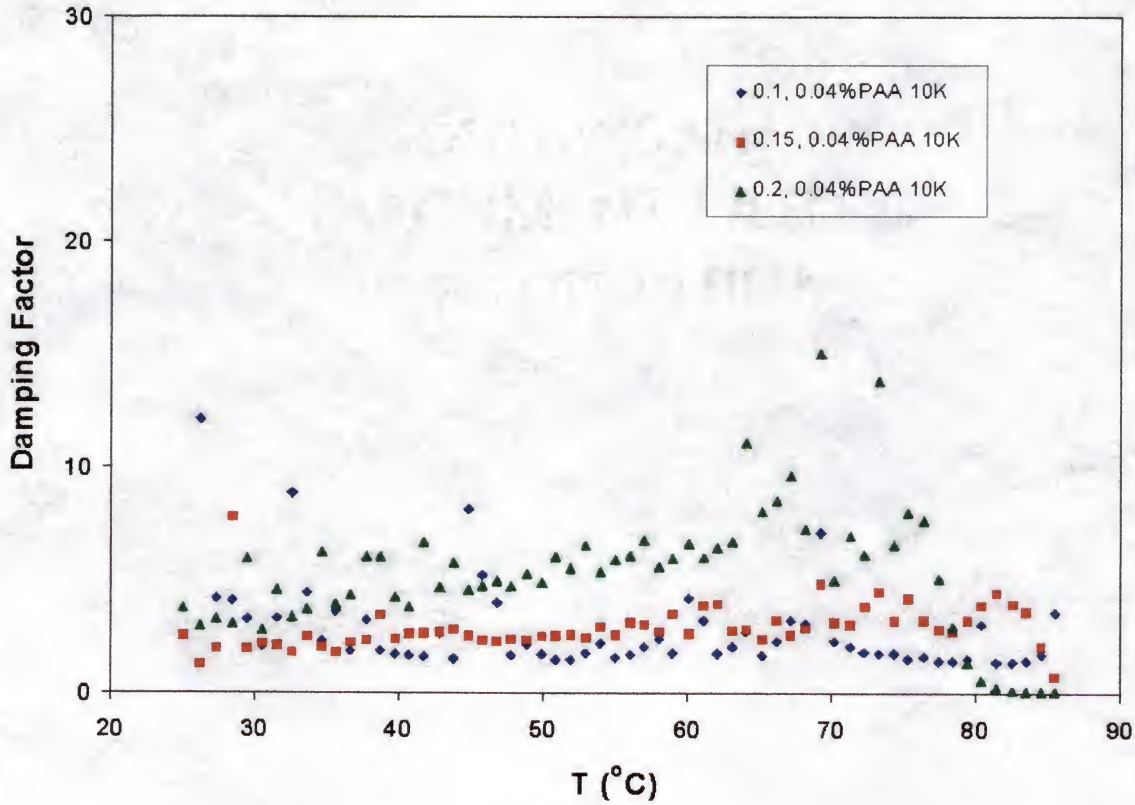

Fig.5-14. The corresponding damping factors to Fig.5-13.

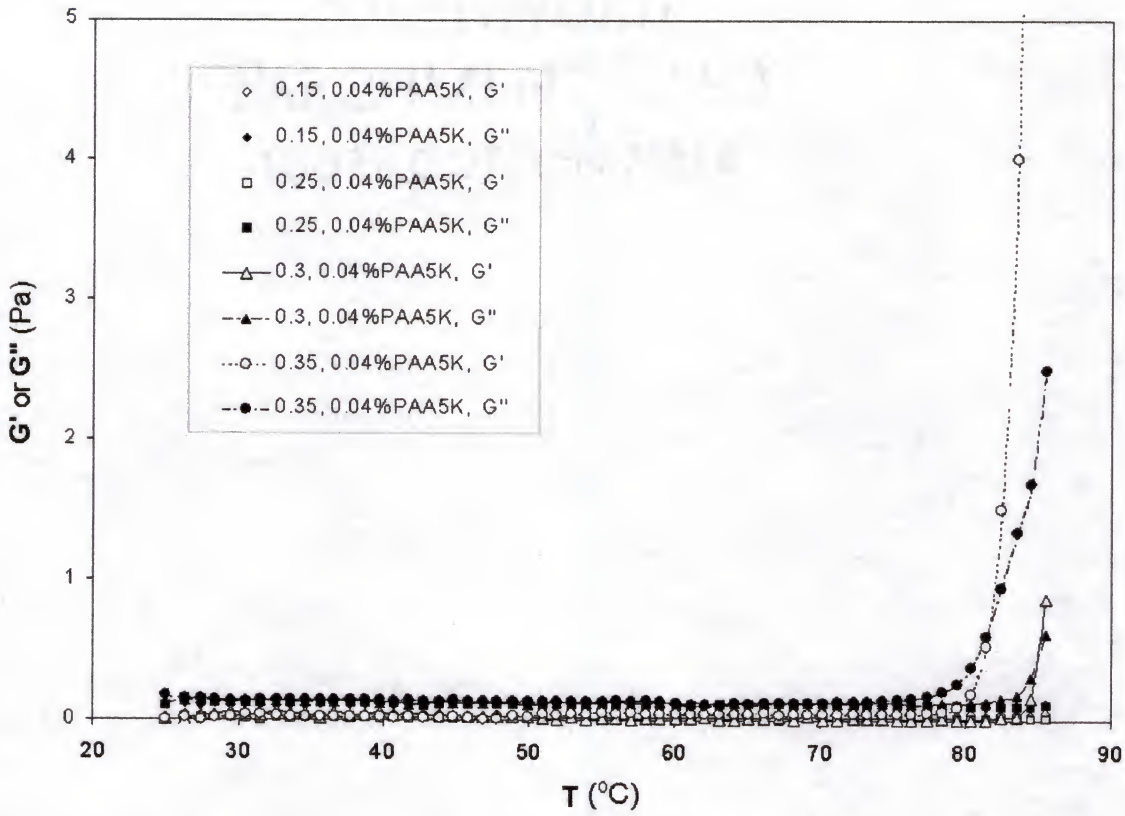

Fig.5-15. Variation of the shear modulus with temperature for the 0.04wt% PAA 5,000 addition suspensions. The volume fraction gelation threshold is about 0.3. Measurements are conducted at 1% strain and 1Hz, with a temperature ramp of 1 °C/min.

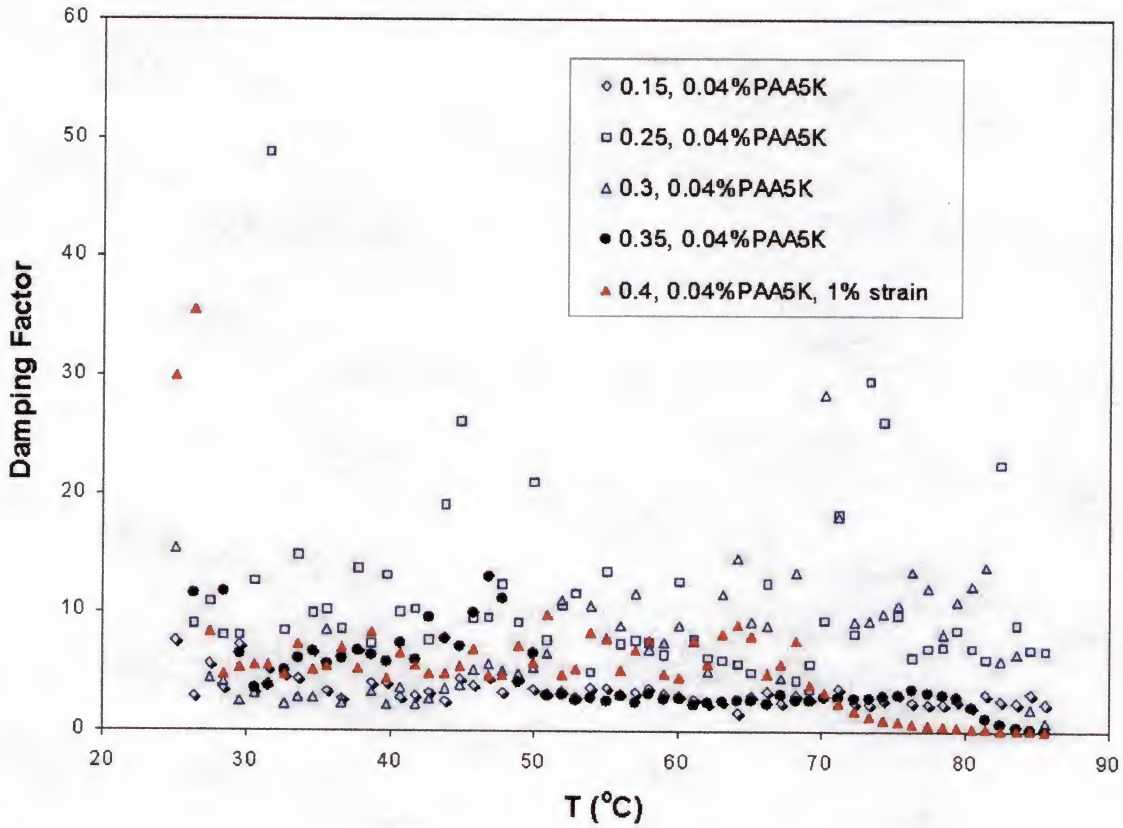

Fig.5-16. The corresponding damping factors to Fig.5-15.

5.4.2 Determination of the Percolative Microstructure Exponent, *s*

Considering the growth of the agglomerate flocs with temperature, the effective volume that is occupied by the growing flocs and the formation of percolation network will require determination of the percolative microstructure exponent. Change Eq. (6-7) to the following form:

$$G'(T, \phi_0) = G'_0(T) \cdot \{\phi_0 \cdot e^{-\Delta U / kT} \cdot e^{d_1 \cdot [d_2 + (T-T_0)/T_0]} / \phi_g - 1\}^s \qquad (6\text{-}8)$$

Take logarithm to both sides of the equation and we get

$$ln\, G' = s \cdot ln\, \{\phi_0 \cdot e^{-\Delta U / kT} \cdot e^{d_1 \cdot [d_2 + (T-T_0)/T_0]} / \phi_g - 1\} + ln(G'_0(T)) \qquad (6\text{-}9)$$

If this percolation model can reflect the intrinsic nature of the gelation for the TIF suspensions, plotting $\boldsymbol{ln}\ G' \sim ln\{\phi_0 \cdot e^{-\Delta U/kT} \cdot e^{d_1 \cdot [d_2 + (T-T_0)/T_0]} / \phi_g - 1\}$ should yield a straight line with slope, s, for all volume fraction suspensions when $\phi_0 > \phi_g$.

During the calculation and plotting, $\boldsymbol{ln}\{\phi_0 \cdot e^{-\Delta U/kT} \cdot e^{d_1 \cdot [d_2 + (T-T_0)/T_0]} / \phi_g - 1\}$ was denoted as $\boldsymbol{ln}\ \{x\}$ for simplicity. The volume fraction of the suspensions are varied from 0.3 to 0.5 with 0.04wt% PAA (Mw~50,000) addition. G' takes the measured storage modulus value at the same temperature as in the calculation of $\boldsymbol{ln}\ \{x\}$. ΔU, d_1, d_2 are fixed to values of – 50 eV, 1.3 and 0.1, respectively. The value used for ϕ_g was determined in section 5.4.1 of this Chapter. For example, ϕ_g is about 0.15 for the 0.04wt% PAA (Mw~50,000) addition alumina suspensions.

Figure 5-17 gives the results for the 0.04wt% PAA of Mw~50,000 addition suspensions while fixing T_0 = 30 °C. The value of T_0 can be estimated from the temperature dependence of the relative viscosity of the 40vol% alumina suspensions with 0.04wt% PAA addition (see Chapter 3). T_0 should be smaller than the critical temperature where the relative viscosity starts to increase, because only after the bridging flocs grow to a size large enough can they increase the suspension viscosity measurably. The variation of T_0 with PAA molecular weight is summarized and shown in Table 5-1. The data points below the line of $\boldsymbol{ln}\ G' = 0$ are those that do not fall in the percolative network region because the network does not yet form in the low temperature range. Therefore, these points are not counted. The points that are far above the line of $\boldsymbol{ln}\ G' = 0$ are those in which the percolation network has been formed at the respective temperature and volume fraction of particles. These points can be fitted to a straight line with slope of

about 4.6 and an intercept on the ***ln*** G' axis of – 4.0 when ***ln*** {x} = 0. Therefore, ***s*** ~ 4.6 and $\boldsymbol{ln}(G_0 \cdot e^{\beta T}) = -4.0$, or $G_0 \cdot e^{\beta T} \sim 0.02$ Pa.

Similar procedures are taken to treat the 0.04wt% PAA of Mw~10,000 and Mw~5,000 alumina suspensions, which are shown in Figure 5-18 and Figure 5-19. From the slopes of the ***ln*** G' ~ ***ln*** {x} plots and the intercept on the ***ln*** G' axis, the values of ***s*** and $G_0 \cdot e^{\beta T}$ are obtained and summarized in Table 5-1.

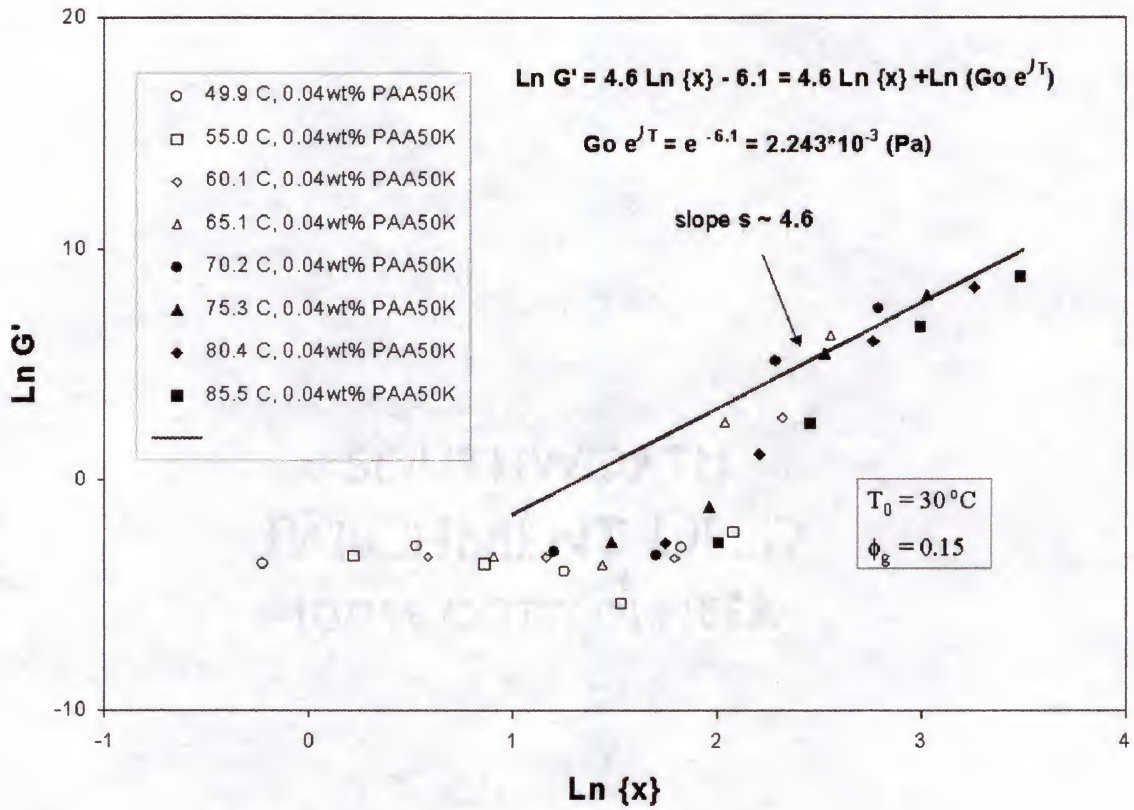

Fig.5-17. Exponent ***s*** determination for AKP53 alumina slurries with 0.04wt% PAA (Mw~50,000). Measurements are conducted at 1% strain, 1Hz, and a temperature ramp of 1 °C/min. The points below the line ***ln***G'= 0 are thought to be away from the formation of the percolation network. The volume fraction of the suspensions is varied from 0.3 to 0.5. The same type marks are for different volume fraction suspensions at the same temperature.

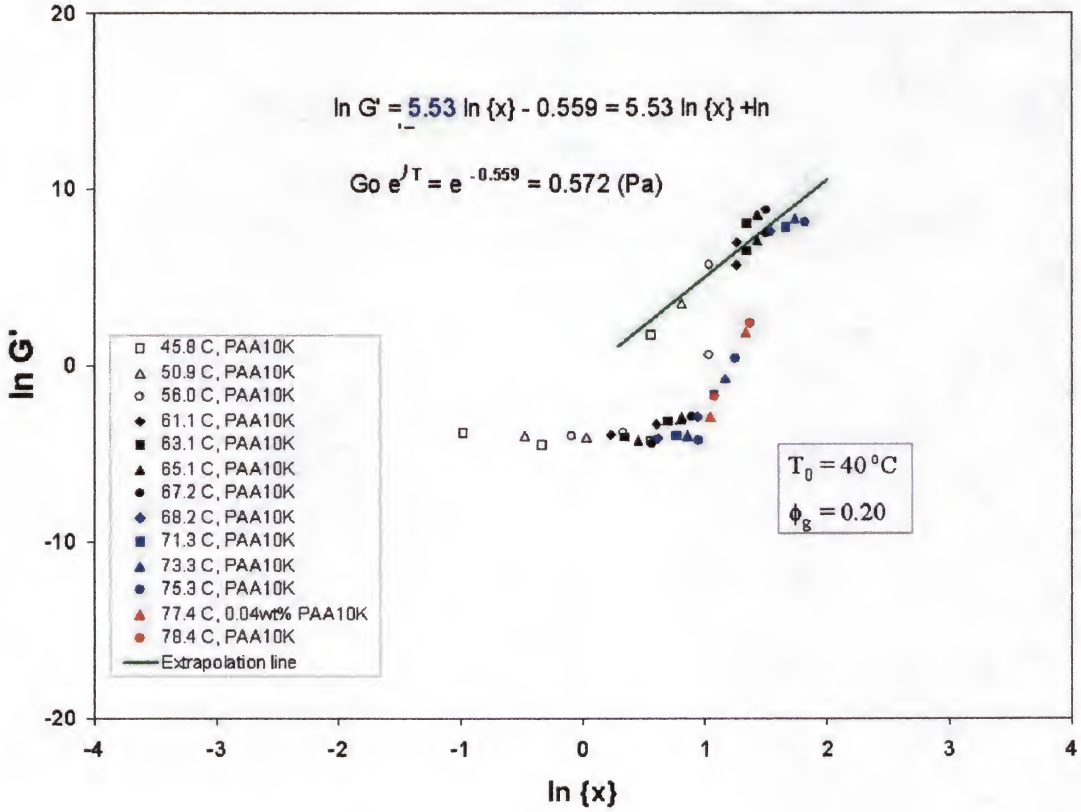

Fig.5-18. Exponent s determination for AKP53 alumina slurries with 0.04wt% PAA (Mw~10,000). Measurements are conducted at 1% strain, 1Hz, and a temperature ramp of 1 °C/min. The points below the line $\ln G' = 0$ are thought to be away from the formation of the percolation network. The volume fraction of the suspension is varied from 0.3 to 0.5. The same type marks are for different volume fraction suspensions at the same temperature.

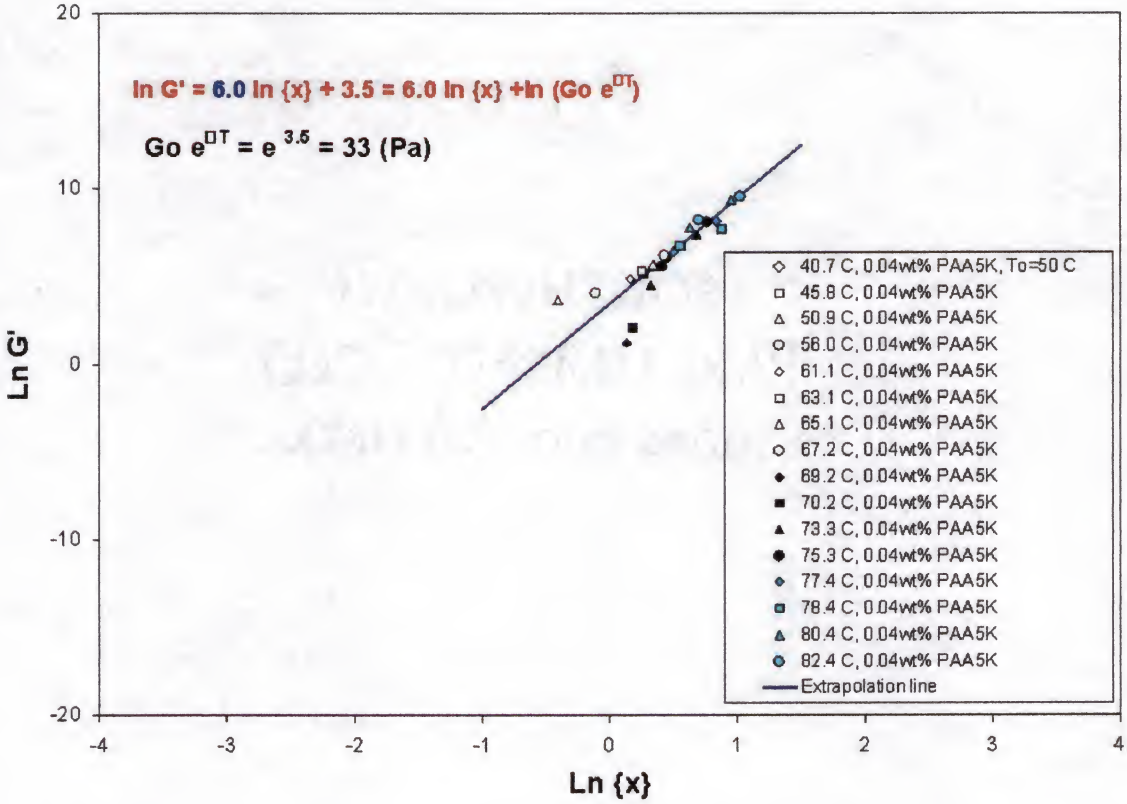

Fig.5-19. Exponent s determination for AKP53 alumina slurries with 0.04wt% PAA (Mw~5,000). Measurements are conducted at 1% strain and frequency of 1Hz, and a temperature ramp of 1 °C/min. T0 = 50 °C, ϕ_g=0.35. The points below the line ***ln***G'= 0 are thought to be away from the formation of the percolation network. The volume fraction of the suspension is varied from 0.3 to 0.5. The same type marks are for different volume fraction suspensions at the same temperature.

Table 5-1. Effect of PAA Molecular Weight on the Parameters in Eq. (5-5).

	PAA Mw~50,000	PAA Mw~10,000	PAA Mw~5,000
s	~ 4.6	~ 5.5	~ 6.0
G_0'	~ 0.02 Pa	~ 0.57 Pa	~ 33 Pa
ϕ_g	~ 0.15	~ 0.20	~ 0.35
T_0	~ 30 °C	~ 40 °C	~ 50 °C

The data in Table 5-1 illustrate that the values of all four parameters increase with decreasing PAA molecular weight. Large values of s are due to the percolative nature of particle networks [96-100]. Smaller s values with respect to the higher molecular weight of PAA reflect the weaker percolative nature in the suspensions, which might be due to the more significant effect of the interactions of polymer/particle instead of the particle/particle to form agglomerates during the percolative network formation. Therefore, lower molecular weight PAA addition suspensions exhibit a more significant percolative nature of particle networks. The larger ϕ_g value for PAA of Mw~5,000 addition suspensions also supports this conclusion because more particles are involved to form the particle percolation networks.

As mentioned in the introduction section of this chapter, G_0' is a reflection of the particle network stiffness and is expected to be positively related to the number density of polymer chains and the weight percent of polymer in the suspension.

T_0 increases with the decreasing of the PAA molecular weight for the same volume fraction alumina suspensions, which might be attributed to the smaller magnitude

of the polymer/particle interaction so that more thermal energy is required to overcome the repulsive energy barrier before the formation of bridging flocs.

The effect of the amount of PAA on the value of ***s*** was also studied. The results show that the ***s*** value decreases to ~ 4 for the 0.5wt% PAA 50,000 addition suspensions compared to ~ 4.6 for the 0.04wt% PAA 50,000 suspensions (Figure 5-20). The value of G_0' ($= G_0 \cdot e^{\beta T}$) increases by more than five times from ~ 0.02 Pa to ~ 0.12 Pa. Therefore, the value of $\mathbf{G_0 \cdot e^{\beta T}}$ increases with the amount of PAA in the suspensions, but the percolation network nature of the particles decreases with the increment of PAA addition, which is reflected by the decrease of the value of ***s***.

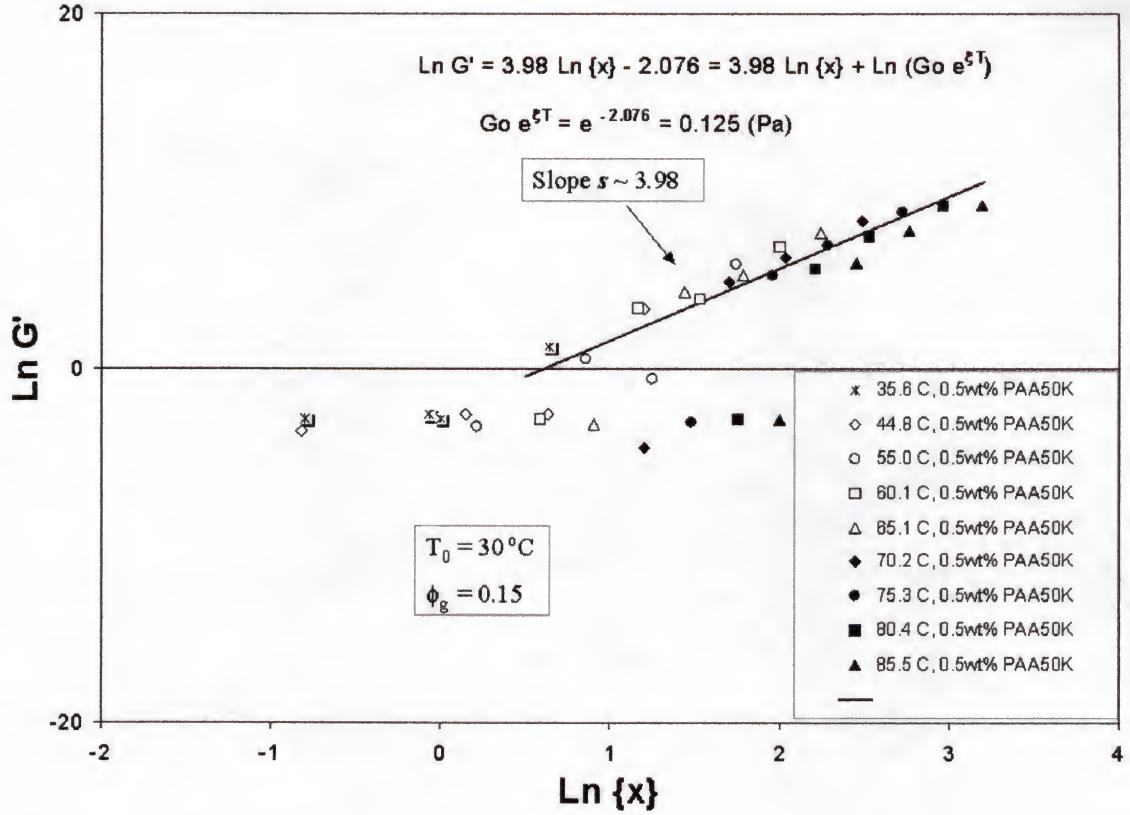

Fig.5-20. Exponent ***s*** determination for the AKP53 alumina slurries with 0.5wt% PAA (Mw~50,000). Measurements are conducted at 1% strain, 1Hz, and a temperature ramp of 1 °C/min. T0 = 30 °C, ϕ_g=0.15. The points below the line ***ln***G'= 0 are thought to be away from the formation of the percolation network. The volume fraction of the suspension is varied from 0.3 to 0.5. The same type marks are for different volume fraction suspensions at the same temperature.

5.5 Comparison of the Calculated and Experimental Results

5.5.1 Effect of Volume Fraction of Particles on the Storage Modulus, G'

Figure 5-21 shows both the calculated results using Eq. (5-5) and the measured data for the 0.04wt% PAA (Mw~50,000) addition alumina suspensions. The volume fraction of particles for each suspension is 0.3, 0.4 and 0.5, respectively. The parameters

shown in Table 1 were used for the calculations. The calculated results fit well with the measured data except at the "transition" region, which might be due to the disregard of the data points that is below the line of lnG' = 0 from Figure 5-17 to Figure 5-19.

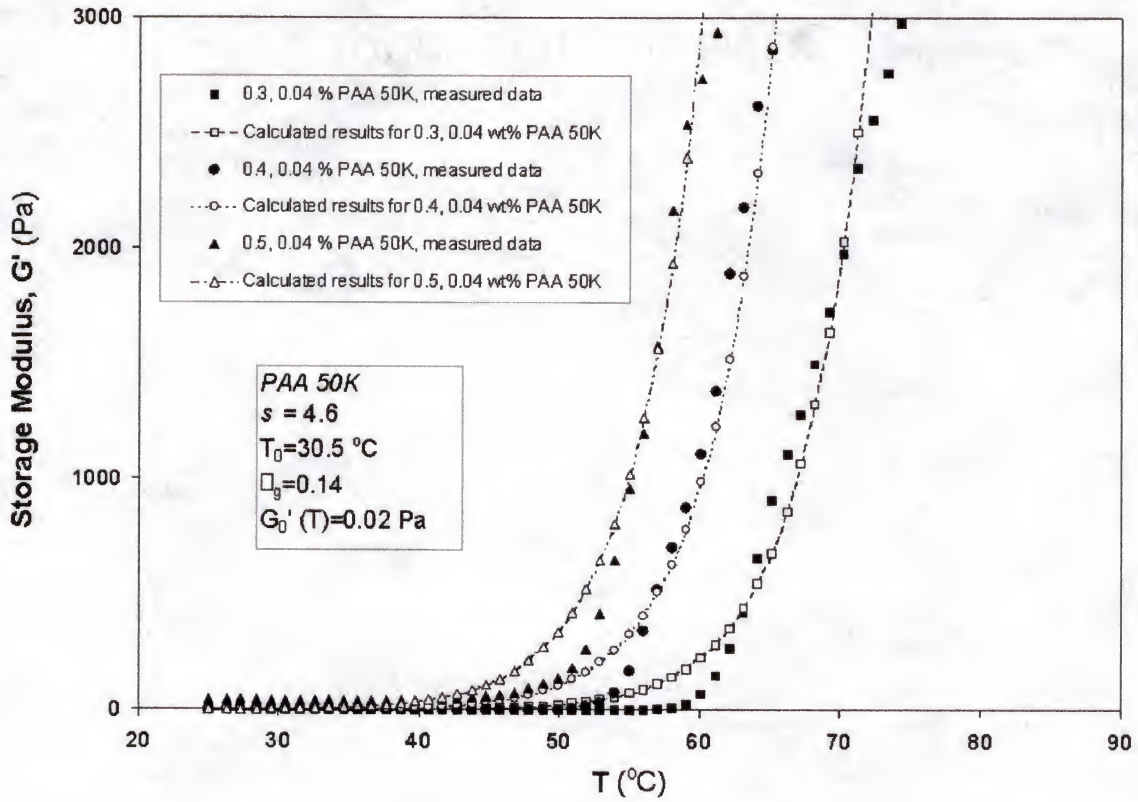

Fig.5-21. Comparison of the calculated data using Eq. (5-5) and the measurement results for 0.04wt% PAA 50,000 addition suspensions with variation in volume fraction of alumina. Measurements are conducted at 1% strain and 1Hz, and a temperature ramp of 1 °C/min. $s = 4.6$, $\phi_g = 0.14$, $T_0 = 30.5$ °C and $G_0' = 0.02$ Pa.

5.5.2 Effect of Molecular Weight of PAA on the Storage Modulus, G'

Figure 5-22 shows how the molecular weight of PAA affects the storage modulus of the 0.4 volume fraction alumina suspensions with 0.04wt% PAA addition. The calculated results for each composition suspensions are also shown as open symbols and solid lines. During the calculation, small variation is made to some parameters that are

shown in Table 5-1. These fitting parameters are summarized in Table 5-2. These adjustments are due to the rough nature of the obtained values in Table 5-1. The calculated results using the adjusted parameters fit the experimental data well in the whole temperature range.

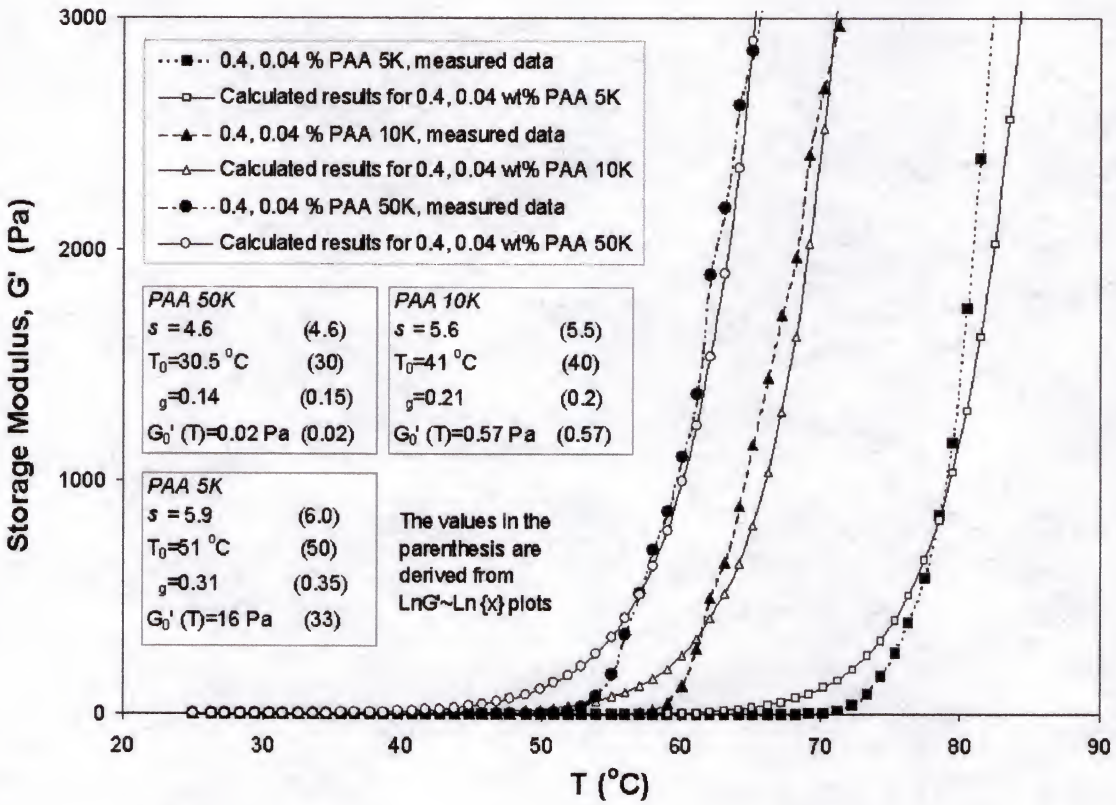

Fig.5-22. Comparison of the calculated data using Eq. (5-5) and the measurement results for 0.4 volume fraction alumina suspensions with variation in molecular weight of PAA. Measurements are conducted at 1% strain, 1Hz, and a temperature ramp of 1 °C/min.

Although our expanded percolation theory model is a good approximation for the temperature dependence of the storage modulus for the actual TIF suspensions, other aspects concerning the detailed evolution of the suspension microstructure should be addressed in order to have a full understanding of the TIF suspensions. For example,

how the agglomerates form and how they interact with each other to form a continuous percolation network, and how to relate this to the time scale.

Table 5-2. The Fitting Parameters Used for Calculations in Fig.5-21 and Fig.5-22.

	PAA Mw~50,000	PAA Mw~10,000	PAA Mw~5,000
s	**4.6**	**5.6**	**5.9**
G_0'	0.02 Pa	0.57 Pa	**16 Pa**
ϕ_g	**0.14**	**0.21**	**0.31**
T_0	**30.5 °C**	**41.0 °C**	**51.0 °C**

5.5.3 Prediction of the Wet Gelled Body Strength Using the Expanded Percolation Model

From above discussions, it can be realized that this expanded percolation model may be used to predict the strength of the wet gelled body. Figure 5-23, Figure 5-24 and Figure 5-25 illustrate the variation of the calculated storage modulus with volume fraction of particles and temperature for PAA addition alumina suspensions with different molecular weights. The parameters used in calculations are shown in Table 5-2.

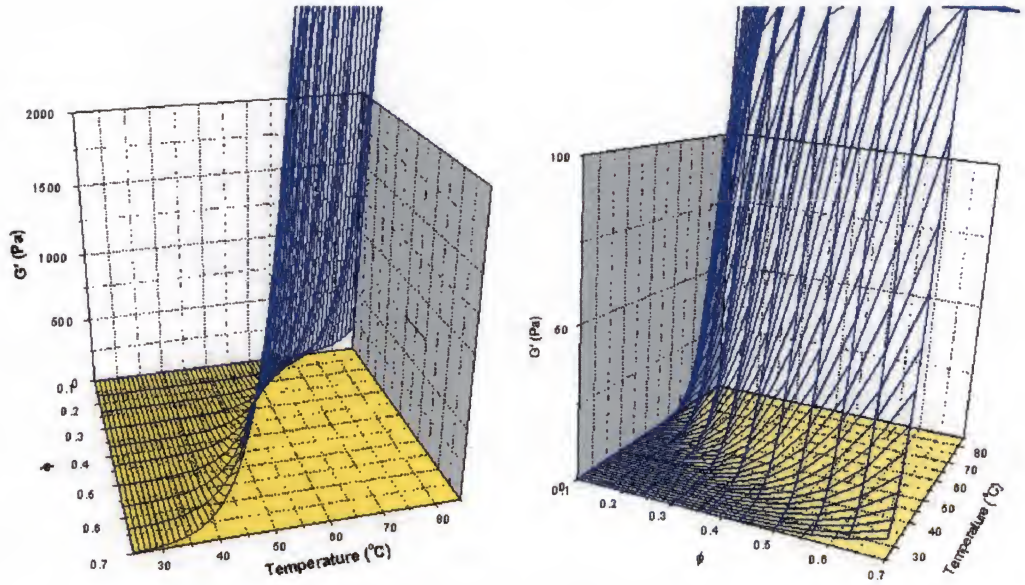

0.04 wt% PAA 50000 addition

$\Phi_g \sim 0.14$, $T_0 \sim 30°C$, s~4.6

Fig.5-23. Three-dimensional plots that relate storage modulus with volume fraction of alumina and the temperature for the 0.04wt% PAA 50,000 addition alumina suspensions. Eq.(5-5) is used for calculations. Two views of the same plot are shown.

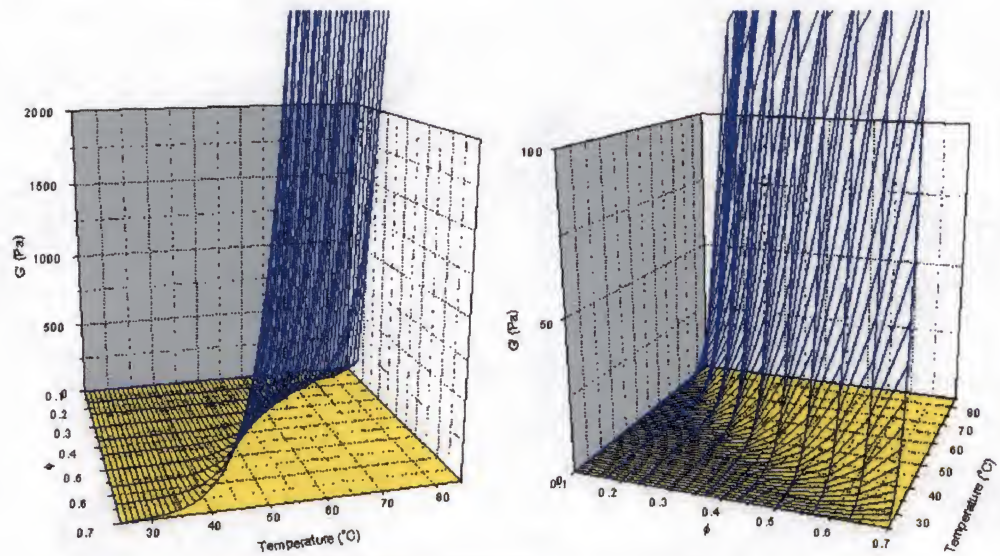

0.04 wt% PAA 10000 addition

$\Phi_g \sim 0.21$, $T_0 \sim 41°C$, s~5.6

Fig.5-24. Three-dimensional plots that relate storage modulus with volume fraction of alumina and the temperature for the 0.04wt% PAA 10,000 addition alumina suspensions. Eq.(5-5) is used for calculations. Two views of the same plot are shown.

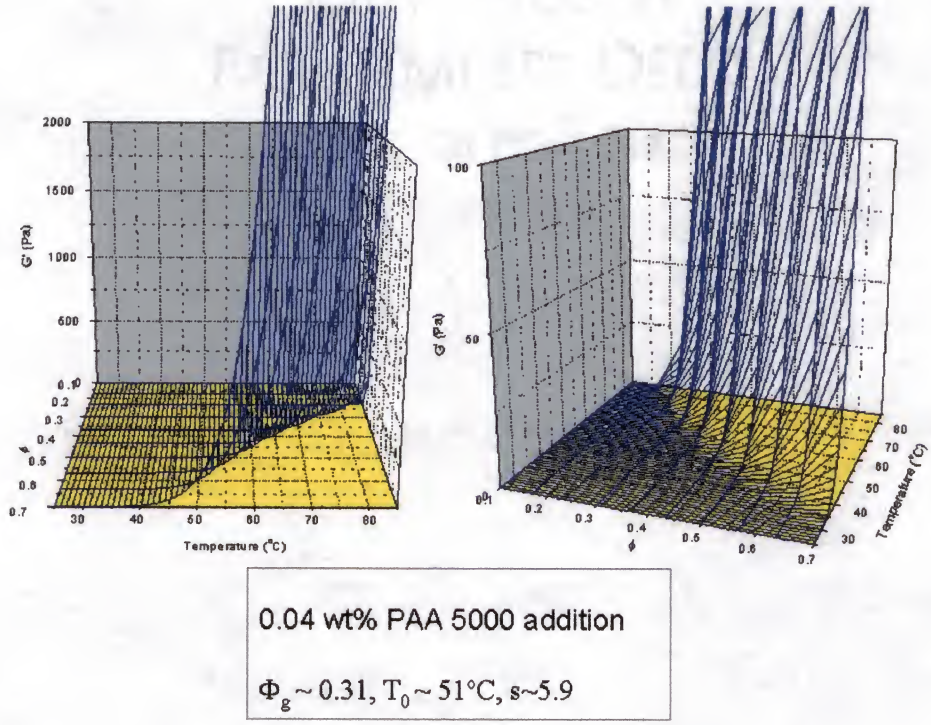

0.04 wt% PAA 5000 addition

$\Phi_g \sim 0.31$, $T_0 \sim 51°C$, s~5.9

Fig.5-25. Three-dimensional plots that relate storage modulus with volume fraction of alumina and the temperature for the 0.04wt% PAA 5,000 addition alumina suspensions. Eq.(5-5) is used for calculations. Two views of the same plot are shown.

5.6 Schematic Drawings of the Possible Percolation Network Formation Process

From the above modeling results and the experimental data, it is clear that the molecular weight of PAA will affect the percolation nature and the volume fraction gelation threshold. The higher volume fraction of particles will increase the stiffness of the backbones of the percolation network. The possible temperature dependence of the percolation network formation process is schematically shown in Figure 5-26 and Figure 5-27 (showing the effect of PAA molecular weight), Figure 5-28 and Figure 5-29 (showing the effect of volume fraction of particles).

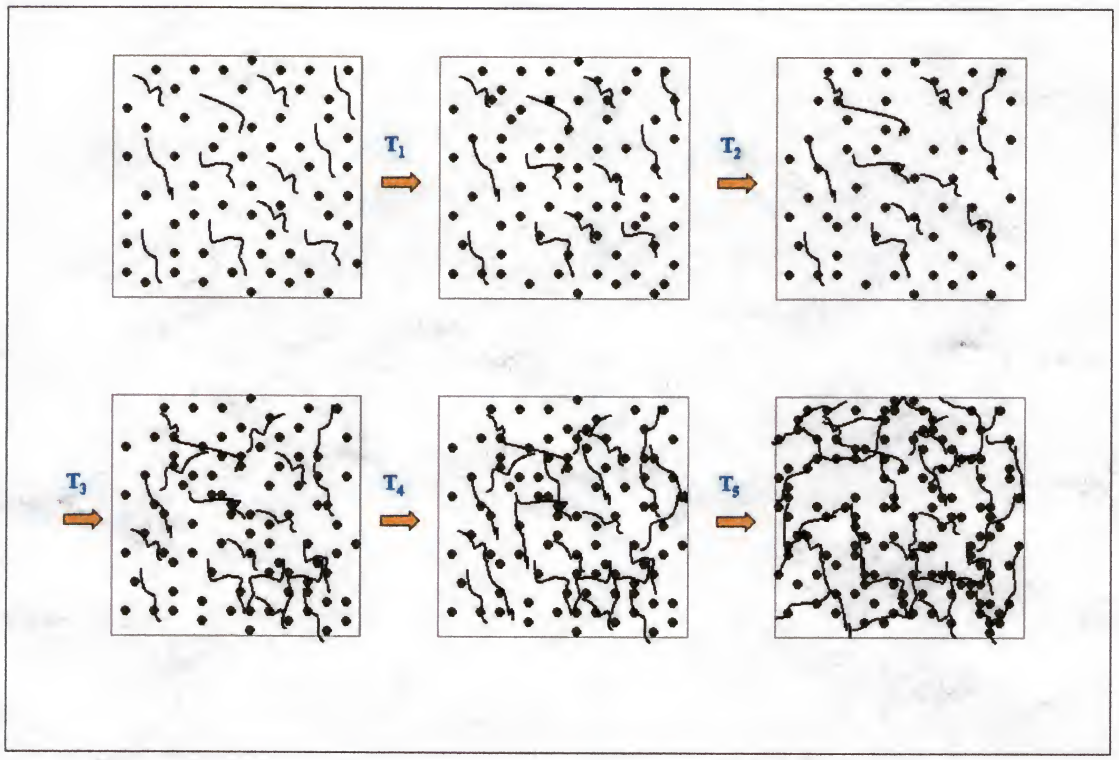

Fig.5-26. Schematic drawing of the percolation network formation process for TIF suspensions having larger Mw PAA. The size of the PAA molecular chains and distance between particles are exaggerated for clarity.

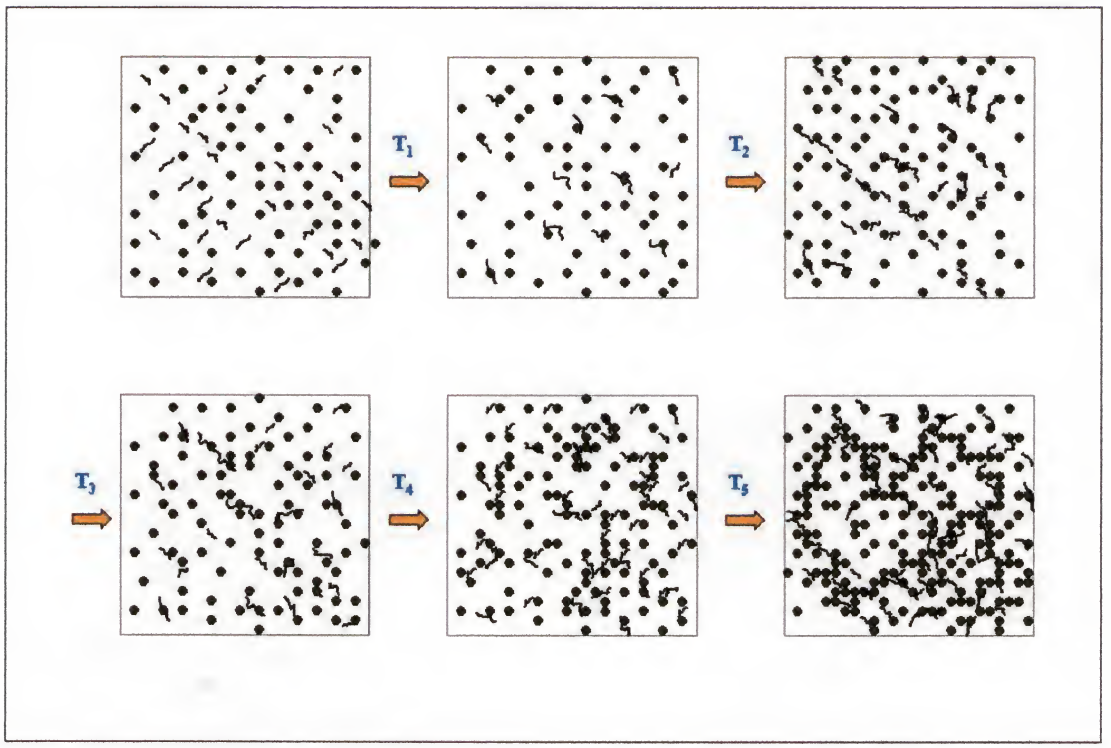

Fig.5-27. Schematic drawing of the percolation network formation process for TIF suspensions having smaller Mw PAA. The size of the PAA molecular chains and distance between particles are exaggerated for clarity.

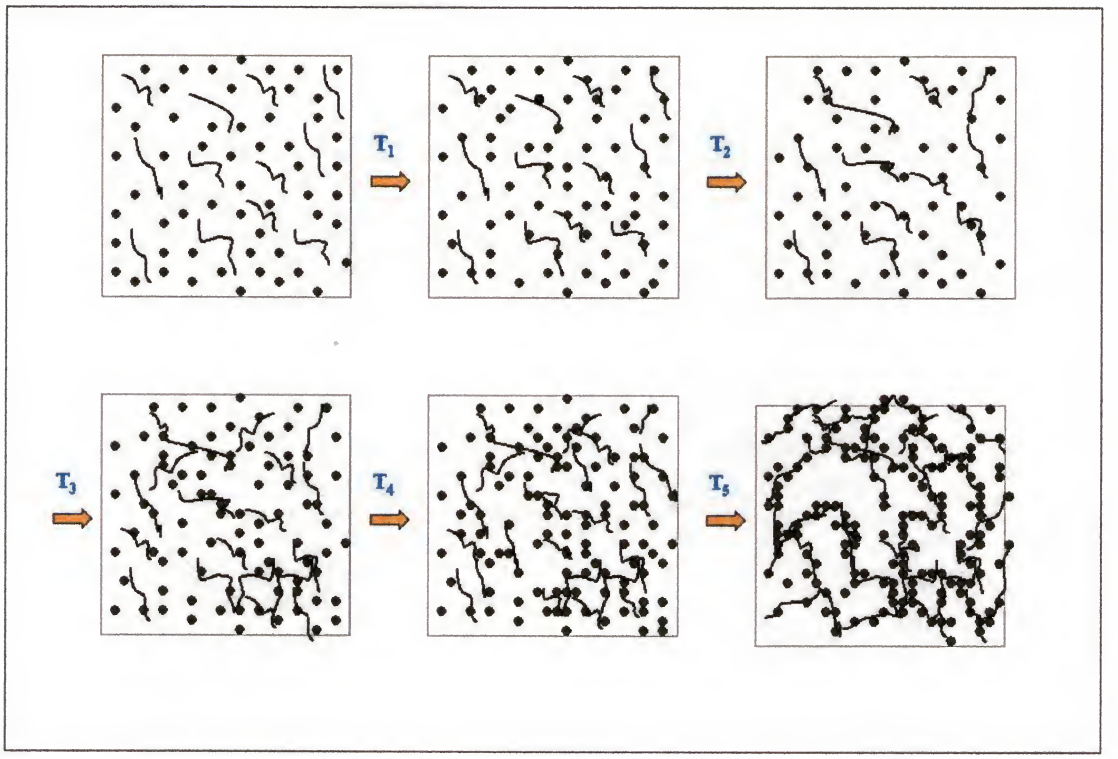

Fig.5-28. Schematic drawing of the percolation network formation process for lower volume fraction TIF suspensions with PAA addition. The size of the PAA molecular chains and distance between particles are exaggerated for clarity.

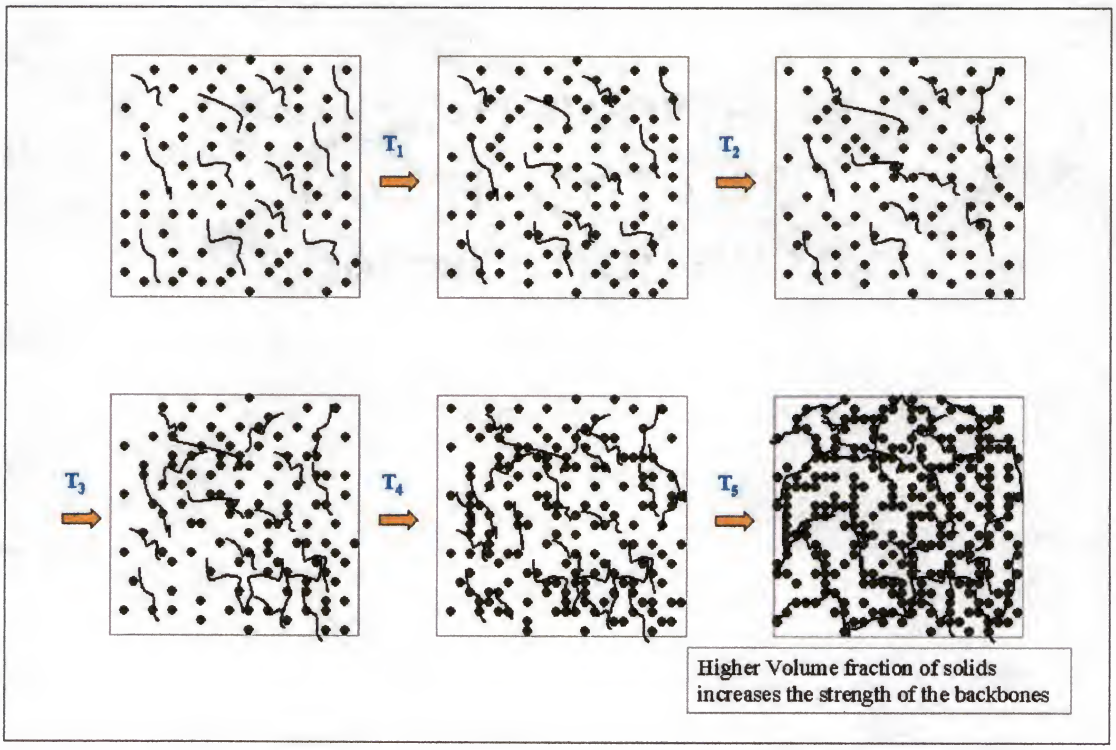

Fig.5-29. Schematic drawing of the percolation network formation process for higher volume fraction TIF suspensions with PAA addition. The size of the PAA molecular chains and distance between particles are exaggerated for clarity.

5.7 Summary of This Chapter

Continuous percolation theory model is established to interpret the evolution of the storage modulus with temperature for the TIF alumina suspensions. Realizing that the effective volume fraction of particles will increase with temperature because of the growth of the agglomerate, a model that relates the storage modulus with temperature and volume fraction of solids is proposed.

Calculated results using this model show that the storage modulus of the suspensions increases with the volume fraction of solids and temperature. The increment of the volume fraction gelation threshold, ϕ_g, decreases the magnitude of the storage modulus. The characteristic temperature T_0 also has significant influence on the calculated value of storage modulus using this model. It is anticipated that ϕ_g and T_0 are always related to each other with respect to the composition of the suspensions. The description of the temperature dependence of the storage modulus for the actual alumina suspensions can be realized by tailoring the specific parameters in this model.

The exponent, s, and the volume fraction gelation threshold, ϕ_g, are derived from experimental data for the PAA containing TIF alumina suspensions. For the same amount of PAA addition, increasing molecular weight of PAA decreases the values of s, ϕ_g and T_0 at the same time. The decrease of the particle percolation nature might be due to the stronger interaction of PAA chains/particles for larger molecular weight PAA.

This model is used to compute the variation of the storage modulus with the volume fraction of solids, and the variation of the storage modulus with the molecular weight of PAA for the 40vol% alumina suspensions. The calculated results using the experimental derived parameters match the measurement data well except at transition region.

CHAPTER 6
STUDY OF THE CONCENTRATED PAA-FREE TIF ALUMINA AQUEOUS SUSPENSIONS

6.1 Theoretical Approach to Design the Composition of the Suspensions

Results in Chapter 3, 4 and 5 show that PAA is a critical component in the alumina suspensions to bring about bridging flocculation and make it gel with applied heat. It is also clear that PAA addition significantly increases the room temperature shear viscosity at the same time. The industry requires higher slurry loading suspensions with relatively low shear viscosity at room temperature so that the suspensions can fill the molds during direct casting or can be deposited from a drop-on-demand nozzle. The results show that not only does an increase in PAA amount and molecular weight increase the shear viscosity, but higher slurry loading increases the viscosity according to the Dougherty-Krieger equation, which is described in Chapter 3. When the slurry loading is above 50vol% for the 0.04wt% PAA addition, for example 60vol% of alumina, the zero shear rate viscosity at room temperature is > 20 Pa·s and that the suspension does not flow easily. An alternative route must be found to overcome this obstacle. In this chapter, a new approach using the DLVO concept is proposed to avoid using PAA in the alumina suspensions while keeping a similar gelation behavior.

DLVO theory proposes that either at high concentrations of counterions, where the layer of counterions is very thin, or near the isoelectic point, where the number density of charged surface sites is small, the particles in the suspension will become

attractive. The dominance of the attractive van der Waals potential will cause the suspension to flocculate. The flocculation of the suspension can be accelerated when the counterions are bivalent or trivalent metal ion complex, which will result in the compression of the double-layer thickness. The thickness is commonly identified with the Debye length, which is the inverse of the Debye parameter, κ:

$$1/\kappa = (\varepsilon\varepsilon_0 \, kT / I)^{1/2} \quad \text{(for 1:1 electrolyte)} \qquad (6\text{-}1)$$

$$I = e^2 \sum (n_i \, z_i^2) \qquad (6\text{-}2)$$

Where e is the electronic charge, n_i the concentration of ions with charge z_i, ε the dielectric constant of the liquid, and ε_0 the permittivity of a vacuum [55,101,102].

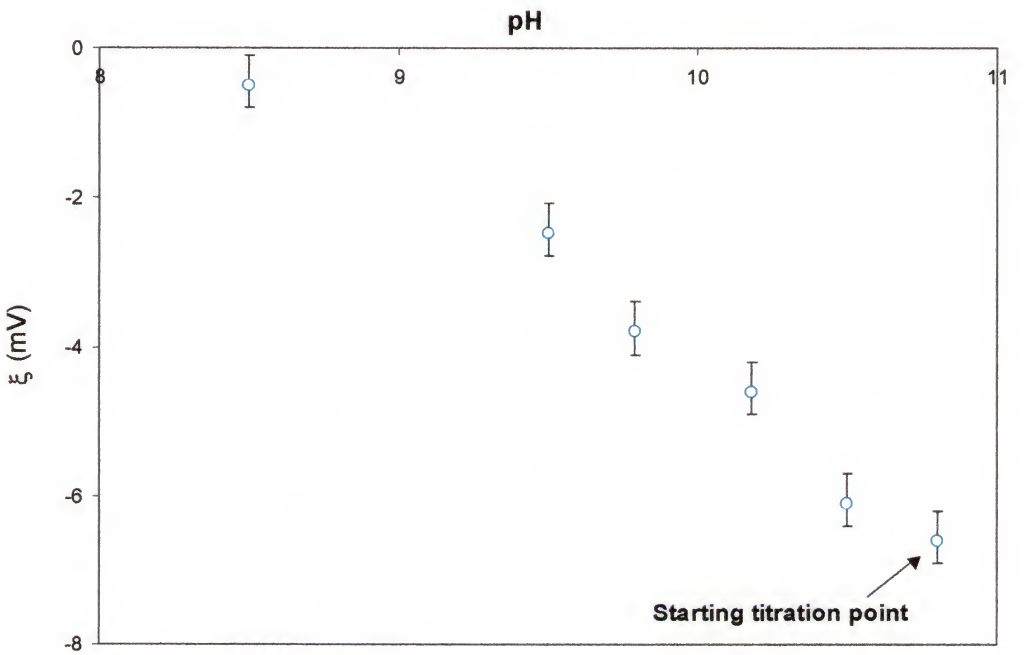

Fig.6-1. Variation of ξ potential with pH for the 3vol% magnesium citrate powders only. The titration is conducted from pH10.8 to pH8.5 using 1N HCl acid. The surface ξ Potentials become absolutely smaller when the pH of the suspension decreases.

Magnesium citrate powder is found to carry negative surface charge at high pH region (Figure 6-1) and dissolves in water when the pH is decreased, which in turn increases the ionic strength in the suspension. Another advantage of this chemical is that the resulting magnesium ion can be a sintering aid for alumina. Therefore, magnesium citrate powder is chosen as a substitute material for PAA.

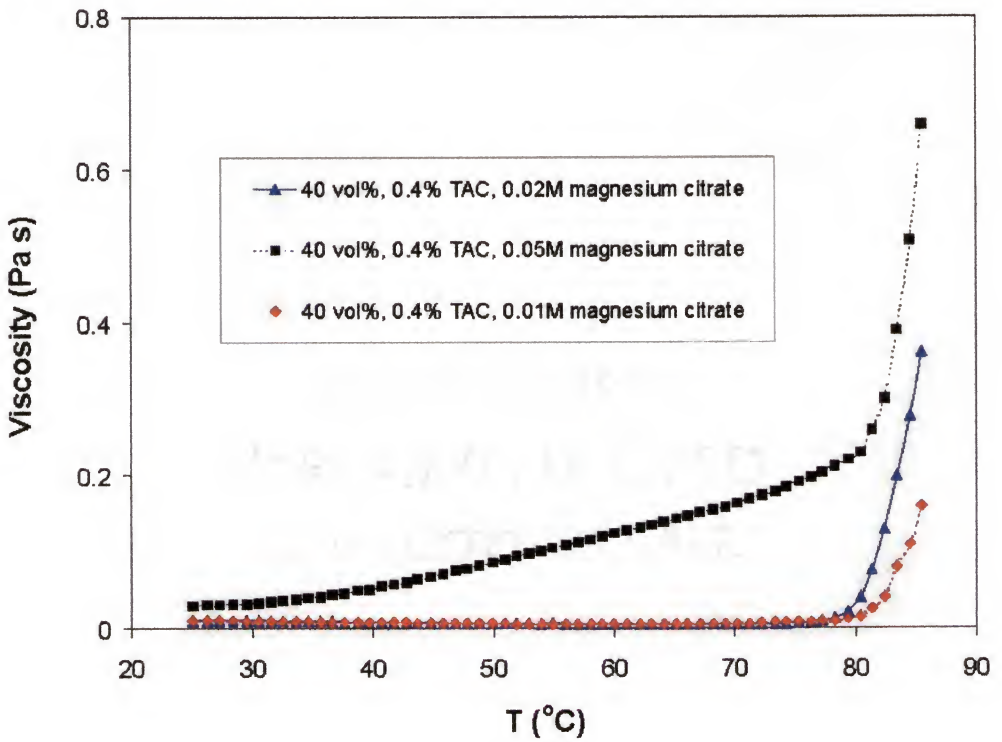

Fig.6-2. The effect of the amount of magnesium citrate on the temperature dependence of the viscosity of the 40vol% AKP53 alumina suspensions. Measurements are conducted at shear rate 20 s^{-1} with temperature ramp of 1 °C/min.

6.2 Temperature Dependence of the Shear Viscosity

6.2.1 Effect of the Amount of Magnesium Citrate

Figure 6-2 shows the variation of the viscosity of the 40vol% AKP53 alumina suspensions with temperature and the amount of the magnesium citrate. It can be seen that the viscosity start to increase when the temperature is above 80 °C for the 0.01M (molar per liter) and 0.02M magnesium citrate addition suspensions. But before 80 °C, the suspension viscosity decreases at the beginning similar to the PAA addition suspensions, which might be due to the viscosity decrease of water with temperature. But for the suspension with 0.05M magnesium citrate, its viscosity increases from 30 °C. The difference might be due to the formation of weak agglomerates in the suspension when the amount of magnesium citrate powders is large, which has a negative ξ potential value less than 8 mV at pH>10.5. When the shear rate increases, these weak agglomerates can be broken up so that the suspension shows shear thinning behavior, as shown in Figure 6-3. The degree of shear-thinning increases with the amount of magnesium citrate.

6.2.2 Effect of the Volume Fraction of Alumina

Figure 6-4 shows the effect of volume fraction of alumina on the temperature evolution of the viscosity for suspensions with 0.02% magnesium citrate. In the figure, the data of the 60vol% alumina suspension with 0.4wt% TAC is also shown. It is obvious that increasing of the volume fraction of alumina can increase the suspension viscosity at a relatively low temperature. For example, the temperatures where the slurry viscosity

starts to increase significantly are at about 80 °C, 70 °C and 55 °C for the 40vol%, 50vol% and 60vol% suspensions, respectively. It can also be observed that a higher volume fraction of alumina yields a higher viscosity, which might be the result of overlapping of the electric double layer.

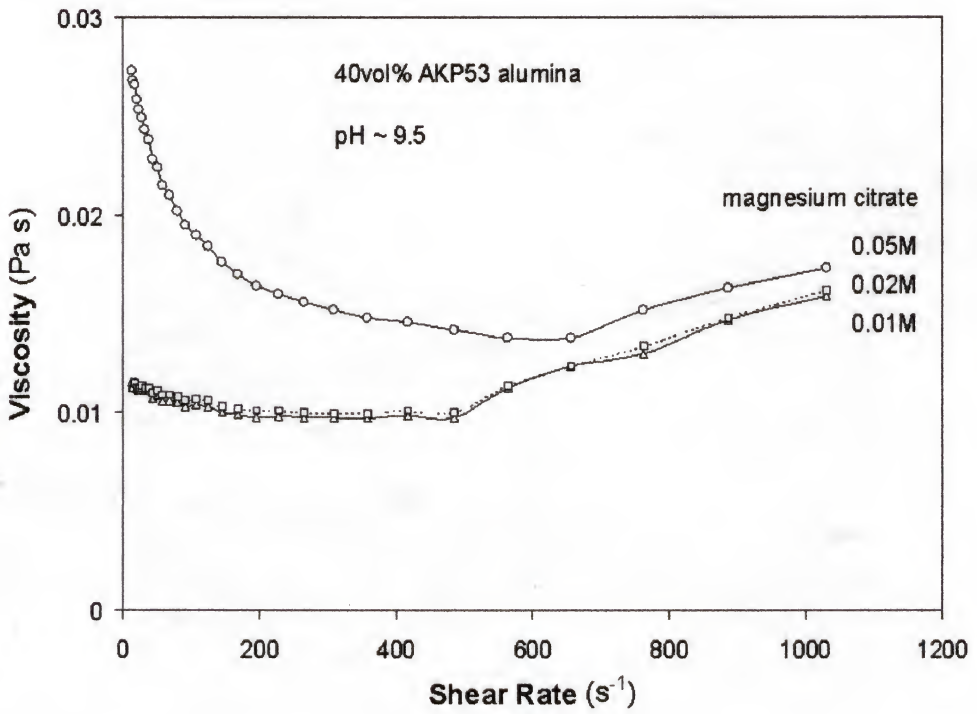

Fig.6-3. Steady shear flow of the magnesium citrate addition 40vol% alumina suspensions. All three suspensions show shear-thinning behavior at low shear rate.

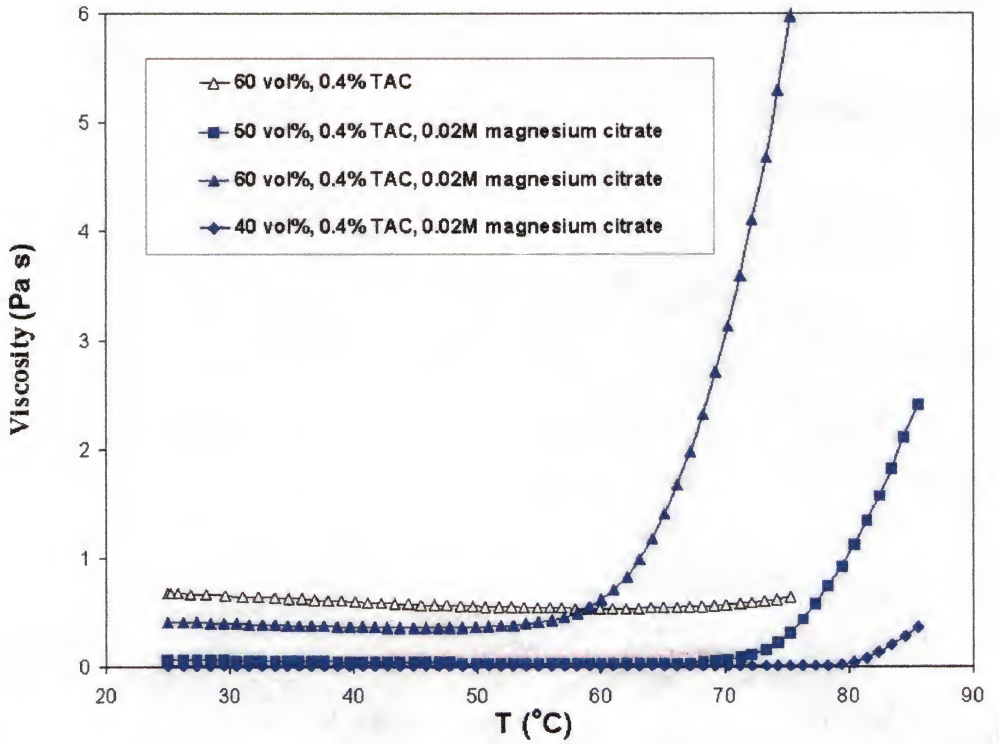

Fig.6-4. Effects of volume fraction of alumina and temperature on the viscosiy of the suspensions with 0.02M magnesium citrate. Measurements are conducted at shear rate 20 s^{-1} with temperature ramp of 1 °C/min.

6.3 Mechanism of Agglomerates Formation

In the as-prepared suspensions, the surface potential of the pure magnesium citrate powder is less than negative 8mV at pH > 10 (Figure 6-1). Even though the magnitude is low, a small amount of magnesium citrate can still form stable suspensions with alumina particles, which has a negative zeta potential with absolute value >50mV. When the temperature is raised, the pH value of the suspensions starts to decrease, as is shown in Figure 6-5. The pH decrease might be due to the increasing dissolution of

alumina with temperature [56,88]. It is also observed that during the pH measurements, agglomerates starts to form at ~ 60 °C, which is correspondent to a pH value of about 8.8.

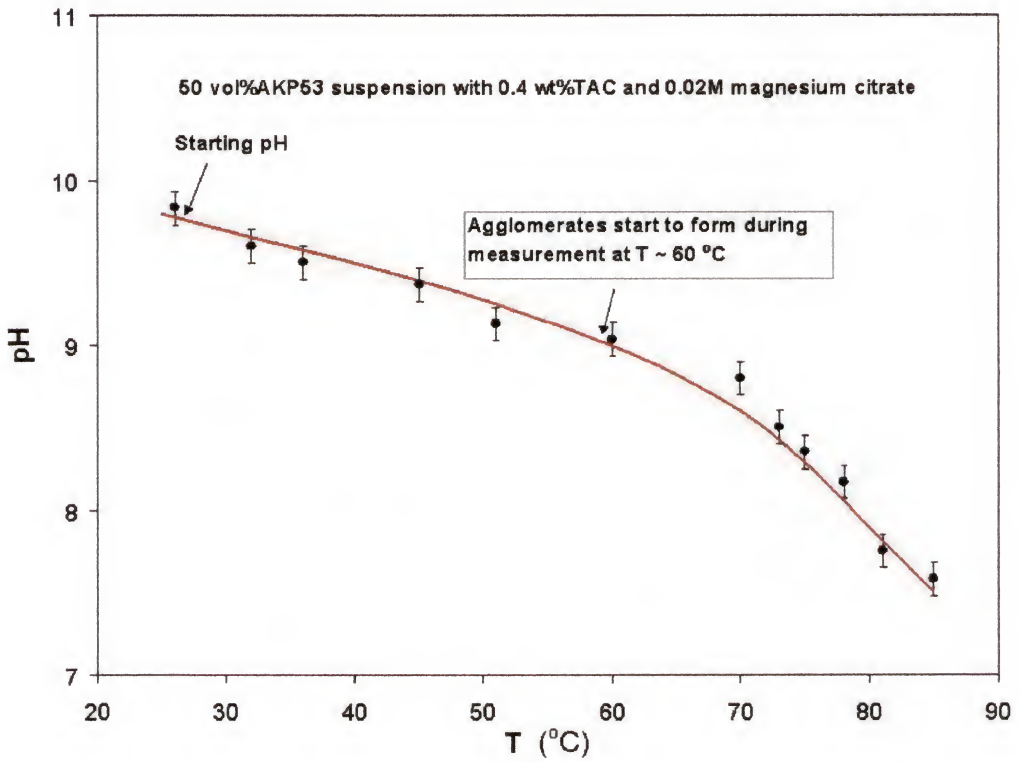

Fig.6-5. Variation of pH with temperature for 50vol% alumina suspension with 0.4wt% TAC and 0.02M magnesium citrate. The initial pH of the suspension is ~ pH10.

The next question is whether the dispersion behavior of the pure magnesium citrate powder varies with pH, because the pH of the suspension decreases with increasing temperature. Figure 6-6 shows the pH dependence of the conductivity for the pure magnesium citrate powder suspensions during titration in an electrophoresis measurement. It can be seen that the conductivity of the suspension increases from pH10 to pH8, indicating that reactions have happened on the magnesium citrate powder surface

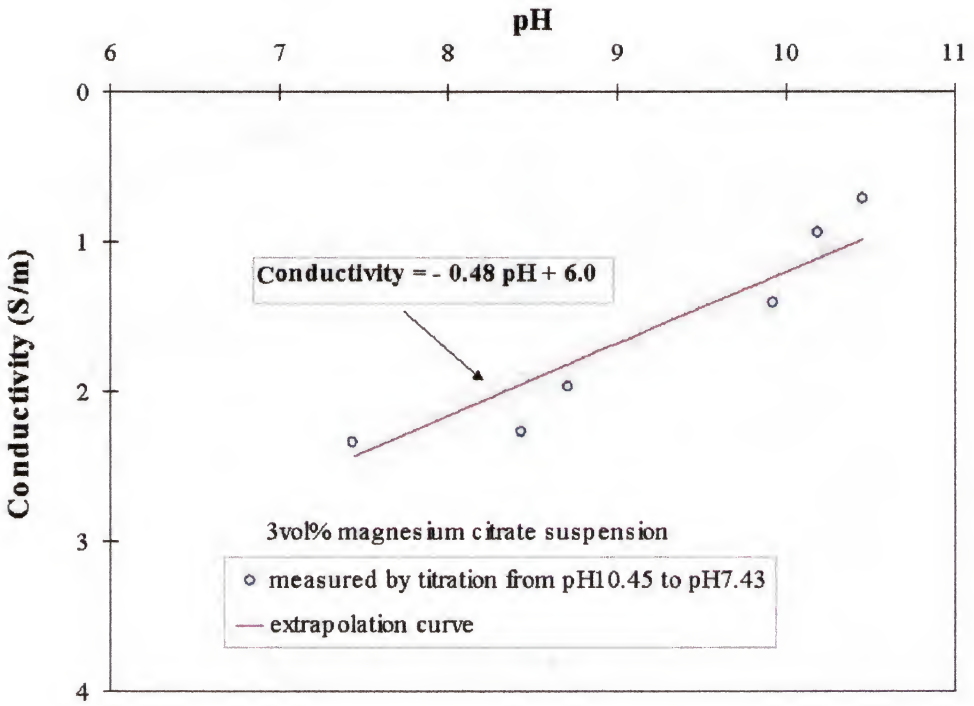

Fig.6-6. The pH dependence of the conductivity for the 3vol% magnesium citrate powder suspensions during titration of the electrophoresis measurement.

with decreasing pH to alter the surface charge complex configurations. The possible reactions might be:

(1) Adsorption of H^+ on the charged magnesium citrate powder:

$$M_gC_6H_5O_7^- + H^+ \rightarrow M_gC_6H_6O_7(OH)_x \qquad (6\text{-}3)$$

(2) Ionization and dissolution of magnesium citrate powder:

$$M_gC_6H_6O_7(OH)_x + 2H^+ \rightarrow M_g^{2+} + C_6H_8O_7 + H_2O \qquad (6\text{-}4)$$

It is noticed that the dissolution reaction did happen and magnesium citrate powders dissolved gradually into water with the increasing acidity in the solution. Since this reaction is directly connected to the ionization reaction, these reactions should yield an increasing concentration of magnesium ions in the suspensions.

To verify this assumption, the variation of the magnesium ion concentrations with the pH of the suspension is measured. These results are shown in Figure 6-7. The measurement data illustrate that the magnesium ion concentration increases with decreasing pH from pH10. This result reflects that the ionization reaction (6-4) takes place in the suspensions with decreasing pH and yields the increase of the ionic strength in the suspensions with temperature. By DLVO theory, this ionic strength increment might compress the EDL thickness and make it possible that the interparticle distance fall into the primary minimum to cause flocculation of the suspension. The continuous increase of viscosity with temperature might be due to the growth of the flocculated aggregates, which will increase the resistance of the movement of water molecules under shear rate.

6.4 Reducing the Low Shear Rate Viscosity by Magnesium Citrate

Figure 6-8 gives the steady shear flow curves for the 0.02M magnesium citrate addition suspensions with different volume fractions of alumina. The 60vol% suspension with 0.4% TAC, and the 60vol% suspension with 0.4% TAC and 0.04% PAA (Mw~50,000) are also shown. It seems that the suspension shows more shear-thinning behavior when the volume fraction of particles is increased, and no shear thickening is observed in the experiment shear rate range for the 50vol% and 60vol% suspensions with

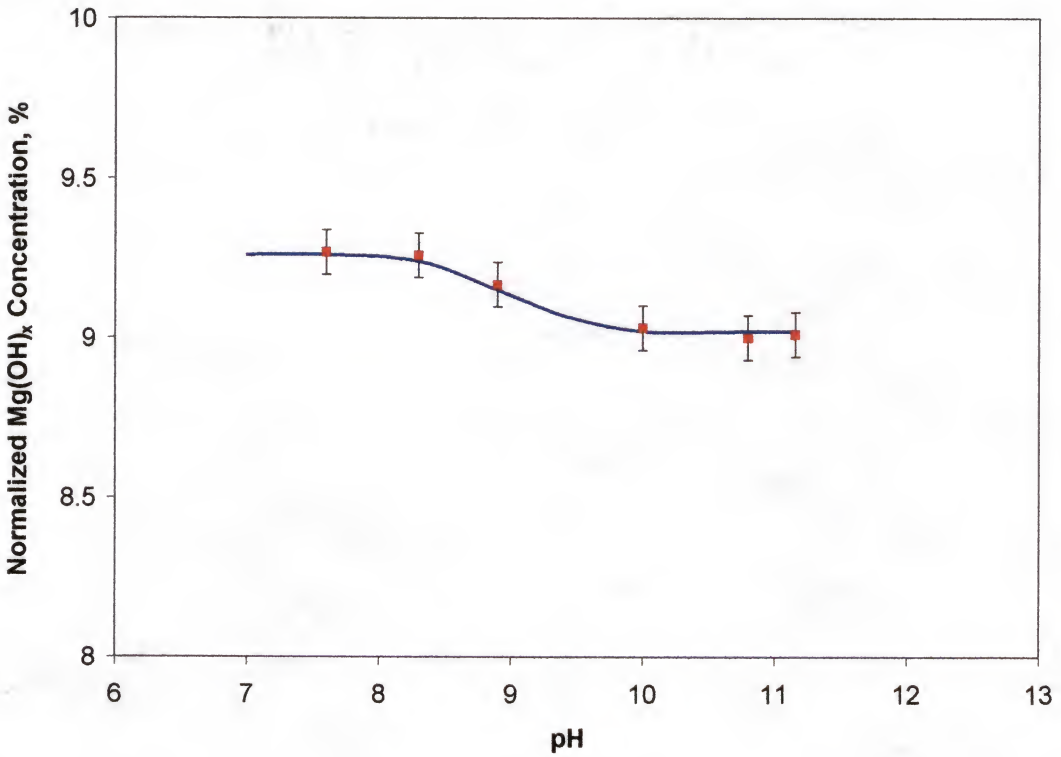

Fig.6-7. Variation of the concentration of $Mg(OH)_x$ ion with pH for the pure magnesium citrate powder suspension. The normalized concentration is defined as the ratio of the measured concentration of Mg ions to that of the initial amount of the magnesium citrate. The Mg ion concentration in the supernatant is measured by using ICP Emission Spectroscopy (PERKIN ELMER, Optima 3200 RL).

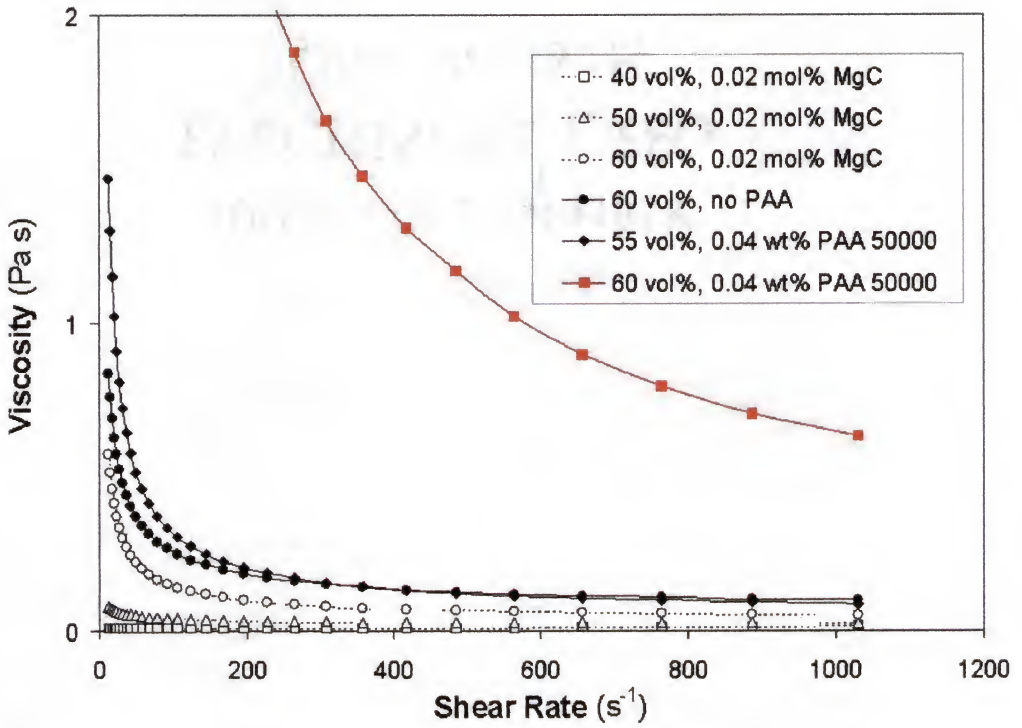

Fig.6-8. Steady shear flow curves for the 0.02M magnesium citrate addition suspensions with different volume fraction of alumina. The 60vol% suspension with 0.4% TAC only, and the 60vol% suspension with 0.4% TAC and 0.04% PAA (Mw~50,000) are also shown. It can be seen that addition of magnesium citrate can reduce the low shear-rate viscosity of the same volume fraction alumina suspensions.

magnesium citrate. If the suspension contains no aggregates before shear, shear thickening is expected to occur because of the ordering rearrangement of the particles along the shear field. If the suspension has weak aggregates, then a shear-thinning behavior would be expected at the small shear rate range because of the breaking down of the aggregates under shear. Therefore, from the shear flow data, it can be realized that the 40vol% alumina suspensions with 0.01 and 0.02M magnesium citrate powders do not have significant amount of aggregates in the as prepared state (Figure 6-3). When the slurry loading is above 50vol%, agglomerates start to form after the preparation of the

suspensions. Comparing the same volume fraction suspensions, it can be realized that introducing of magnesium citrate powder instead of PAA can dramatically decrease the shear viscosity at low shear rate range, which is favorable to industrial direct casting. For the 60vol% alumina suspensions, using magnesium citrate can even yield a suspension with lower viscosity in the experimental shear rate range than the 60vol% suspension with 0.4wt% TAC only, the stabilization effect of magnesium citrate is still under investigation.

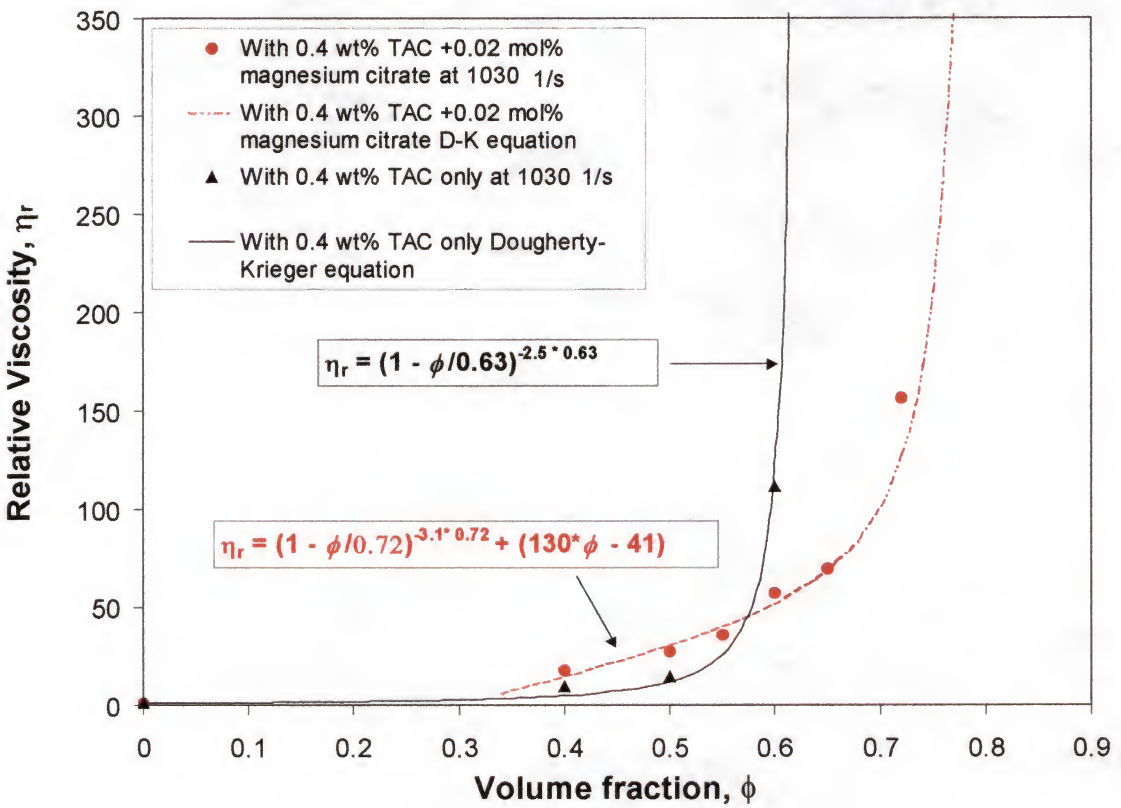

Fig.6-9. Variation of the relative viscosity (at shear rate of $1030s^{-1}$) with the volume fraction of alumina for the suspensions with and without magnesium citrate addition. The modified Dougherty-Krieger equations are used to fit the experiment data. The maximum volume fraction for the magnesium citrate suspensions can be ~ 0.72, and the suspensions with TAC only is ~ 0.63.

Figure 6-9 is the plots using the modified Dougherty-Krieger (D-K) equations to fit the experiment data for the 0.02mol% magnesium citrate addition suspensions and the 0.4wt% TAC only addition suspensions. The D-K equation is $\eta_r = (1 - \phi/\phi_m)^{-[\eta]\,\phi m}$. For the later suspensions, a set of fitting parameters are $[\eta] = 2.5$ and $\phi_m = 0.63$, and the D-K equation is $\eta_r = (1 - \phi/0.63)^{-2.5\times0.62}$. For the magnesium citrate adding suspensions, the modified D-K equation $\eta_r = (1 - \phi/0.72)^{-3.1\times0.72} + (130\phi - 41)$ is proposed to fit the experimental data. The fitting parameters are $[\eta] = 3.1$ and $\phi_m = 0.72$. Therefore, according to the fitting parameters, the maximum volume fraction of particles can be increased to 0.72 with magnesium citrate powder addition while keeping the temperature induced forming characters.

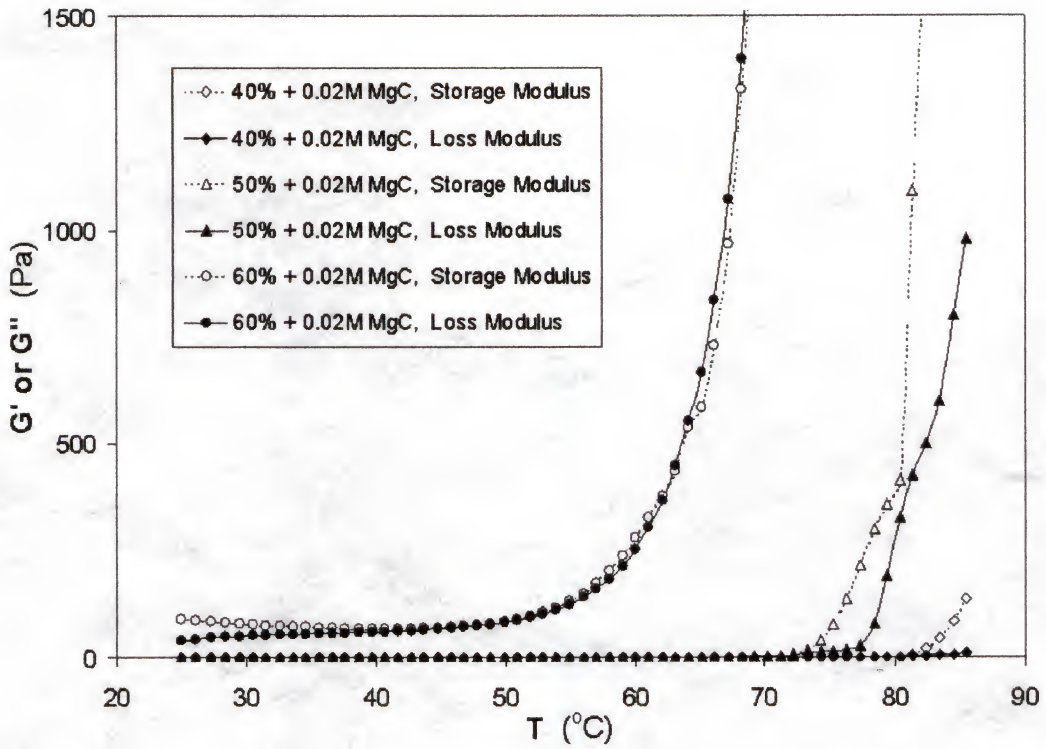

Fig.6-10. Variation of the shear modulus with temperature for the different volume fraction alumina suspensions with 0.02M magnesium citrate. The storage modulus, G' clearly starts to increase at 80°C, 70°C and 50°C for 40vol%, 50vol% and 60vol% suspensions, respectively. Measurements are conducted at 1% strain amplitude and a frequency of 1Hz, the temperature is raised at 1 °C/min.

6.5 Temperature Dependence of the Shear Modulus

Figure 6-10 shows the variation of the shear modulus with temperature for the different volume fraction alumina suspensions with 0.02M magnesium citrate. The storage modulus, G' clearly starts to increase at 80°C, 70°C and 50°C for 40vol%, 50vol% and 60vol% suspensions, respectively. In other words, this specific temperature decreases with increasing volume fraction of particles, and the suspension has a quite

different microstructure above this temperature. Similar to the PAA addition TIF alumina suspensions, the gelation of the suspension with magnesium citrate might be the result of the growth of the aggregates and the formation of the particle percolation networks. As discussed in the previous part, the flocculation of the suspension is due to the ionization reaction of the magnesium citrate with temperature. The increasing ionic strength compresses the EDL thickness, and the van der Waals attractive potential starts to dominate. Then the small, weak agglomerates will form in the suspension. If the thermal energy kT is not large enough to break these aggregates apart, larger size aggregates will form by the adhesion of particles on the existing agglomerates. Finally, these aggregate flocs connect and form a continuous particle percolation network, which yields the observed increase of the storage modulus.

When the volume fraction is increase from 40vol% to 50vol%, the interparticle distance is reduced and it is easier for the particles to form bonding by the van der Waals force at the same temperature. Therefore, the particle network can form at a lower temperature in the 50vol% suspension than in the 40vol% suspension. But with further increase in the volume fraction of particles, the probability of two or more particles meeting together increases significantly, and the interaction between particles tends to hold these particles together as multiplets at room temperature [62]. These aggregate flocs are favored to grow to a larger size thermodynamically in order to reduce the total surface energy. Therefore, for the 60vol% suspension, the particle network could be formed at about 50°C.

6.6 Percolation Theory Model for the PAA-Free TIF Alumina Suspensions

The percolation theory model described in Chapter 5 can also be applied to the magnesium citrate addition suspensions. Take the expression for the temperature dependence of the storage modulus as

$$G'(T, \phi_0) = G_0'(T) \cdot \{\phi_0 \cdot e^{-\Delta U / kT} \cdot e^{d_1 \cdot [d_2 + (T-T_0)/T_0]} / \phi_g - 1\}^s \qquad (6\text{-}5)$$

Then

$$\ln G' = s \cdot \ln \{\phi_0 \cdot e^{-\Delta U / kT} \cdot e^{d_1 \cdot [d_2 + (T-T_0)/T_0]} / \phi_g - 1\} + \ln G_0'(T) \qquad (6\text{-}6)$$

Plotting $\ln G' \sim ln\{\phi_0 \cdot e^{-\Delta U / kT} \cdot e^{d_1 \cdot [d_2 + (T-T_0)/T_0]} / \phi_g - 1\}$ should yield a straight line with slope, s.

From Figure 6-4 and Figure 6-10 the volume fraction gelation threshold can be determined to be about 0.4, or $\phi_g \sim 0.4$. The determination of exponent, s, involves the same procedures as described in Chapter 6. During calculation, $d_1 = 1.3$, $d_2 = 0.1$, and $\Delta U = -50$ eV. T_0 is the temperature where the relative viscosity starts to increase and can be obtained from the relative viscosity (at shear rate of 20 s^{-1}) vs. temperature plots. Its value is about 45 °C.

If $ln\{\phi_0 \cdot e^{-\Delta U / kT} \cdot e^{d_1 \cdot [d_2 + (T-T_0)/T_0]} / \phi_g - 1\}$ is notified **as** $ln\{x\}$, Then the plot of $\ln G' \sim ln\{x\}$ can be shown in Figure 6-11. The slope values of the straight lines and the interceptions on the ln G' axis are summarized in Table 6-1.

The values of s illustrated in Table 6-1 are much larger that that obtained in Chapter 5, indicating that the magnesium citrate suspensions have a higher order particle percolation network [96-100]. It is reasonable because in these suspensions, only

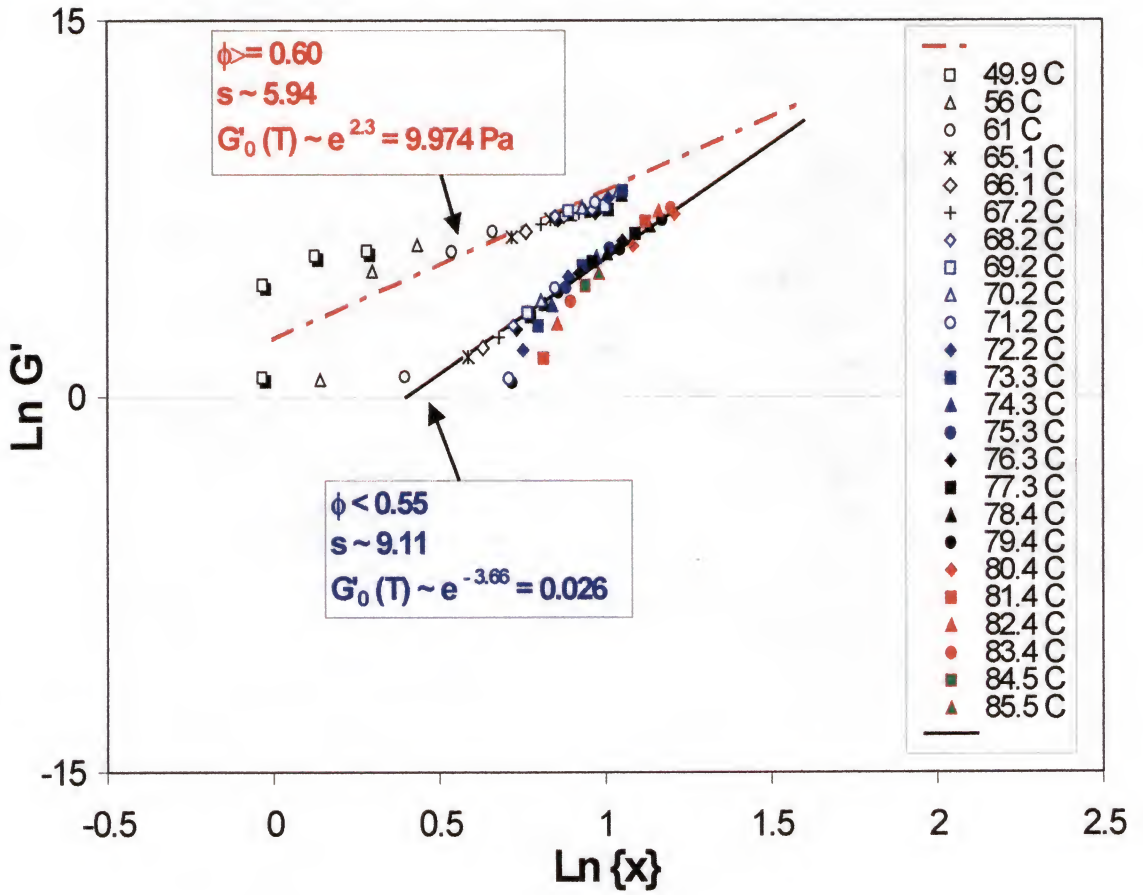

Fig.6-11. The ***ln*** G' ~ *ln {x}* plots using Eq. (6-6) for the alumina suspensions with 0.02M magnesium citrate addition. The values of s and $G'_0(T)$ can be obtained from the slope and interception of the line on the Ln G' axis, respectively.

Table 6-1. Effect of Volume Fraction on the Parameters in Eq. (6-6).

	$\phi < 0.55$	$\phi > 0.6$
s	~ 9.11	~ 5.95
G_0' (T)	~ 0.025 Pa	~ 9.98 Pa
ϕ_g	~ 0.40	~ 0.40
T_0	~ 45 °C	~ 45 °C

particles forms agglomerates and finally yields a space particle network, whereas the interaction of the PAA molecular chains also contributes to the formation of the percolation network in the PAA addition TIF suspensions.

The value of the pre-exponent term is larger for the higher volume fraction suspension, which is also observed in the PAA addition TIF alumina suspensions in Chapter 5. Since this term, G_0' (T), is a reflection of the strength or stiffness of the network chain backbones, higher volume fraction of particles will yield a higher packing density and therefore can transmit a higher stress before breaking down.

Figure 6-12 shows the calculated results using the percolation theory model (Eq. 7-3), the parameters used during calculation are shown in the figure. It is clear that the computed results can match the measurement data quite well. Therefore, it can be concluded that the gelation of the magnesium citrate-addition TIF alumina suspensions might be due to the formation of the particle percolation network. This model can be used to predict and control the gelation degree of this type of suspension.

Considering the higher percolation nature for the PAA-free TIF suspensions, the gelation and percolation network formation process can be shown schematically as in Figure 6-13.

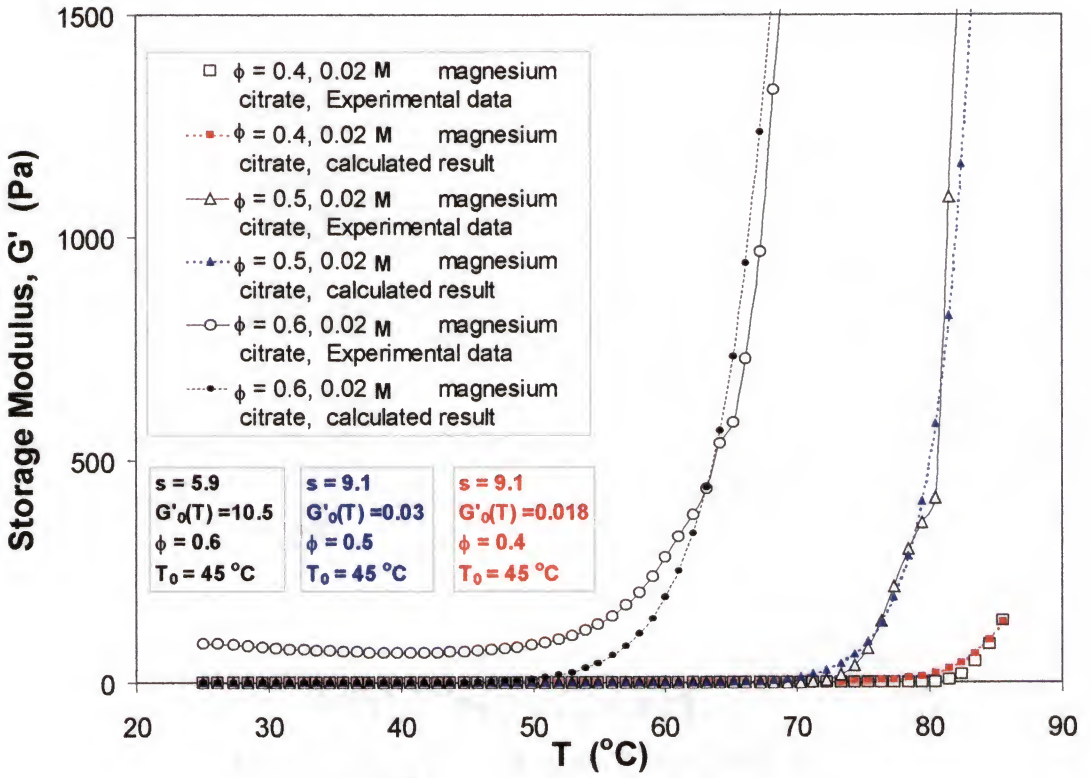

Fig.6-12. Comparison of the calculated result using the expanded percolation theory model (Eq. 6-6) and the experiment data, the parameters used during calculation are shown in the figure. It is clear that the model calculation results fit the measured data quite well.

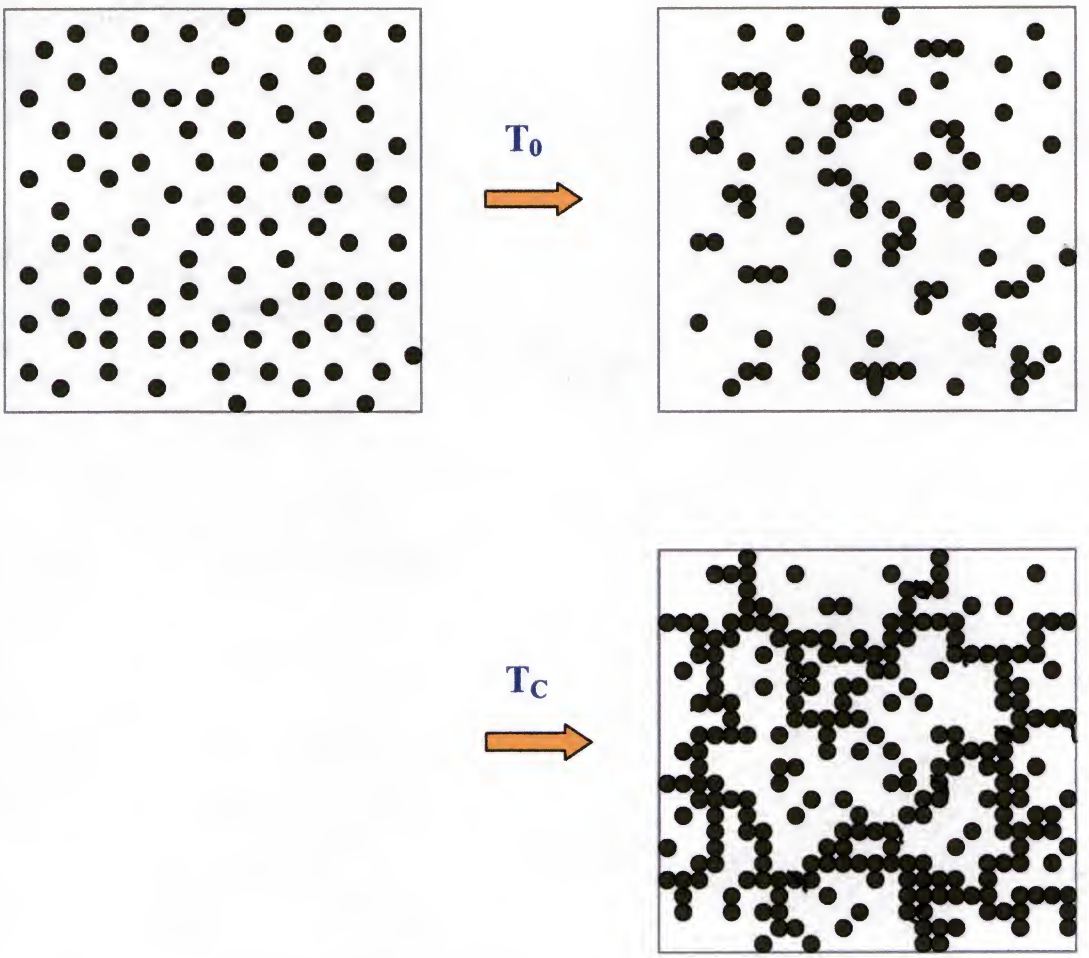

Fig. 6-13. The proposed gelation and percolation network formation process. The size of the alumina particles and distance between particles are exaggerated for clarity.

6.7 Summary of This Chapter

The PAA-free TIF alumina suspensions have been successfully produced by introducing magnesium citrate powders. The variations of both the shear viscosity and shear modulus with temperature are similar to that of the PAA addition suspensions.

Both the viscosity and storage modulus of the suspensions show an evident increase when the temperature is above a critical temperature. The magnitude of this

temperature decreases with increasing volume fraction of the alumina particles. Compared with the PAA addition TIF suspensions, the same volume fraction PAA-free suspension has a higher critical temperature. The flocculation of the magnesium citrate-addition TIF suspensions is controlled by the ionization reaction of the magnesium citrate that increases the ionic strength in the suspensions. The ionization reaction is controlled by the pH of the suspensions, which decreases with increasing temperature.

Comparing the 60vol% TIF alumina suspensions with the PAA addition and the suspension using TAC only, addition of magnesium citrate can decrease the room temperature shear viscosity significantly, which is favorable to industrial direct casting applications.

Variation of the relative viscosity with the volume fraction of alumina for the 0.4wt% TAC and 0.02M magnesium citrate addition suspensions can be fitted to the modified Dougherty-Krieger equation as $\eta_r = (1 - \phi/0.72)^{-3.1\times0.72} + (130\phi - 41)$.

Percolation theory model can be successfully applied to this type of suspension. Therefore, the gelation of the magnesium citrate-addition TIF alumina suspensions might be due to the formation of the particle percolation network. Compared with the PAA addition TIF suspensions, larger values of percolation exponent, ***s***, are expected and verified by the experimental data for these PAA-free TIF suspensions, indicating that these suspensions have higher degree of particle percolation.

The calculation results using the expanded percolation model fit the measured data well. Therefore, this model can be used to predict and control the gelation degree of the PAA-free TIF alumina suspensions.

CHAPTER 7
DIRECT CASTING USING THE TIF AQUEOUS ALUMINA SUSPENSIONS

7.1 Direct Casting Parts and Analysis

The compositions of the direct casting suspension are 40vol% AKP52 alumina with 0.4wt% TAC and 0.04wt% PAA of molecular weight 50000. The preparation and direct casting procedures are described in the Appendix-1 of this dissertation.

Figure 7-1 shows the green bodies of some ceramic parts fabricated by TIF direct casting. It can be realized that the resultant green body has good surface finish. The success of utilizing TIF suspensions into direct casting opens an alternative method to prepare rather complex shape engineering ceramic parts. Its simple processing makes TIF direct casting promise of readily automation.

The SEM morphology of the natural surface for the dried green body fabricated by the TIF direct casting is shown in Figure 7-2. It is seen that alumina particles are closely packed. The density of the dried green body is ~ 65% of theory density of alumina.

Figure 7-3 shows the Energy Dispersion X-ray Spectrum of the green body surface in Figure 7-2. It is observed zirconium element in the green body can not be detected evidently under the resolution of the probe, which excludes the significance of introduction of much zirconia into the alumina green body during ball mill mixing using zirconium oxide milling balls. This observation also excludes the effect of other impurities contributing to the gelation of TIF alumina suspensions.

Fig.7-1. The green bodies of some ceramic parts fabricated by TIF direct casting. The suspension compositions are 40vol% alumina, 0.4wt% TAC and 0.04wt% PAA 50000.

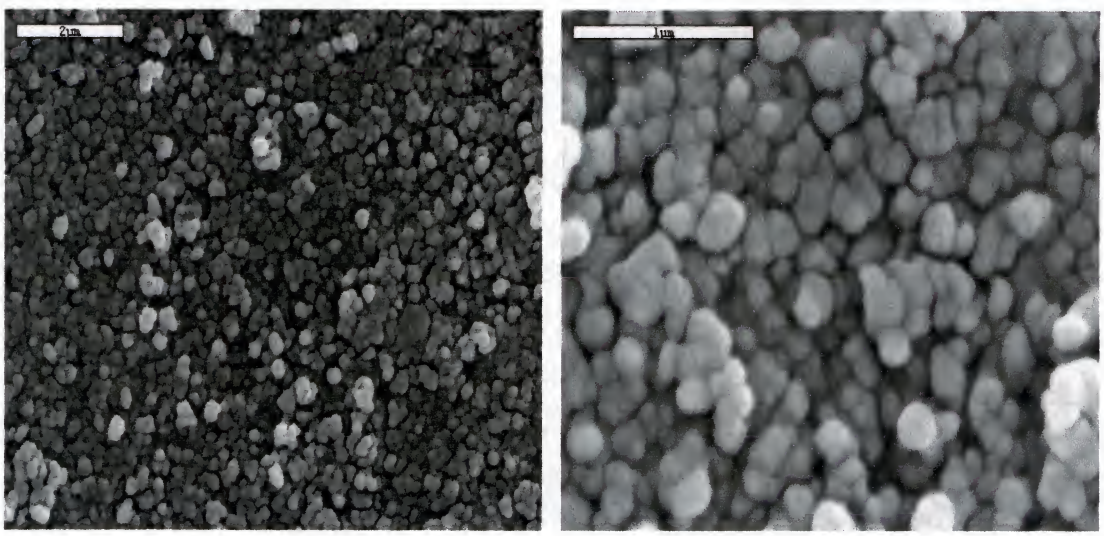

Fig.7-2. SEM surface morphology of the AKP53 ceramic green body fabricated by TIF direct casting using the same composition suspensions in Fig.7-1.

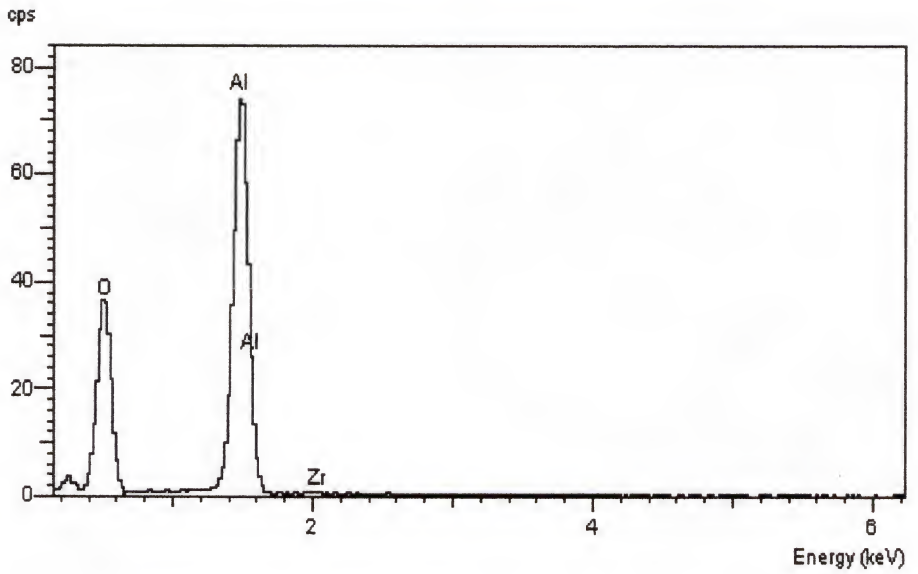

Fig.7-3. EDXS analysis of the AKP53 alumina green body fabricated by TIF direct casting.

7.2 Sintering of TIF Direct Casting Parts and Microstructure Observation

The alumina green body is sintered at 1550 °C for 2h. The sintered samples are translucent and have ~100% of theoretical density. The SEM surface morphology of the sintered sample is shown in Figure 7-4. It can be seen that there is no abnormal grain growth in the sample and the alumina grain size is ~ 1.5μm. The residual pore size is less than 0.2 μm and uniformly distributed in the grain boundary. Therefore, the microstructure shows that TIF process can eliminated the strength limiting defects, such as abnormal grain growth, large pores.

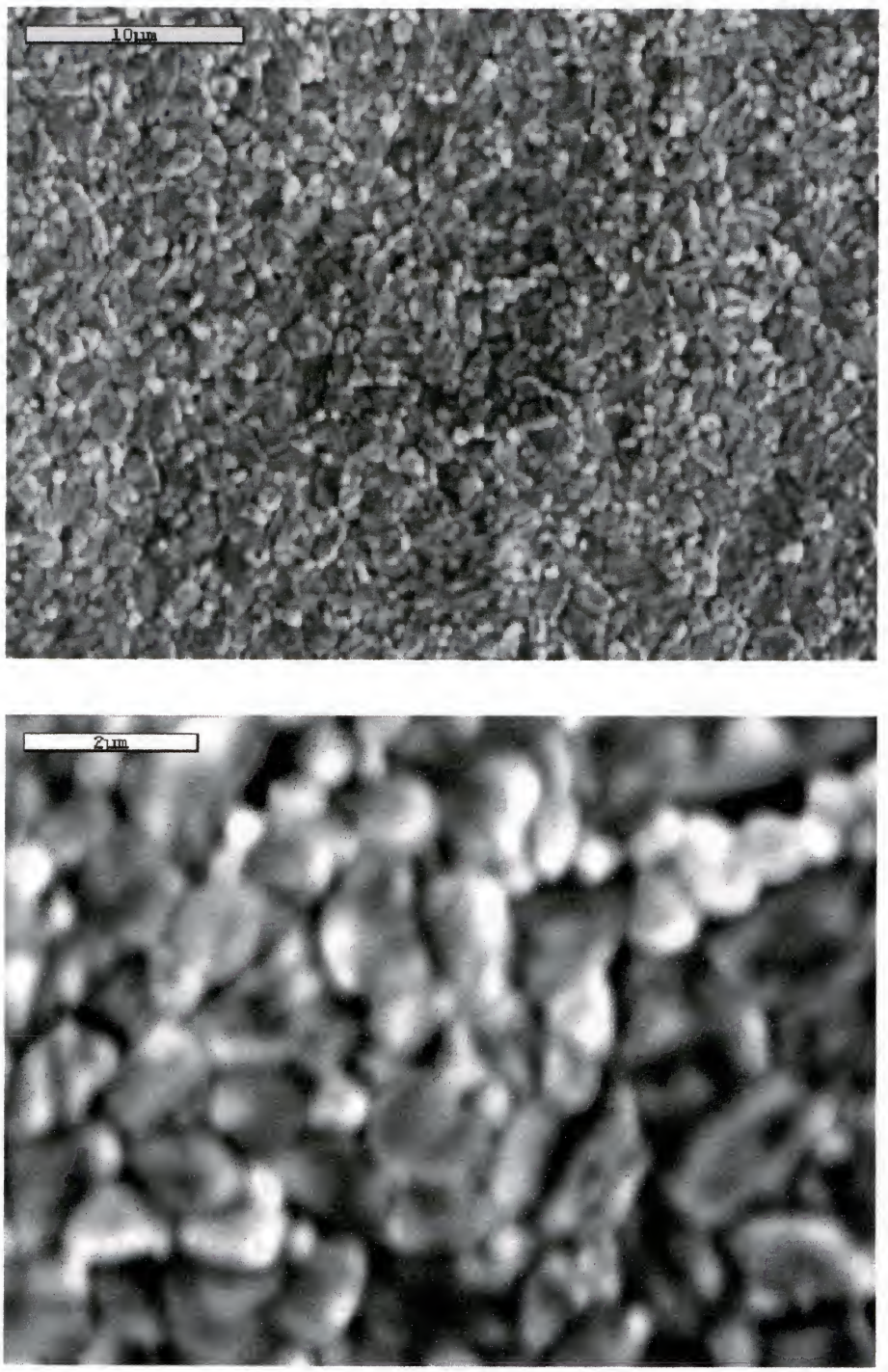

Fig.7-4. SEM surface morphology of the sintered AKP53 alumina parts fabricated by TIF direct casting. The sintering condition is 1550 °C and 2h.

7.3 Phase Determination in the TIF Direct Casting Parts

Figure 7-5 gives the XRD spectrum of the AKP53 alumina powder, green body and the sintered sample under 1550 °C for 2h. The peaks shift to higher angle for both the green body and sintered samples compared with the peak positions of the powder. This might be due to the hydration reaction of alumina powder in water to form the aluminum hydroxide phase on the surface, which will transform to γ-Al_2O_3 phase after sintering.

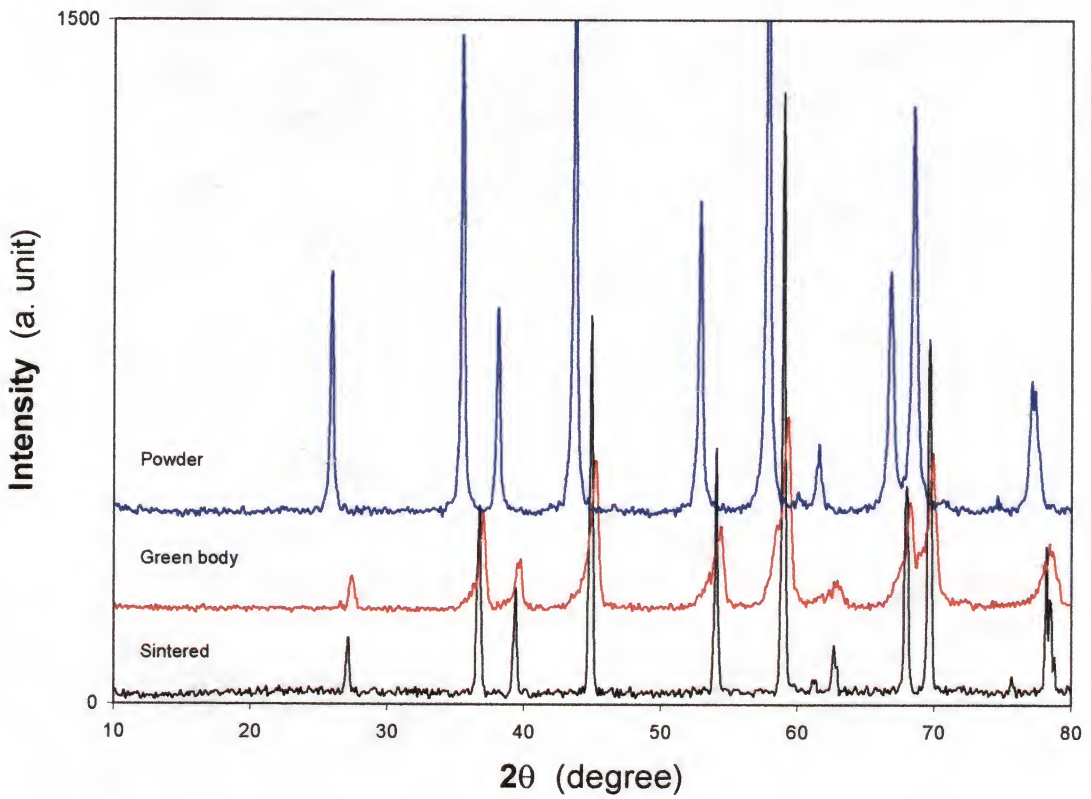

Fig.7-5. XRD spectrum of the AKP53 alumina powder, green body and the sintered body.

7.4 Summary of This Chapter

Complex-shape engineering ceramic parts have been successfully fabricated by TIF direct casting using the TIF alumina suspensions described in previous chapters.

SEM observation shows that the particles are closely packed in the green body. The TIF direct casting parts have a relative density of ~ 65% of theory value of alumina. For the sintered sample at 1550 °C for 2h, the SEM surface morphology shows that the grain size is uniform and no abnormal grain size growth is observed. The grain size is ~ 1.5μm. The residual pore size is < 0.2μm and uniformly distributed. These microstructure results in a translucent sintered sample.

No evident observation of zirconium element in the dried green body by using EDAX analysis, thus assures that the gelation of TIF suspensions does not come from the effect of other impurities that might be introduced during powder processing.

CHAPTER 8
SUMMARY AND OUTLOOK

In the research work shown in this dissertation, the viscoelastic properties of TIF alumina suspensions are characterized with variation in volume fraction of particles, PAA amount and the molecular weight of PAA. The temperature dependence of the suspension shear viscosity and shear modulus are also measured and analyzed. A continuous percolation theory model is proposed to explain the experimental data. PAA-free TIF alumina suspensions is also successfully introduced. The TIF suspensions are successfully used for direct casting complex engineering ceramic parts. The main results are summarized as follows:

(1) TIF alumina suspensions have been successfully prepared by adding 0.4wt% of ammonium citrate powder and <0.1wt% PAA into the suspensions. The optimum amount of ammonium citrate powder is determined experimentally to be ~ 0.4wt%.

(2) The gelation diagrams that relate the volume fraction of particles, PAA amount and the gelation degree are experimentally determined and plotted. The results show that ~ 0.04wt% of either PAA50,000 or PAA 10,000 is enough to flocculate and gel the TIF alumina suspensions when the volume fraction of particles is no less than 0.3.

(3) Increasing the volume fraction of alumina will increase the 25 °C steady shear viscosity, which can be fitted by the Dougherty-Krieger equation. For the PAA 50,000 addition suspensions, the fitted D-K equation is $\eta_r = [1 - (\phi / 0.57)]^{-2.4 \times 0.57}$.

While for suspensions in the absence of PAA, the fitted D-K equation is

$\eta_r = [1 - (\phi / 0.64)]^{-2.18 \times 0.64}$.

(4) The volume fraction of particles affects the degree of the relative viscosity increment with temperature. Higher volume fraction of particles will enhance the viscosity increment more.

(5) Molecular weight of PAA has a significant effect on the 25 °C shear viscosity of the alumina suspensions. Larger molecular weight PAA tends to increase the shear viscosity, decrease the gelation threshold of the alumina suspensions where the suspension relative viscosity starts to increase rapidly, and decrease the temperature where the suspension shows visible increase of its viscosity.

(6) Shear modulus is used to characterize the viscoelastic properties of the TIF suspensions. For the suspensions with volume fraction less than 0.5, there is a "crossover" temperature. The suspensions have "solid-like" behavior with G'>G'' when the temperature is above this temperature. This "crossover" point can be easily observed in the damping factor vs. temperature plots.

(7) Higher volume fraction of particles tends to shift the "crossover" to a lower temperature and increases the magnitude of the storage modulus. Increasing the amount or the molecular weight of PAA can shift the "crossover" to a lower temperature and enhances in the formation of particle space-filling network at lower temperature.

(8) The evolution of the shear modulus with time at a temperature shows that higher temperatures increase the shear modulus more rapidly than at lower temperature. Both the storage and the loss modulus of the suspension with PAA 50,000 increase

much more rapidly than the suspensions with PAA 10,000. Therefore, higher M_w PAA can improve the gelation degree under the same experimental conditions, but at an expense of increasing the zero shear rate viscosity that is not favorable for a direct casting process.

(9) Realizing that the effective volume fraction of particles will increase with temperature because of the growth of the agglomerate, an expanded continuous percolation theory model is established to interpret the evolution of the storage modulus with temperature and slurry loading for the TIF alumina suspensions.

(10) Calculated results using the percolation model show that the storage modulus of the suspensions increases with the volume fraction of solids and temperature. The increment of the volume fraction gelation threshold, ϕ_g, decreases the magnitude of the storage modulus. The characteristic temperature T_0 also has significant influence on the calculated value of storage modulus using this model. It is assumed that ϕ_g and T_0 are always related to each other with respective to the composition of the suspensions. The description of the temperature dependence of the storage modulus for the actual alumina suspensions can be realized by tailoring the specific parameters in this model.

(11) The exponent, s and the volume fraction gelation threshold, ϕ_g are derived from experimental data for the PAA containing TIF alumina suspensions. For the same amount of PAA addition, increasing molecular weight of PAA decreases the values of s, ϕ_g and T_0 at the same time.

(12) This model is used to compute the variation of the storage modulus with the volume fraction of solids and the molecular weight of PAA. The measurement data fit the calculated results the well.

(13) The PAA-free TIF alumina suspensions have been successfully introduced using magnesium citrate powders. The variations of both the shear viscosity and shear modulus is similar to that of the PAA addition suspensions. Both the viscosity and storage modulus of the suspensions show an evident increase when the temperature is above a critical temperature. The magnitude of this temperature decreases with increasing volume fraction of the alumina particles. Compared with the PAA addition TIF suspensions, the same volume fraction PAA-free suspension has a higher critical temperature.

(14) The flocculation of the magnesium citrate-addition TIF suspensions is controlled by the ionization reaction of the magnesium citrate that increases the ionic strength in the suspensions. The ionization reaction is controlled by the pH of the suspensions, which decreases with increasing temperature.

(15) Comparing the 60vol% TIF alumina suspensions with the PAA addition and the suspension using TAC only, addition of magnesium citrate can decrease the room temperature shear viscosity significantly, which is favorable to industrial direct casting applications. Variation of the relative viscosity with the volume fraction of alumina for the 0.4wt% TAC and 0.02M magnesium citrate addition suspensions can be fitted to the modified Dougherty-Krieger equation as $\eta_r = (1 - \phi/0.72)^{-3.1\times0.72} + (130\phi - 41)$.

(16) Percolation theory model can be successfully applied to this type of suspension. Therefore, the gelation of the magnesium citrate-addition TIF alumina suspensions might be due to the formation of the particle percolation network. Compared with the PAA addition TIF suspensions, larger values of percolation exponent, ***s***, are expected and verified by the experimental data for these PAA-free TIF suspensions, indicating that these suspensions have higher degree of particle percolation. The measurement data fit well with the calculated results using the percolation model. Therefore, this model can be used to predict and control the gelation degree of the suspensions.

(17) Complex-shape engineering ceramic parts have been successfully fabricated by TIF direct casting using the TIF alumina suspensions.

(18) SEM observation shows that the particles are closely packed in the green body. The TIF direct casting parts have a relative density of ~ 65% of theory value of alumina. For the sintered sample at 1550 °C for 2h, the SEM surface morphology shows that the grain size is uniform and no abnormal grain size growth is observed. The grain size is ~ 1.5μm. The residual pore size is < 0.2μm and uniformly distributed. These microstructure results in a translucent sintered sample.

(19) No evident observation of zirconium element in the dried green body by using EDAX analysis, thus assures that the gelation of TIF suspensions does not come from the effect of other impurities that might be introduced during powder processing.

Future Work

The author suggests that the following experiments need to be done so as to get a further understanding and to apply this novel technology to the industrial production of ceramic parts.

(1) Apply the TIF gelation mechanism to other ceramic material systems, especially to non-oxide ceramic systems;

(2) Design and apply TIF suspension to the solid freeform fabrication area to produce prototypes or fabricate complex ceramic parts directly;

(3) Theoretical understanding of the formation process of the percolation network with time at a fixed temperature and build a universal model to give useful guides for the processing control.

APPENDIX A

RAW MATERIALS, SLURRY PREPARATION AND MEASUREMENTS

A.1 Raw Materials

Raw materials used in the experiments are listed in Table A-1.

Table A-1. Raw materials used in this research.

Material	Source	Purity / Other Specification	Physical Form
AKP53 Alumina	Sumitomo, Japan	>99.999%	powder
Ammonium Citrate	Aldrich, USA	98%	powder
Poly(Acrylic Acid)	Polysciences, USA	Mw ~ 50,000	25% aqueous solution
Poly(Acrylic Acid)	Polysciences, USA	Mw ~ 10,000	25% aqueous solution
Poly(Acrylic Acid)	Polysciences, USA	Mw ~ 5,000	50% aqueous solution
Calcium Nitrate	Aldrich, USA	99+%	powder
Sodium Chloride	Aldrich, USA	99+%	powder
Magnesium Citrate	Alfa Aesar, USA	CAS# 144-23-0	powder

A.2 Characterization of the AKP53 Alumina Powder

The particle size of AKP53 was measured by LS Particle Size Analyzer (COULTER) and yielded a $d_{50} \sim 0.4\mu m$. The particle size distribution of the powder is shown in Figure A-1. The SEM morphology of the as-received powder is illustrated in Figure A-2. The surface area of the alumina powder as measured by standard BET (NOVA 1200) N_2 adsorption was 14.8 m^2/g.

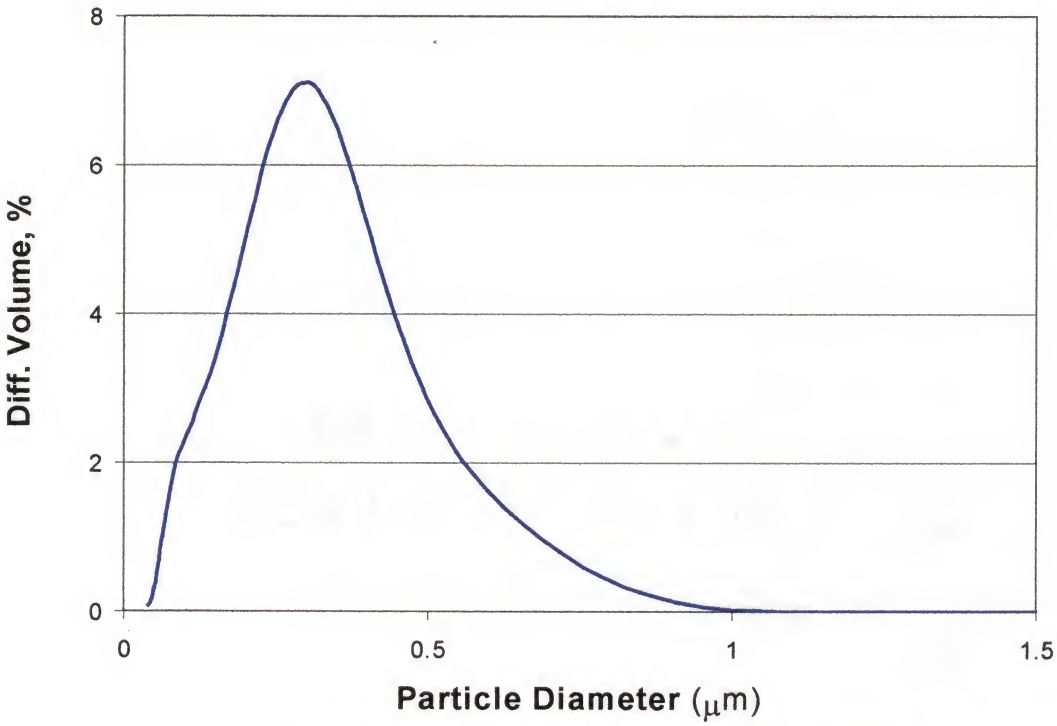

Fig.A-1. Paticle size distribution of the AKP53 alumina powders.

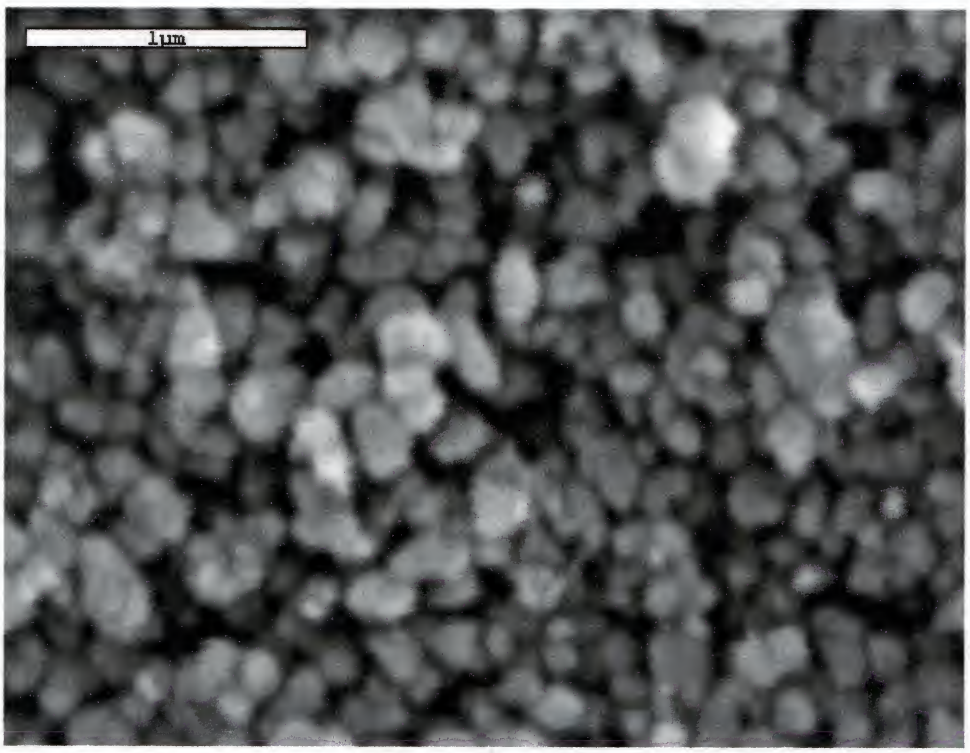

Fig.A-2. SEM morphology of the as-received AKP53 alumina powders.

Electroacoustic Measurement is conducted to measure the surface zeta potential of the as-received AKP53 powders. The variations of the zeta potential with pH are shown in Figure A-3. The point of zero charge (PZC) is about pH9.2.

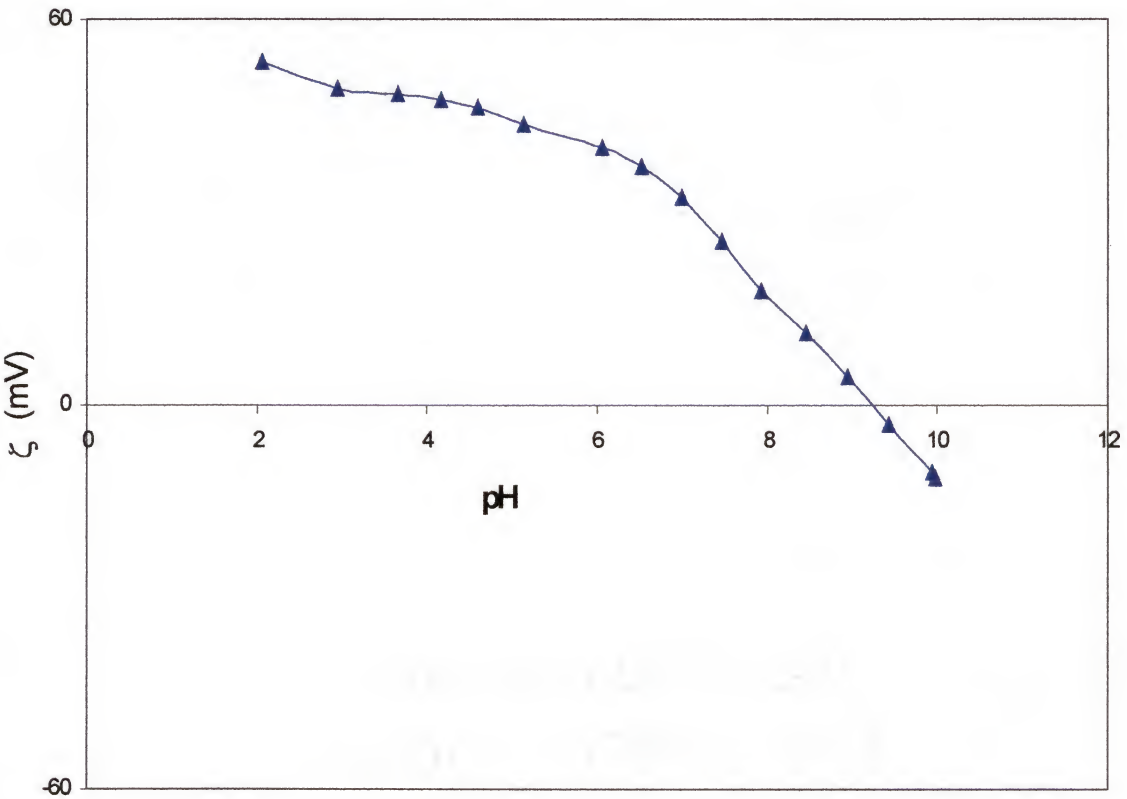

Fig.A-3. Zeta potential measurement by titration of the as received AKP53 alumina powders. The concentration of Na^+ is 0.01 mol/L. The volume fraction of alumina is 0.03 and the starting pH of the slurry is ~ pH2. The base used for titration is 1.0 mol/L KOH.

A.3 Electroacoustic Measurement

Zeta potential determinations were performed with an electrokinetic sonic amplitude measurement (ESA) apparatus (Acoustosizer Matec Applied Sciences, Hopkinton, MA). In this device the suspension is subjected to an alternationg electric field, at magahertz frequencies, which creats relative movement between the ceramic particles and the surrounding liquid. This motion generates a sound wave at the same frequency as the electric field detected by the transducer. The acoustic energy generated is proportional to the dynamic mobility. A correlation between these ESA measurements and the zeta potential values (ζ) was established through O'Brien's formula: [A1]

$$\zeta = \mu_d(\omega)\, \eta\, G(\alpha)^{-1}\, \varepsilon^{-1}$$

where μ_d is the dynamic mobility, ω the angular frequency of the applied field, η the viscosity of the liquid, ε the dielectric permittivity of the suspension, and $G(\alpha)$ a term which corrects for the inertia of the particles in the alternating field, which acts to reduce the velocity amplitude of the particle motion for a given zeta potential. $G(\alpha)$ is dependent on ω, on the particle radius, and on the kinematic viscosity of the liquid.

A.4 Slurry Preparation

A.4.1 Planetary Ball Mill

The Pulverisette 5" Laboratory Planetary Mill (Fritsch GmbH, Germany) is used for the mixing and homogenizing of different starting materials. The rotation speed can be adjusted to 350rpm/min. The mill jar material is alumina. The material of milling ball used is zirconia.

A.4.2 Slurry Preparation Process

The suspension preparation process is shown schematically as Figure A-4:

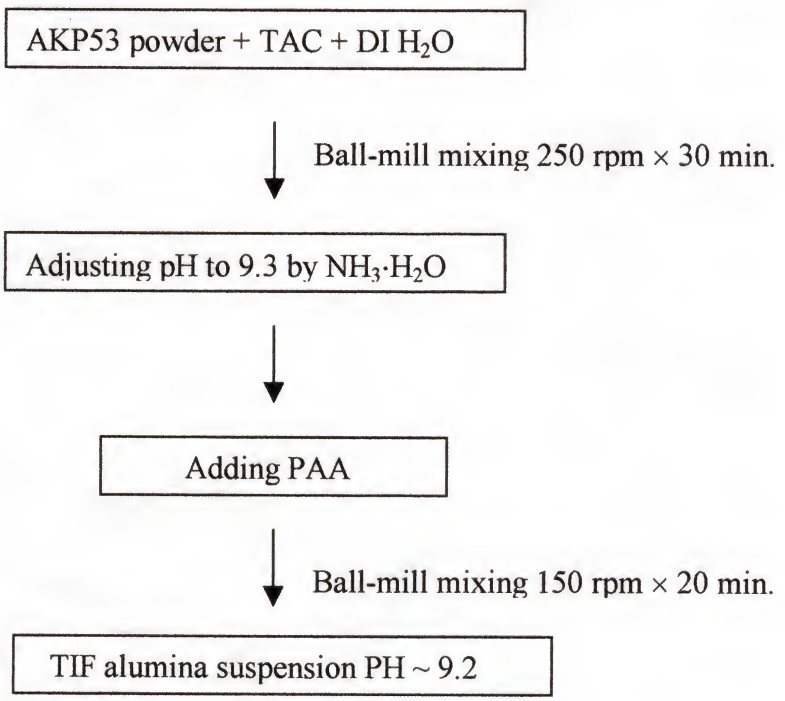

Fig.A-4. Flowchart of the TIF suspension preparation process.

The exact amount of alumina powders, TAC and respective amount of deionized water were mixed for 30 minutes at a speed of 250 rpm first. Then the pH was adjusted to about 9.3 with analytical 4.94N ammonium hydroxide before adding the exact amount of PAA. The above suspensions were then ball-milled for about 20 minutes to get the final suspensions. The pH value of the suspension is ~ 9.2. Without specific statement, the amount of ammonium citrate and the amount of PAA are taken as the weight percent of the dry ceramic powders.

A.5 Viscoelastic Property Measurements

A.5.1 Modular Compact Rheometer

The MCR300 Modular Compact Rheometer (Paar Physica, USA) is used to measure the viscoelastic properties of the suspensions. The MCR300 is the newest rheometer and offering research-grade capabilities of controlled-stress and controlled-strain rheometers in one package. It is versatile to use in temperature control with all measuring geometries (cylinder, cone/plate, plate/plate). In our experiment measurements, cylinder geometry is used with a name of CC27. The standard tests modes used in our experiments are (1) rotational test with controlled shear stress (CSS), and (2) oscillatory test with controlled strain, and (3) temperature sweep test in both rotation and oscillation modes.

A.5.2 Steady Shear Flow Curves and Shear Viscosity Measurements

The shear flow with shear rate is conducted at 25°C, and the shear rate varies from 0.1 s^{-1} to 1030 s^{-1}. The time duration between two measuring points is 15 s. The temperature ramp rotation mode was used to measure the temperature dependence of suspension viscosity. During measurement, the shear rate was 20 s^{-1} and the temperature was raised at a rate of 1 °C/ min with the start temperature at 25 °C. The relative viscosity was computed out using the ratio of the measured viscosity to that of the water at the same temperature. A polynomial expression for the temperature dependence of viscosity of water can be fixed to data from the CRC Handbook, as can be shown in the following expression.

$$\eta_{Water} = 0.0017-(4.73\times10^{-5})\,T+(7.45\times10^{-7})\,T^2-(6.25\times10^{-9})\,T^3+(2.13\times10^{-11})\,T^4$$

Where T is the temperature of the suspension with a unit of degree centigrade (°C).

A.5.3 Shear Modulus Measurement

The temperature dependence of the storage and loss modulus were measured using the temperature ramp oscillation mode with the fixed shear strain of 1%, the frequency of 1 Hz, and the temperature ramp of 1 °C/ min. From the measurement, we can also get the data of the shear stress, loss angle, η' and η''.

The time dependence of the storage modulus and the loss modulus at a temperature were conducted in the time test oscillation mode. During measurement, the temperature was increased to the set temperature point at a rate about 20 °C/ min. The strain was kept at 2% and the frequency was fixed at 1 Hz.

A.6 Citrate Adsorption and Ionic Concentration Measurements

Eppendorf Centrifuge 5810 from Brinkmann Instruments, Inc. is used to prepare the samples for ionic concentration measurements or for citrate adsorption measurements. Fixed-angle rotor with cover for 6×85mL tubes is used.

The suspensions for adsorption measurements were centrifuged at 3600 rpm for 3 hours (Centrifuge 5810, Eppendorf), and then the upper clear supernatants were drawn out carefully. The citrate anion adsorption measurement was conducted using the UV-Persulfate TOC Analyzer (DOHRMANN, Phoenix 8000), where a calibration curve was obtained first by using ammonium citrate stock solutions. After getting the carbon

content in the supernatant, it can be converted into the concentration of the remaining citrate anion in the supernatant.

For the measurements of the concentration of magnesium ions in Chapter 6, six 100mL beakers are filled with 40mL DI water (R~18.2 MΩ), and the pH are adjusted by 30wt% potassium hydroxide to pH11.2, 10.8, 9.8, 8.9, 8.3, 7.6, respectively. Then 0.404 g of magnesium citrate is dispersed into each above beaker while stirring. After stirring 24 h, the above suspensions are removed into the 45mL centrifuge PE tubes. Then they are all put in the centrifuge (Centrifuge 5810, Eppendorf) at 3600 rpm for 1.5 h. The clear supernatants are drawing out later carefully and diluted using DI water for ICP measurements. The Mg^{2+} concentration in the supernatant was measured by using ICP Emission Spectroscopy (PERKIN ELMER, Optima 3200 RL).

A.7 Preparation of the Silicon Mold for Direct Casting

Silicon rubber molds were used for direct casting to make ceramic parts. The mold material is a mixture of ELASTOSIL A and ELASTOSIL B (Wacker Silicones Corp.) by the weight ratio of 9:1 and can be cured readily at 75°C for 1 hour. The rubber mixture of A and B is first de-aired under vacuum for 40 min., and then it is poured into a container that have the prototype of the desired part. After putting the container in oven of 75°C for 1 hour, the prototype part can be removed so that the ceramic mold with the desired shape and dimension cavity is obtained.

A.8 Direct Casting Procedure and Control

The suspension preparation procedure is the same as reported above. The resultant suspension is de-aired under vacuum for 30 min before pouring into the mold. Then a thin layer of vegetable oil to prevent water vaporizing covers the surface of the suspension in the mold. After staying in the oven of 65 °C for 2h, the gelled ceramic part is obtained after de-molding. The following drying step yields the dry green body. The TIF direct casting process can be summarized in Figure A-5.

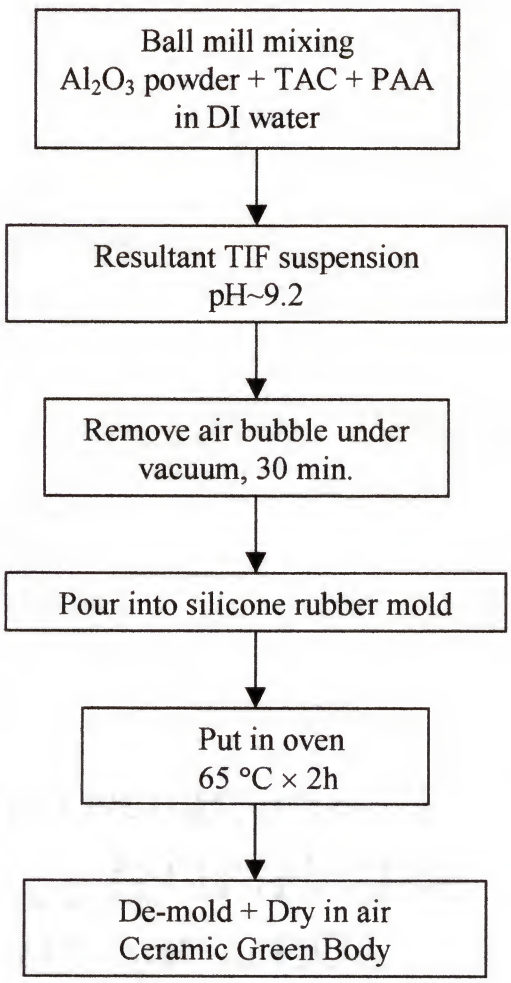

Fig.A-5. Schematic flowchart of the TIF direct casting process.

A.9 Microstructure Analysis and Phase Determination

A.9-1 Scanning Electronic Microscopy (SEM)

Scanning Electronic Microscopy (SEM) (JOEL JSM-6400) is used to observe the morphology of the powder, the green body and the sintered sample. The as-received powder and the as-prepared green body are coated with Au-Pt before SEM observations. The sintered sample is first etched in 10wt% HF acid for 15 min, and then ultrasonic is used to clean the sample surface for 30 min. After coated with Au-Pt, the sample surface morphology is investigated under SEM. Under SE mode, the Energy Dispersion x-ray Spectrometer (EDXS) is used to detect the existing elements in the sample.

A.9-2 X-ray Diffraction (XRD)

X-ray Diffraction (XRD) (Philips APD3720) is used to determine the phase composition in the samples, where Cu K_α (λ = 1.540 and 1.543 A) is used as anode of x-ray source. The scanning angle is from 10 to 80 degree and with a scanning speed of 3°/min.

APPENDIX B

LISTS OF PAPERS WRITTEN DURING THE RESEARCH OF THIS DISSERTATION

1. "Effect of volume fraction of particles on the viscoelastic properties of the temperature induced forming (TIF) alumina suspensions," *Journal of American Ceramic Society*, in press (2001).

2. "Rheological properties, gelation diagram and direct casting process of the temperature induced forming (TIF) alumina suspensions," *Journal of Material Synthesis and Processing*, 9[1] 103-109 (2001).

3. "Effect of calcium addition on the adsorption of citrate anions on alumina surface in the temperature induced forming (TIF) alumina suspensions," *Journal of Material Science Letters*, in press (2001).

4. "Effect of calcium addition on the gelation behavior of the temperature induced forming (TIF) alumina suspensions," submitted to *Journal of Material Science*, (2000).

5. "Estimation of the volume fraction gelation threshold for the temperature induced forming (TIF) alumina suspensions using rheological measurement," submitted to *Journal of Ceramic Processing Research*, (May 2001).

6. "Percolation theory model for the temperature induced forming (TIF) alumina suspensions, Part 1: Model calculations," submitted to *Journal of European Ceramic Society*, (May 2001).

7. "Percolation theory model for the temperature induced forming (TIF) alumina suspensions, Part 2: Determination of the model equation parameters," submitted to *Journal of European Ceramic Society*, (May 2001).

8. "Effect of the molecular weight of poly (acrylic acid) on the rheological properties and percolation microstructure of the temperature sensitive alumina suspensions," submitted to *Journal of American Ceramic Society*, (June 2001).

9. "Effect of the molecular weight of poly (acrylic acid) on the volume fraction gelation threshold for the temperature sensitive alumina slurries," submitted to *Journal of Materials Science Letters*, (June 2001).

10. "A new approach using DLVO theory to prepare highly loaded poly (acrylic acid)-free temperature sensitive alumina suspensions," finished and to be submitted to *Journal of Material Synthesis and Processing*, (July 2001).

LIST OF REFERENCES

[1] F.F. Lange, "Powder Processing Science and Technology for Increased Reliability," J. Am. Ceram. Soc., 72 [1], 3 (1989).

[2] G. V. Franks and F. F. Lange, "Mechanical Behavior of Saturated, Consolidated, Alumina Powder Compacts: Effect of Particle Size and Morphology on the Plastic-to-Brittle Transition," Colloids and Surfaces A: Physicochemical and Engineering Aspects 146, 5 (1999).

[3] Ceramic Transactions, *Forming Science and Technology for Ceramics*, edited by Michael J. Cima, Vol 26, 1992.

[4] H.K. Bowen, "Basic Research Needs on High Temperature Ceramics for Energy Applications," Mater. Sci. Eng., 44, 1 (1980).

[5] J.R. Merhar, "Designing for Metal Injection Molding," presented at the Powder Injection Molding International Symposium, July 15-17, 1991, Albany, NY.

[6] M. Savitz, "Commercialization of Advanced Structural Ceramics Patience Is A Necessity, Part II," Am. Ceram. Soc. Bulletin, 3 (1999).

[7] T. Wohlers, "Creating Parts by Layers," Cadence, 5, 73 (1989).

[8] C. Deckard and J. Beaman, "Recent Advances in Selective Laser Sintering," pp.447-52 in Proceedings of the 14th Conference on Product Research and Technology, University of Michigan, October 1987.

[9] E. Sachs, M. Cima, P. Williams and D. Brancazio, "Rapid Tooling and Prototyping by Three Dimensional Printing," Trans. NAMRI/SME, 41 (1990).

[10] M. J. Cima and E. M. Sachs, "Three Dimensional Printing: Form, Materials, and Performance," in Proceedings of the Solid Freeform Fabrication Symposium, Austin, TX, 1991.

[11] L. M. Sheppard, "Computer Software Product Design," Ceramic Industry, 30 (1999).

[12] M. F. Berard, "Rapid Prototyping," Ceramic Industry, 12 (1997).

[13] M. F. Berard, "Rapid Prototyping II," Ceramic Industry, 1 (1998).

[14] Helysis, Inc. Homepage: http://helisys.com/. Layered Material Technology for Rapid Prototyping, Modeling, Pattern Making, Production Tooling and Manufacturing, 6/2000.

[15] A. Griffin, "Rapid Prototyping with Engineered Ceramics," Ceramic Industry, 4 (1997).

[16] E. A. Griffin, D. R. Mumm and D. B. Marshall, "Rapid Prototyping of Functional Ceramic Composites," Am. Ceram. Soc. Bull., 75 [7] (1996).

[17] C.W. Griffin, J. Daufenbach and S. McMillin, "Desktop Manufacturing: LOM versus Pressing," Am. Ceram. Soc. Bull., 73 [8] (1994).

[18] M. Feygin and B. Hsieh, "Laminated Object Manufacturing: A simple Process," presented at The Second Freeform Fabrication Symposium, University of Texas at Austin, Aug. 1991.

[19] J. Grau, M. Cima and E. Sachs, "Fabricating Alumina Molds for Slip Casting with 3-D Printing," Ceramic Industry, 7 (1996).

[20] S. Baskaran, G. D. Maupin and G. L. Graff, "Freeform Fabrication of Ceramics," Am. Ceram. Soc. Bull., 77[7] (1998).

[21] J. H. Song, M. J. Edirisinghe and J. R. G. Evans, "Formulation and Multilayer Jet Printing of Ceramic Inks," J. Am. Ceram. Soc., 82 [12], 3374 (1999).

[22] http://www.sanders-prototype.com/. 3D MoldMaker™ Plotter System, 6/1999.

[23] http://www.sandia.gov/. Robocasting: Free Forming of Ceramic Parts without Moulds or Machining, 7/1999.

[24] J. Cesarano III and I. A. Aksay, "Processing of Highly Concentrated Aqueous α-Alumina Suspensions Stabilized with Polyelectrolytes," J. Amer. Ceram. Soc., 71[12], 1062 (1988).

[25] J. Cesarano III and R. Segalman, "Robocasting Provides Moldless Fabrication from Slurry Deposition," Ceramic Industry, 4 (1998).

[26] D. Dimos and P. Yang, "Simplifies Fabrication of Thick-Film Hybrids," Ceramic Industry, 12 (1997).

[27] 3D Systems, Inc. Homepage: http://www.3dsystems.com/. 3D Systems'™ ThermoJet™ Solid Object Printer, 2/2000.

[28] S. Kirihara, Y. Miyamoto and K. Kajiyama, "Fabrication of Ceramic/Eposy Photonic Crystals by Stereolithgraphy," presented in 24th Annual Cocoa Beach Conference

and Exposition: An International Conference on Engineering Ceramics and Structures, Cocoa Beach, FL, January 23-28, 2000 (Paper No.C-083-00).

[29] Cubital Homepage: http://www.cubital.com/cubital/. Direct Photoshaping, 6/1999.

[30] W. Wang, J. G. Conley, H. W. Stoll and R. Jiang, "Rapid Process Selection for Rapid Tooling in Sand Casting," Proceedings of the 10th Solid Freeform Fabrication Symposium, University of Texas at Austin, August 10, 1999, pp19-27.

[31] G. M. Lous, I. A. Cornejo, T.F. Mcnulty, A. Safari and S.C. Danforth, "Fabrication of Piezoelectric Ceramic/Polymer Composite Transducers Using Fused Deposition of Ceramics," J. Am. Ceram. Soc., 83 [1], 124 (2000).

[32] A. Bandyopadhyay, R.K. Panda, T.F. McNulty, F. Mohammadi, S.C. Danforth and A. Safari, "Piezoelectric Ceramics and Composites via Rapid Prototyping Techniques," Rapid Prototyping J., 4 [1], 37 (1998).

[33] S. C. Danforth, A. Safari, M. Agarwala, A. Bandyopadhyay, R. van Weeren, N. Langrana and V. Jamalabad, "Solid Freeform Fabrication Methods," U.S. Pat. No. 5,738,817, April 14,1998.

[34] A. Safari, V. F. Janas, A. Bandyopadhyay, R. K. Panda, M. Agarwala and S. C. Danforth, "Ceramic Composites and Methods for Producing Same," U.S. Pat. No.5,818,149, Oct. 6,1998.

[35] T. F. McNulty, F. Mohammadi, A. Bandyopadhyay, D. J. Shanefield, S. C. Danforth and A. Safari, "Development of a Binder Formulation for Fused Deposition of Ceramics," Rapid Prototyping J., 4 [4], 144 (1998).

[36] J.C. Nelson, "Selective Laser Sintering of Polymer-coated Silicon Carbide Powders," Ind. Eng. Chem. Res., 34, 1641 (1995).

[37] P. K. Subramanian and H. L. Marcus, "Selective Laser Sintering of Alumina Using Alumina Binder," Mater. Manuf. Processes, 10, 689 (1995).

[38] M. K. Agarwala, D. L. Bourell, A. Manthiram, B. R. Birmingham and H. L. Marcus, "High T_c Dual Phase Ag-$Yba_2Cu_3O_{7-x}$ Composites Prepared by Selective Laser Sintering and Infiltration," J. Mater. Sci., 30, 459 (1995).

[39] A. Nickel, "Analysis of Thermal Stresses in Shape Deposition Manufacturing of Metal Parts," Ph.D. Thesis, Stanford University, August 1999.

[40] K. Sakamoto, "Gel Casting of Metal Powder for MoldSDM," M.Sc. Thesis, Stanford University, June 1999.

[41] J. H. Kao, "Process Planning for Additive/Subtractive Solid Freeform Fabrication using Medial Axis Transform," Ph.D. Thesis, Stanford University, June 1999.

[42] X. C. Li, J. Stampfl and F.B. Prinz, "Mechanical and Thermal Expansion Behavior of Laser Deposited Metal Matrix Composites of Invar and TiC," Materials Science and Engineering A, 282(1-2), 86 (2000).

[43] A. Nickel, D. Barnett, G. Link and F. Prinz, "Residual Stresses in Layered Manufacturing," Proceedings of the Solid Freeform Fabrication Symposium, University of Texas at Austin, Austin, Texas, August 1999.

[44] A.G. Cooper, S. Kang, J.W. Kietzman, F.B. Prinz, J.L. Lombardi and L.E. Weiss, "Automated Fabrication of Complex Molded Parts using Mold Shape Deposition Manufacturing," Materials and Design, 20[2/3], 83, (1999).

[45] S. Kang, A. G. Cooper, J. Stampfl, F. Prinz, J. Lombardi, L. Weiss and J.Sherbeck, "Fabrication of High Quality Ceramic Parts using Mold SDM," Proc. Solid Freeform Fabrication Symposium, University of Texas at Austin, Austin, Texas, August 1999.

[46] Y.L. Cheng, J. Stampfl, R. Leitgeb and F. Prinz, "Additive/Subtractive Material Processing for Mesoscopic Parts," Proc. Solid Freeform Fabrication Symposium, University of Texas at Austin, Austin, Texas, August 1999.

[47] Y.C. Chang, J.M. Pinilla, J.H. Kao, J. Dong, K. Ramaswami and F.B. Prinz, "Automated Layer Decomposition for Additive/Subtractive Solid Freeform Fabrication," Proc. Solid Freeform Fabrication Symposium, University of Texas at Austin, Austin, Texas, 1999.

[48] A. G. Cooper, S. Kang, J. W. Kietzman, F. B. Prinz, J. L. Lombardi and L. Weiss, "Automated Fabrication of Complex Molded Parts Using Mold SDM," Proceedings of the Solid Freeform Fabrication Symposium, University of Texas at Austin, Austin, Texas, August 1998.

[49] J. W. Kietzman and F. B. Prinz, "Material Strength in Polymer Shape Deposition Manufacturing," Proceedings of the Solid Freeform Fabrication Symposium, University of Texas at Austin, Austin, Texas, August 1998.

[50] G.R. Link, J.Fessler, A.Nickel and F.Prinz, "Rapid Tooling Die Case Inserts using Shape Deposition Manufacturing," Materials and Manufacturing Processes, 13[2], 263 (1998).

[51] P. F. Blazdell and J. R. G. Evans, "The Computer Aided Manufacture of Ceramics Using Multilayer Jet Printing," J. Mater. Sci. Lett., 14 [22], 1562 (1995).

[52] W. D. Teng and M. J. Edirisinghe, "Development of Ceramic Inks for Direct Continuous Jet Printing," J. Am. Ceram. Soc., 81 [4], 1033 (1998).

[53] B. V. Velamakanni, J. C. Chang, F. F. Lange and D. S. Pearson, "New Method for Efficient Colloidal Particle Packing via Modulation of Repulsive Lubricating Hydration Forces," Langmuir, 6 [7], 1323 (1990).

[54] M. Colic, G. V. Franks, M. L. Fisher and F. F. Lange, "Effect of Counterion Size on Short Range Repulsive Forces at High Ionic Strength," Langmuir, 13[12], 3129 (1997).

[55] R. G. Horn, "Surface Forces and Their Action in Ceramic Materials," J. Am. Ceram. Soc., 73 [5], 1117 (1990).

[56] W. M. Sigmund, N. S. Bell and L. Bergström, "Novel Powder Processing Methods for Advanced Ceramics," J. Am. Ceram. Soc., 83 [7], 1557 (2000).

[57] H. A. Barnes, J. F. Hutton and K. Walters, *An Introduction to Rheology*, Elsevier, New York, 1989, pp121-122.

[58] H. A. Barnes, J. F. Hutton and K. Walters, *An Introduction to Rheology*, Elsevier, New York, 1989, pp37-54.

[59] J. A. Yanez, T. Shikata, F. F. Lange and D. S. Pearson, "Shear Modulus and yield Stress Measurements of Attractive Alumina Particle Networks in Aqueous Suspensions," J. Am. Ceram. Soc., 79[11], 2917 (1996).

[60] L. Bergström, "Shear Thinning and Shear Thickening of Concentrated Ceramic Suspensions," Colloids and Surfaces, A: Physicochemical and Engineering Aspects, 133, 151 (1998).

[61] S. Stoll and J. Buffle, "Computer Simulation of Bridging Flocculation Processes: The Role of Colloid to Polymer Concentration Ratio on Aggregation Kinetics," J. Colloid Interf. Sci., 180, 548 (1996).

[62] W. Liang and K. Kendall, "Aggregate Formation in Colloidal Dispersions," Colloids and Surfaces, A: Physicochemical and Engineering Aspects, 131, 193 (1998).

[63] L. G. B. Bremer, B. H. Bijsterbosch, R. Schrijvers, T. van Vliet and P. Walstra, "On the Fractal Nature of the Structure of Acid Casein Gels," Colloids Surf., 51, 159 (1990).

[64] H. G. E. Hentschel, "Fractal Dimension of Generalized Diffusion-Limited Aggregates," Phys. Rev. Lett., 52 [3], 212 (1984).

[65] W. Wolthers, D. van den Ende, V. Breedveld, M. H. G. Duits, A. A. Potanin, R. H. W. Wientjes and J. Mellema, "Linear Viscoelastic Behavior of Aggregated Colloidal Dispersions," Physical Review E, 56, 5726 (1997).

[66] C. J. Rueb and C. F. Zukoski, "Viscoelastic Properties of Colloidal Gels," J. Rheol., 41[2], 197 (1997).

[67] D. Stauffer, *Introduction to Percolation Theory.* Taylor & Friends, London, 1985.

[68] J. A. Yanez, E. Larrz and L. Bergström, "Viscoelastic Properties of Particle Gels," J. Colloid Interface Sci., 209, 162 (1999).

[69] L. Bergström, C.H. Schilling and I.A. Aksay, "Consolodation Behavior of Flocculated Alumina Suspensions," J. Am. Ceram. Soc., 75[12], 3305 (1992).

[70] J.C. Chang, B.V. Velamakani, F.F. Lange and D.S. Pearson, "Centrifugal Consolidation of Al_2O_3/ZrO_2 Composite Slurries Versus Interparticle Potentials: Particle Packing and Mass Segregation," J. Am. Ceram. Soc., 74[10], 2201 (1991).

[71] C. Ballard, "Ceramic Injection Molding Meets the Demand for Manufacturing Complex Shapes," Ceramic Industry, 3 (1997).

[72] A. F. Henriksen, "The Art of Forming Near Net Shapes," Ceramic Industry, 4 (1997).

[73] R. M. German and R. G. Cornwall, "Demand for Injection Molded Components to Grow," Ceramic Industry, 9 (1997).

[74] J.R.G. Evans, "Interfacial Aspects of Ceramic Injection Molding," in Surface and Colloidal Chemistry in Advanced Ceramics Processing, ed. R.J. Pugh and L. Bergström, Marcel Dekker, New York, 1994, pp. 309-351.

[75] T. J. Graule, L. J. Gauckler and F. H. Baader, "Direct Coagulation Casting, A New Green Shaping Technique, Part I: Processing Principles," Industrial Ceramics, 16 [1], 31 (1996).

[76] T. J. Graule, F. H. Baader and L. J. Gauckler, "Shaping of Ceramic Green Compacts Direct form Suspension by Enzyme Catalyzed Reactions," CFI/Ber, DKG, 71, 317 (1994).

[77] R. W. Adams, W. B. Householder and C. A. Sundback, "Application of Quickset Injection Molding to Intelligent Processing of Ceramics," Ceram. Eng. Sci. Proc., 12, 2062 (1991).

[78] C. A. Sundback, B. E. Novich, A. E. Karas and R. W. Adams, "Complex Ceramic and Metallic Shaped by Low Pressure Forming and Sublimative Drying," US Patent 5,047,182, 10 Sept. 1991.

[79] Y. Zhang and K. Uematsu, "A Novel Consolidation Approach for Ceramic Colloidal Forming," Proceedings of CICC-1, Beijing, China (1999).

[80] L. Bergström and E. Sjöström, "Temperature Induced Gelation of Concentrated Ceramic Suspensions: Rheological Properties," J. Eur. Ceram. Soc., 5, 1 (1999).

[81] L. Bergström, "Method for Forming Ceramic Powders by Temperature Induced Flocculation," US Patent 5,540,532, 23, August 1994.

[82] T. Kosmac, S. Novak and M. Sajko, "Hydrolysis-Assisted Solidification (HAS): A New Setting Concept for Ceramic Net-Shaping," J. Eur. Ceram. Soc., 17, 427 (1997).

[83] A. J. Fanelli, R. D. Silvers, W.S. Frei, J. V. Burlew and G. B. Marsh, "New Aqueous Injection Molding Processes for Ceramic Powders," J. Am. Ceram. Soc., 72[8], 1833 (1989).

[84] Z. Xie, L. Zhou and Y. Huang, "Gelation Forming of Ceramic Compacts Using Agarose," British Ceramic Transactions, 98[2], 58 (1999).

[85] O. O. Omatete, M. A. Janney and R. A. Strehlow, "Gel Casting - A New Ceramic Forming Process," Am. Ceram. Soc. Bulletin, 70, 1641 (1991).

[86] L. Zhou, Y. Huang and Z. Xie, "Gelacasting of Concentrated Aqueous Silicon Carbide Suspension," J. Eur. Ceram. Soc., 20, 85 (2000).

[87] F. Aldinger, W. Sigmund and J. Yanez, "Formgebungsmethodde für Keramiken unde Metalle in Wässrigen Systemen mittels Temperaturäandering Aktenzeichen," German patent 197,51,696.3, 1998.

[88] N. S. Bell, L. Wang, W. M. Sigmund and F. Aldinger, "Temperature Induced Forming: Application of Bridging Flocculation to Near-Net Shape Production of Ceramic Parts," Z. Metallkd., 90 [6], 388 (1999).

[89] P.C. Hidber, T. J. Graule and L. J. Gauckler, "Citric Acid — A Dispersant for Aqueous Alumina Suspensions," J. Am. Ceram. Soc., 79 [7], 1857 (1996).

[90] R. Kummert and W. Stumm, "The Surface Complexation of Organic Acids on Hydrous γ-Al_2O_3," J. Colloid Interf. Sci., 75 [2], 373 (1980).

[91] P. C. Hidber, T. J. Graule and L. J. Gauckler, "Competitive Adsorption of Citric Acid and Poly(Vinyl alcohol) onto Alumina and Its Influence on the Binder Migration during Drying," J. Am. Ceram. Soc., 78 [7], 1775 (1995).

[92] E. Ringenbach, G. Chauveteau and E. Pefferkorn, "Effect of Soluble Alumina Ions on Polyelectrolyte-Alumina Interaction: Kinetics of Polymer Adsorption and Colloid Stabilization," Colloids and Surfaces, A: Physicochemical and Engineering Aspects, 99, 161 (1995).

[93] A. Ogawa, H. Yamada, S. Matsuda, K. Okajima and M. Doi, "Viscosity Equation for Concentrated Suspensions of Charged Colloidal Particles," J. Rheol., 41[3], 769 (1997).

[94] Th. F. Tadros, "Correlation of Viscoelastic Properties of Stable and Flocculated Suspensions with Their Interparticle Interactions," Advances in Colloid and Interface Science, 68, 97 (1996).

[95] D. Santhiya, G. Nandini, S. Subramanian, K. A. Natarajan and S. G. Malghan, "Effect of Polymer Molecular Weight on the Adsorption of Polyacrylic Acid at the Alumina-Water Interface," Colloids and Surfaces, A: Physicochemical and Engineering Aspects, 133, 157 (1998).

[96] S. Feng and P. N. Sen, "Percolation on Elastic Networks: New Exponents and Threshold," Phys. Rev. Lett., 52 [3], 216 (1984).

[97] J. A. Yanez, T. Shikata, F. F. Lange and D. S. Pearson, "Shear Modulus and Yield Stress Measurements of Attractive Alumina Particle Networks in Aqueous Slurries," J. Am. Ceram. Soc., 79 [11], 2917 (1996).

[98] R. C. Sonntag and W. B. Russel, "Elastic Properties of Flocculated Networks," J. Colloid and Interface Sci., 116 [2], 485 (1987).

[99] W. H. Shih, W. Y. Shih, S. I. Kim, J. Liu and I. A. Aksay, "Scaling Behavior of the Elastic Properties of Colloidal Gels," Phys. Rev. A, 42 [8], 4772 (1990).

[100] R. Buscall, P. D. Mills, J. W. Goodwin and D. W. Lawson, "Scaling Behavior of the Rheology of Aggregate Networks Formed from Colloidal Particles," J. Chem. Soc., Faraday Trans. 1, 84 [12], 4249 (1988).

[101] http://www.mse.ufl.edu/~adair/software/. STABIL© 4.5 for Windows™, 1999.

[102] R. Ettelaie and R. Buscall, "Electrical Double Layer Interactions for Spherical Charge Regulating Colloidal Particles," Advances in Colloid and Interface Science, 61, 131 (1995).

[A-1] R. W. O'Brien, "Electroacoustic Effects on a Dilute Suspension of Spherical Particles," J. Fluid. Mech., 190, 71 (1988).

BIOGRAPHICAL SKETCH

Yunpeng Yang was born in HeNan Province of the People's Republic of China. He got his BS degree in materials science in 1991 from the Department of Materials Science and Engineering of Zhejiang University, Hangzhou, P. R. China. He then got his Master's degree in advanced ceramic materials in 1993 from the Department of Materials Science and Engineering of Tianjin University, Tianjin, P. R. China. From 1994 to 1997, he worked in Tianjin University as an assistant professor and lecturer. He came to the University of Florida in the fall of 1997 and joined Dr. Sigmund's group in the summer of 1999 to study the colloidal processing and solid freeform fabrication (SFF) of ceramics. He got his Ph.D. in August of 2001. He enjoyed the life at UF and the beautiful weather of the sunshine state. He is one of the five recipients of *the Outstanding Academic Achievement Award for An International Student* in College of Engineering of the University of Florida on 4/25/2001.

I certify that I have read this study and that in my opinion it conforms to acceptable standards of scholarly presentation and is fully adequate, in scope and quality, as a dissertation for the degree of Doctor of Philosophy.

Wolfgang M. Sigmund, Chairman
Assistant Professor of Materials Science and Engineering

I certify that I have read this study and that in my opinion it conforms to acceptable standards of scholarly presentation and is fully adequate, in scope and quality, as a dissertation for the degree of Doctor of Philosophy.

E. Dow Whitney
Professor of Materials Science and Engineering

I certify that I have read this study and that in my opinion it conforms to acceptable standards of scholarly presentation and is fully adequate, in scope and quality, as a dissertation for the degree of Doctor of Philosophy.

Ronald Baney
Associate Engineer of Materials Science and Engineering

I certify that I have read this study and that in my opinion it conforms to acceptable standards of scholarly presentation and is fully adequate, in scope and quality, as a dissertation for the degree of Doctor of Philosophy.

Laurie Gower
Assistant Professor of Materials Science and Engineering

I certify that I have read this study and that in my opinion it conforms to acceptable standards of scholarly presentation and is fully adequate, in scope and quality, as a dissertation for the degree of Doctor of Philosophy.

Chang-Yu Wu
Assistant Professor of Environmental
Engineering Science

This dissertation was submitted to the Graduate Faculty of the College of Engineering and to the Graduate School and was accepted as partial fulfillment of the requirements for the degree of Doctor of Philosophy.

August 2001

Pramod Khargonekar
Dean, College of Engineering

Winfred M. Phillips
Dean, Graduate School